TECHNISCHE UNIVERSITÄT WIEN

INSTITUT FÜR MECHANIK UND MECHATRONIK
Mechanics & Mechatronics

DISSERTATION

A Multi-Level Cooperative Strategy for Reducing Fuel Consumption and Transient Pollutant Emissions of Hybrid Electric Vehicles.

ausgeführt zum Zwecke der Erlangung des akademischen Grades
DOKTOR DER TECHNISCHEN WISSENSCHAFTEN
der
FAKULTÄT FÜR MASCHINENWESEN UND BETRIEBSWISSENSCHAFTEN
der
TECHNISCHEN UNIVERSITÄT WIEN
von

Alexis Benaitier
Matrikelnummer: 12038904

unter der Leitung von
Associate Prof. Dipl.-Ing. Dr.techn. Christoph Hametner
Forschungsgruppe Regelungsmethoden-Antriebssysteme
Institut für Mechanik und Mechatronik

Wien, am August 26, 2024

Alexis Benaitier

Ma famille
Mes amis

Danksagung

Leider läßt sich eine wahrhafte Dankbarkeit mit Worten nicht ausdrücken.

Johann Wolfgang von Goethe (1749-1832)

Diese Arbeit wurde von der Christian Doppler Laboratory for Innovative Control and Monitoring of Automotive Powertrain Systems und der TU Wien Bibliothek im Rahmen des Open Access Funding Programme unterstützt.

Ich nehme zur Kenntnis, dass ich zur Drucklegung meiner Arbeit unter der Bezeichnung Dissertation nur mit Bewilligung der Prüfungskommission berechtigt bin.

Eidesstattliche Erklärung

Ich erkläre an Eides statt, dass die vorliegende Arbeit nach den anerkannten Grundsätzen für wissenschaftliche Abhandlungen von mir selbstständig erstellt wurde. Alle verwendeten Hilfsmittel, insbesondere die zugrunde gelegte Literatur, sind in dieser Arbeit genannt und aufgelistet. Die aus den Quellen wörtlich entnommenen Stellen, sind als solche kenntlich gemacht.

Das Thema dieser Arbeit wurde von mir bisher weder im In- noch Ausland einer Beurteilerin/einem Beurteiler zur Begutachtung in irgendeiner Form als Prüfungsarbeit vorgelegt. Diese Arbeit stimmt mit der von den Begutachterinnen/Begutachtern beurteilten Arbeit überein.

Ich nehme zur Kenntnis, dass die vorgelegte Arbeit mit geeigneten und dem derzeitigen Stand der Technik entsprechenden Mitteln (Plagiat Erkennungssoftware) elektronischtechnisch überprüft wird. Dies stellt einerseits sicher, dass bei der Erstellung der vorgelegten Arbeit die hohen Qualitätsvorgaben im Rahmen der geltenden Regeln zur Sicherung guter wissenschaftlicher Praxis „Code of Conduct“ an der TU Wien eingehalten wurden. Zum anderen werden durch einen Abgleich mit anderen studentischen Abschlussarbeiten Verletzungen meines persönlichen Urheberrechts vermieden.

Wien, am August 26, 2024 Alexis Benaitier

Kurzfassung

Diese Doktorarbeit untersucht eine mehrstufige Energiemanagementstrategie zur Optimierung der Drehmomentaufteilung und Gangwahl für Hybridfahrzeuge mit Verbrennungsmotor (HEVs). Sie präsentiert drei wesentliche Beiträge, die jeweils in Fachpublikationen detailliert beschrieben sind und darauf abzielen, den Kraftstoffverbrauch und die Schadstoffemissionen in HEVs weiter zu reduzieren. Während die Hybridisierung von Fahrzeugen bereits erfolgreich zur Senkung des Kraftstoffverbrauchs eingesetzt wird, sind neue Herausforderungen, vor allem bezüglich der Minimierung von Schadstoffemissionen, entstanden.

Der erste Beitrag dieser Arbeit zielt auf die systematische Kooperation zwischen den Reglern und den Komponenten des Antriebsstranges ab. Die Kooperation wird dabei durch parametrische Regler erzielt, die die Einflüsse der anderen Regler bei der Aktualisierung der Reglerparameter berücksichtigen. Angewendet auf ein HEV zeigt die Methode eine erhebliche Kraftstoffreduktion durch verbesserte Zusammenarbeit zwischen den Reglern für Motor und Getriebe. Der zweite Beitrag konzentriert sich auf die Modellierung und Minimierung von Schadstoffemissionen während transienter Betriebszustände. Hier wird eine generische Optimierungsmethode vorgestellt, die die transienten Betriebszustände basierend auf einer funktionalen Darstellung der Stellgrößen berücksichtigt. Angewandt auf ein Diesel-Hybridfahrzeug zeigt die Methode eine signifikante Reduktion der transienten Emissionen dank gleichmäßigeren Betrieb. Der letzte Beitrag stellt ein generisches prädiktives Reglerdesign für die präzise Aktuatorregelung der Antriebskomponenten vor. Eine modulare Vorsteuerung, die basierend auf Messdaten identifiziert wurde und für nichtlineare Systeme geeignet ist, wird zur Regelung des Luftpfads eines Dieselmotors eingesetzt. Dieser Regler liefert vergleichbare Ergebnisse zur optimalen Lösung, jedoch mit deutlich geringerem Rechenaufwand.

Die Beiträge dieser Arbeit wurden durch Simulationen mit detaillierten und experimentell validierten Plattformen überprüft. Die Ergebnisse unterstreichen die Bedeutung der Komponentenkooperation und der Berücksichtigung transienter Betriebszustände bei der effektiven Reduzierung von Kraftstoffverbrauch und Schadstoffemissionen. Dank ihrer Modularität können die entwickelten Lösunge auf verschiedene HEV-Architekturen und Komponentenkonfigurationen angewendet werden. Anhand spezifischer Fallstudien zeigt diese Arbeit signifikante eduktionen der Schadstoffemissionen bei Hybridfahrzeugen mit Verbrennungsmotoren.

Abstract

This PhD thesis investigates a multi-level energy management strategy to optimize torque distribution and gear selection of hybrid electric vehicles (HEVs) with an internal combustion engine. The thesis presents three significant contributions, each detailed in a dedicated journal publication, to further reduce fuel consumption and pollutant emissions of HEVs. While hybridization has long been recognized for its potential to lower fuel consumption, new challenges have emerged, particularly in minimizing pollutant emissions to achieve cleaner transportation.

The first contribution of this thesis is the systematic cooperation between control loops and powertrain components. This cooperation is achieved using parametric controllers, where the update of each controller's parameters considers the reaction of the other controllers. Applied to an HEV, the proposed method demonstrates notable fuel reduction through enhanced collaboration between torque split and gear selection controllers.

The second contribution focuses on modeling and minimizing pollutant emissions during transient operations. This thesis introduces a generic transient optimization method based on a functional representation of the control variables. The proposed optimization method is applied to control the engine torque, significantly reducing transient emissions of a diesel HEV thanks to smooth engine operations.

The last contribution introduces a generic predictive controller design for precise control of powertrain component actuators, ensuring accurate tracking of reference trajectories. A modular feedforward controller structure, identified from measurement data and suitable for nonlinear systems, is proposed and applied to control the air path of a diesel engine. This identified controller yields results comparable to an optimal solver but with substantially lower computational complexity.

The contributions of this thesis have been validated through simulations on detailed and experimentally validated platforms. The findings highlight the critical role of component cooperation and transient operations in effectively reducing fuel consumption and pollutant emissions. Emphasizing modularity, the developed solutions are applicable to various HEV architectures and component configurations. Applied to specific case studies, this thesis demonstrates significant reductions in pollutant emissions for hybrid electric vehicles with combustion engines.

Contents

List of Figures

List of Tables

Chapter 1

Overview

Hybridization of vehicles is a promising step toward sustainable transport. Indeed, the battery and electric motor allow more freedom regarding the control of the combustion engine. Using a state-of-the-art multi-level energy management strategy (EMS), this thesis proposes three main contributions toward further reductions of fuel consumption and pollutant emissions.

This work is organized as a cumulative thesis with an introduction chapter followed by a chapter composed of three selected publications aiming at further reducing fuel consumption and transient pollutant emissions of internal combustion engine hybrid electric vehicles (HEVs). The first chapter of this thesis describes the motivation and problem statement and summarizes the thesis's main contributions. Chapter 2 comprises the three journal publications detailing the main contributions of this thesis, accompanied by an outline of the author's contribution.

The main outcomes achieved in the proposed thesis are the guaranteed cooperation between the powertrain components in Publication A, the minimization of transient pollutant emissions in Publication B, and the control of engine actuators to realize transient trajectory tracking in Publication C.

1.1 Motivation

To pursue the announcement of the European Green Deal in 2020, not only vehicles' fuel consumption must decrease but also their pollutant emissions [1]. Therefore, a smooth transition toward climate-neutral vehicles is necessary, resulting in a large-scale hybridization of the European transport sector. Nowadays, increased efforts in EMS for internal combustion engine HEVs are required to continue the pursuit of climate-neutral vehicles.

This thesis focuses on further reducing fuel consumption and pollutant emissions of HEVs with an internal combustion engine and a gearbox. A multi-level EMS is employed in this thesis, with a low-level layer splitting the torque required by the driving

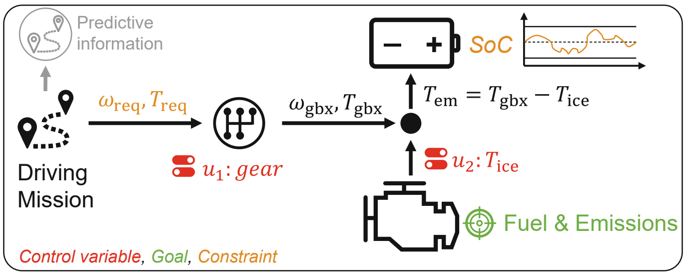

Figure 1.1: Control problem for an HEV with an internal combustion engine.

mission between the engine and the electric motor and defining the gear selection. The actuators are controlled in a second control layer to realize the expected torque split and the gear selection. Lastly, a high-level control layer is employed to take advantage of predictive information to update the EMS parameters depending on the predicted driving conditions. The predictive information comprises the predicted vehicle speed and road altitude from GPS data, onboard sensors, and communication from the vehicle to its environment. The predicted information is consequently not always accurate, and the prediction horizon can vary depending on the availability of the information.

The goal of the EMS is to reduce a cost including fuel consumption, pollutant emissions, and the number of gearshifts for this thesis, while maintaining the state of charge (SoC) within its feasible operating range. The minimization of this cost is achieved through the control of the powertrain components. Figure 1.1 illustrates the role of the EMS, first defining the components' trajectories, i.e., the control variables composed of the engine torque T_{ice} and gear selection *gear*, to then control the components' actuators. During this thesis, different component variants have been considered for the vehicle, and all the contributions are first introduced in a modular framework. The outcomes of this thesis are, consequently, technical solutions adaptable to different HEV architectures and component variants.

This thesis identified three main directions to reduce fuel consumption and emissions further. First, a method is proposed in Publication A to ensure cooperation between powertrain components, demonstrating the need for cooperation between engine and gearbox to reduce the EMS costs efficiently. Then, a functional representation of the engine torque is proposed in Publication B to account for transient operations, significantly reducing pollutant emissions. Finally, the precise control of the engine actuators during transient operations is achieved with an automated feedforward controller design presented in Publication C, guaranteeing efficiency and low emissions levels.

1.2 State-of-the-art overview

The main task of an EMS for HEVs is to control the torque split between the engine and the electric motor. Numerous EMSs have already been investigated, primarily focusing on the torque split [2]. Offline methods have been proposed when the entire driving mission is known before departure to generate a reference or evaluate the optimum fuel consumption. Dynamic programming (DP), Pontryagin maximum principle (PMP), and nonlinear optimization are the most employed methods to generate references before the beginning of the driving mission [2, 3]. The equivalent consumption minimization strategy (ECMS) is widely employed for an online implementation, i.e., to be employed during the driving mission, thanks to its simplicity and robustness [4]. Numerous other online methods exist, such as rule-based, fuzzy logic, optimization methods, or machine learning. Despite the vast number of studies, the new emissions thresholds oblige a drastic update of the standard torque split control strategies [5].

Further fuel and emission reductions are possible when considering the interactions between the powertrain components. As shown by [6] considering the engine while controlling the gear selection can further reduce fuel consumption. More interestingly, considering cooperation between the gear selection and the torque split controller can be beneficial toward achieving lower fuel consumption and emissions [7]. Multiple other powertrain components, such as the battery management system or the exhaust aftertreatment systems, could also benefit from component cooperation. Having a central optimization routine suffers from low modularity and considerable complexity. However, communication between decentralized controllers is seen as a possible perspective. Sharing references between component controllers to find a consensus or using a hierarchical structure is currently the main investigated research direction for cooperative EMS [2].

The emissions of internal combustion engines depend on the engine operating points and are further amplified by engine transient operations [8, 9]. Some models have been proposed to capture the transient emissions, using the torque variations [10] or the derivative of the power [10]. Considering such transient emissions models in the EMS showed considerable emissions reduction [11]. Indeed, standard optimization methods, such as PMP, ignore the transient engine operations, resulting in significant torque variations and pic emissions. A few offline methods, such as DP, can consider transient operations but are impractical online due to their complexity [12]. In contrast, for online methods, the state-of-the-art real-time applicable method is to filter the actuator signal resulting in only a slight reduction of transient emissions [13].

Another key aspect of recent EMS is the consideration of predictive information. Indeed, using GPS data and onboard sensors, the EMS can estimate the future vehicle speed and road elevation, hence optimizing the EMS over a receding horizon [14]. Therefore, model predictive control methods constitute the state-of-the-art to optimize the powertrain behavior considering available predictive information [15]. However, the complexity of predictive algorithms remains a limiting factor for real-time implementation. Consequently, multi-level control has been proposed as a promising solution to consider predictive information while guaranteeing real-time feasibility. Indeed, a high-level layer can be employed to generate reference trajectories for the different powertrain components [16]. Then, a low-level layer controls the powertrain components to follow the references from the high-level layer [17]. The references can be generated during the driving mission as proposed, for example by [17], when the predictive information is not fully available before departure.

The low-level layer of a multi-level EMS defines reference trajectories for the powertrain components. However, accurately following these trajectories can be challenging for nonlinear and multivariate systems with strong output coupling, such as internal combustion engines [18, 19]. As a result, a component-level layer can be added, where the powertrain component actuators are controlled to follow the trajectories provided by the low-level layer. Different methods exist for realizing such a task, with recent studies emphasizing the need for predictive methods to accurately track the reference trajectory during transient operations [20, 19].

The state-of-the-art review concludes that the EMS for internal combustion HEV needs essential updates to further reduce fuel consumption and pollutant emissions. First, the interaction between the engine and the other components, such as the gearbox, must be systematically considered in the EMS. Second, mitigating pollutant emissions requires consideration of the transient engine operations. Third, a real-time and modular predictive control method is needed to control the components actuators to achieve precise reference following.

This thesis proposes important contributions to further reduce fuel consumption and pollutant emissions of HEVs. Using a state-of-the-art multi-level EMS, the first contribution of this thesis guarantees systematic cooperation between the powertrain components. Using parametric controllers in the low-level, the high-level optimized the low-level controllers' parameters independently, yet considering the overall powertrain reaction. The second contribution is a generic method to consider control variable derivatives in an optimization problem. Applied to control the engine torque, the transient emissions are effectively reduced thanks to the smooth operations of the engine. Finally, an automated feedforward controller synthesis is proposed. Identified directly from measurement data, this modular method is applied to control the engine air path actuators to follow transient reference trajectories.

1.3 Outline

1.3.1 Objectives

Considering the large-scale hybridization of the European transport sector and the ambition of climate-neutral vehicles, the main objective pursued in this thesis is formulated:

Key objective (O)

Further reducing fuel consumption and pollutant emissions of internal combustion engine HEVs

This objective practically corresponds to three subordinate goals

- Systematically taking advantage of powertrain components' cooperation;
- Minimizing the pollutant emissions during transient engine operations;
- Controlling the engine actuators to precisely track reference trajectories during transient engine operations.

1.3.2 Problem statement

Achieving the goal (O) corresponds to answering the following research question: (Q) How to further reduce fuel consumption and pollutant emissions of internal combustion engine HEVs?

To develop an exhaustive answer to the research question (Q) a collection of subordinate research questions is formulated.

First, the different components of the powertrain need to cooperate with one another to achieve the goals (O). The first conditions to successfully answer (Q) is therefore formulated:

Components cooperation (Q-1)

How to ensure systematic cooperation between different powertrain components?

The pollutant emissions during transient engine operations constitute the largest part of the total emissions, the following subordinate question is consequently defined:

Transient pollutant emissions (Q-2)

How to further reduce pollutant emissions during transient engine operations?

Defining references for the powertrain components, such as the engine, implicitly implies an accurate output tracking control, especially during transient operations. Additionally, a modular and straightforward calibration method would be beneficial for faster development cycles of powertrain control strategies. The third subordinate question is consequently formulated:

> Transient trajectory tracking (Q-3)
>
> How to systematically identify a feedforward controller for accurate transient output tracking of powertrain components?

In the following of this thesis, a solution is developed for each of the subordinate research questions in order to achieve the overall goal (O).

1.3.3 Scientific approach

A collection of technical properties is employed throughout this thesis as a scientific approach framework to address all the subordinate research questions, hence answering the main research question (Q).

Multi-level control structure (F-1)
A multi-level control structure is considered throughout this thesis. Indeed, different levels can simultaneously consider different aspects of the EMS to efficiently take advantage of predictive information while ensuring modularity and real-time feasibility.

Predictive control (F-2)
Predictive control is a crucial point to effectively achieve the objectives (O). Using predictive information such as vehicle speed and road altitude allows for efficient updates of the controllers.

Functional representation (F-3)
This thesis employs a functional representation of the input to realize simple yet accurate and efficient control laws and guarantee real-time feasibility.

Parametric modeling (F-4)
Employing parametric models and control laws is highly advantageous for modularity and guaranteeing real-time capability. Additionally, parametric controllers' behaviors are predictable, hence allowing systematic components' cooperation.

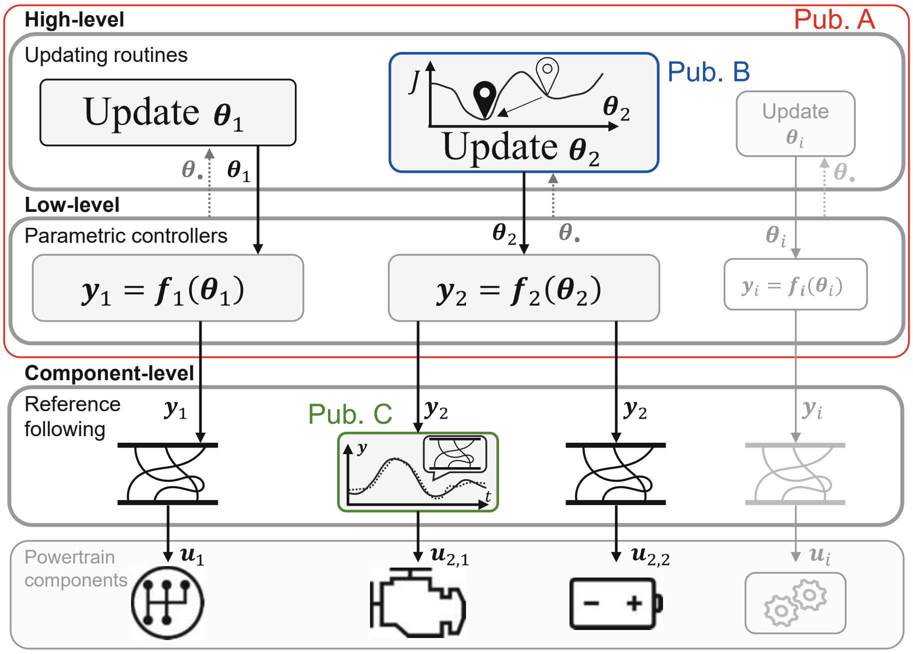

Figure 1.2: Overview of the thesis.

Optimization methods **(F-5)**
Optimization methods play a crucial role in achieving the objectives (O) while taking advantage of predictive information. Additionally, optimization methods can be re-employed for different components of the same nature, strengthening modularity.

The three main contributions of this thesis are proposed within a multi-level EMS. Different layers are indeed used to reduce the overall complexity and increase the EMS modularity. The low-level control layer is used to define references for each component. The component-level layer controls the actuators of each powertrain component to track the low-level reference trajectories. Finally, a high-level layer updates the low-level controllers based on available predictive information.

The first contribution of this thesis is the use of parametric controllers in the low-level layer to make components' cooperation systematically possible for the updating routine in the high-level control layer. Indeed, when updating a specific controller, the associated updating routine in the high-level layer can precisely estimate the reaction of the other controllers of the low-level layer, efficiently answering (Q-1). Further details are provided in Publication A, where this strategy is successfully applied to ensure cooperation between the torque split and the gear selection controllers. Successfully demonstrating modularity and efficiency, the method has been submitted to the European Patent Office [21].

The second contribution of this thesis is the parametrization of the engine torque with smooth basis functions to minimize pollutant emissions during transient engine operations. A generic method is proposed to consider the input variations when minimizing fuel consumption and pollutant emissions over a predictive horizon. Using a detailed model of an internal combustion engine HEV, the proposed method demonstrated performances close to optimality, largely reducing pollutant emissions for only a marginal increase in fuel consumption. The proposed method is exhaustively detailed in Publication B.

The last main contribution of this thesis is an automated method to identify a controller to realize precise transient trajectory tracking. Using a novel model structure, a feedforward controller can be easily identified for a generic nonlinear multivariate system and employed for a precise trajectory following. This method has been detailed and successfully applied to control a diesel engine air path in Publication C and has been protected with a patent [22]. Furthermore, a nonlinear Kalman filter has been proposed to accurately estimate the system's physical output to be tracked [23], allowing the use of a feedback loop to enhance steady-state tracking accuracy.

1.3.4 Scientific outcome

The main scientific outcomes of this thesis are:

1. A method to systematically take advantage of cooperation between control loops of HEVs. Within a state-of-the-art multi-level EMS, the method relies on independent parametric controllers for real-time control of the powertrain components. Each controller's parameters can be updated independently based on predictive information and the reactions of other controllers. This method allows systematic cooperation between control loops of an EMS and is adaptable to various powertrain configurations. Applied to an HEV, it has shown encouraging results in ensuring cooperation between the torque split and gear selection controllers.
2. A generic method has been proposed to minimize the EMS costs over a horizon considering transient operations. The input variations are inherently considered in the developed method, thanks to a functional input representation. Indeed, the input is proposed to be represented as a sum of smooth basis functions. When applied to reduce transient emissions in an HEV, this method delivers smooth engine torque, closely approximating the optimal solution found with DP but with significantly lower computational requirements.
3. An automated feedforward controller synthesis for multivariate nonlinear systems has been proposed. This approach uses a novel model structure identified directly from measurement data, allowing for convenient feedforward control via a straightforward least-squares algorithm. The method enables rapid controller synthesis for any powertrain components, thanks to its robustness to model order selection and non-minimum phase systems. Applied to control the actuators of a diesel engine air path, it achieves precise reference trajectory following, particu-

larly during transient operations.

These contributions were developed and tested through a collaborative research effort between TU Wien and AVL List GmbH. The key findings, along with additional related outcomes, have been documented in several publications in scientific journals and presented at international conferences. Furthermore, two patents have been submitted to protect two of the primary contributions of this thesis.

Journal papers

The method employing a parametric controller to systematically ensure cooperation between control loops and powertrain components is summarized in Section 1.4.1 and detailed in:

> **A. Benaitier**, F. Krainer, S. Jakubek, and C. Hametner. A Modular Approach for Cooperative Energy Management of Hybrid Electric Vehicles Considering Predictive Information. *IEEE Access*, Vol. 12 (2024), pages 60588-60600, DOI: 10.1109/ACCESS.2024.3395019.

The optimization algorithm employing basis functions to consider transient operations is presented in Section 1.4.2 and exhaustively described in:

> **A. Benaitier**, F. Krainer, S. Jakubek, and C. Hametner. Optimal energy management of hybrid electric vehicles considering pollutant emissions during transient operations. *Applied Energy*, Vol. 344 (2023), pages 121267, DOI: 10.1016/j.apenergy.2023.121267.

The automated feedforward controller synthesis introduced in Section 1.4.3 is thoroughly explained in:

> **A. Benaitier**, S. Jakubek, F. Krainer, and C. Hametner. Automated nonlinear feedforward controller identification applied to engine air path output tracking. *International Journal of Control*, Vol. 1 (2023), pages 1-12, DOI: 10.1080/00207179.2023.2227740.

Conference papers

Additionally to the feedforward controller applied to an engine air path, a nonlinear observer using an unscented Kalman filter has been proposed to simplify a PI implementation. This observer is presented and tested in simulation in:

A. Benaitier, F. Krainer, S. Jakubek, and C. Hametner. Robust physical quantities estimation for diesel engine emission reduction using sensor fusion. *2022 IEEE Conference on Control Technology and Applications (CCTA)*, Trieste, Italy; 22.08.2022 - 25.08.2022, DOI: 10.1109/CCTA49430.2022.9966196.

The benefits of adding an electrically heated exhaust aftertreatment system to reduce pollutant emissions have been studied, and a real-time feasible control law has been proposed in:

A. Benaitier, F. Krainer, S. Jakubek, and C. Hametner. Optimal control of aftertreatment electric heaters for mild hybrid vehicles during cold start. *2022 IEEE Vehicle Power and Propulsion Conference (VPPC)*, Merced, CA, USA; 01.11.2022 - 04.11.2022, DOI: 10.1109/VPPC55846.2022.10003358.

An exhaustive study of the advantages of considering torque vectoring capabilities in the EMS has been studied and documented in:

D. Köppel, **A. Benaitier**, L. Kügerl, and C. Hametner. Efficient optimization-based control of a fuel cell hybrid electric vehicle with torque vectoring. *IEEE 2023 Vehicle Power and Propulsion*, Milan, Italy; 24.10.2023 - 27.10.2023, DOI: 10.1109/VPPC60535.2023.10403338.

Patents

To protect the novel automated feedforward synthesis method, a patent has been successfully submitted:

F. Krainer, C. Hametner, and **A. Benaitier**. *Verfahren zur Identifizierung eines Gesetzes zur Vorwärtssteuerung eines Steuerungsparameters eines Antriebsstrangs aus Messdaten.* Status: patent granted (European Patent Office number
DE102023111180).

The method for ensuring cooperation between control loops and powertrain components has also been submitted for a patent:

F. Krainer, C. Hametner, and **A. Benaitier**. *Kontrollverfahren und Kontrollsystem für einen Hybridantriebsstrang.* Status: patent submitted (Austrian registration number: A50304/2022).

1.4 Methodology

This section summarizes the main ideas and outcomes of this thesis's contributions. While all the details of each proposed solution are available in the publications included in Chapter 2, this section intends to provide the main ideas and outcomes in a concise form.

A summary of the method for achieving systematic components cooperation as introduced in Publication A is first presented. Using parametric controllers in the low-level layer enables component cooperation in the high-level layer, where predictive information is used to update the EMS parameters. Encouraging simulation results are provided, emphasizing the benefit of cooperation between the torque split and the gear selection controllers. Then, a functional representation of the engine input to efficiently minimize transient emissions is summarized as proposed in Publication B. A significant reduction of the transient emissions is achieved using a detailed HEV simulation platform. Finally, the automated feedforward controller design proposed in Publication C is succinctly detailed. Applied to control the air path of a diesel engine, this method shows results close to a state-of-the-art reference tracking controller using only a fraction of its computational complexity.

For the scope of this thesis, the EMS costs to be minimized comprise the fuel consumption $\dot{m}_{\text{fuel}}$, the pollutant emissions $\dot{m}_{\text{emi}}$, and the mitigation of the number of gearshifts. The considered components' trajectories communicated from the low-level to the component-level are the engine torque T_{ice} and the gear selection $gear$. The purpose of the EMS is to control the components' actuators to follow the components' trajectories defined to minimize the cost

$$[T_{\text{ice}}, gear] = \arg\min \sum_{k\in\mathcal{C}} \left(\left(\alpha_{\text{fuel}}\dot{m}_{\text{fuel}}\left(k\right) + \alpha_{\text{emi}}\dot{m}_{\text{emi}}\left(k\right)\right) T_{\text{s}} + Q_{gear}\Delta gear\left(k\right)\right) \tag{1.1}$$

with α_{fuel} and α_{ice} the relative trade-off between fuel consumption and pollutant emissions, Q_{gear} the equivalent cost of a gearshift, and $\mathcal{C}$ an arbitrary driving mission with a constant sampling time T_{s}. Additionally, the torque request from the driving mission must always be fulfilled, and the battery SoC should stay in a feasible range.

1.4.1 Components cooperation

The torque split between the engine and the electric motor has already been extensively studied. Also, the other powertrain components are usually optimized separately and eventually share their predicted trajectory with the torque split controller. Cooperation between powertrain components is, however, necessary to answer (Q) for example, cooperation between the gearbox and the engine has already been shown to significantly reduce fuel consumption and emissions [6, 7]. This thesis proposes to use independent parametric controllers to avoid the need for controller interactions while guaranteeing cooperative updates of the controller parameters. Using this proposed method, the cooperation between the torque split and the gear selection controllers is shown to be primordial to achieve efficient fuel reduction while mitigating the number of gearshifts.

Main idea

In a multi-level EMS (F-1), cooperation is usually achieved by sharing reference trajectories between the controllers or making iterative decisions to meet a consensus. This thesis proposes to use independent parametric controllers (F-4) to avoid the need for controller interactions. Instead, the controllers are updated independently by a specific predictive (F-2) updating routine that considers the reaction of the other controllers due to their known structure. Besides its simplicity and usefulness for real-time feasibility, this method is also highly modular, as each component has its own low-level controller and high-level updating routine.

The technical aspect of this contribution resides in the use of independent parametric controllers in the low-level control layer. Each controller possesses its own updating routine in the high-level control layer as illustrated in Figure 1.2. Each updating routine updates the parameters of only a single controller yet considers the reaction of the other controllers as their structure is known and parameters communicated. As such, each updating routine only optimizes a reduced number of parameters, ensuring real-time feasibility. Also, the communication between the low-level and high-level control layers is reduced to only parameters. The proposed EMS structure has been successfully applied to emphasize the need for cooperation between the engine and the gearbox to attain further fuel reduction while mitigating the number of gearshifts.

Cooperation between gear selection and torque split

The proposed cooperative multi-level strategy is applied to a passenger HEV as described in Figure 1.1. The main focus is to guarantee cooperation between the engine and the gearbox to reduce fuel consumption further while mitigating the number of gearshifts. Two parametric controllers are used in the low-level layer, with a dedicated updating routine in the high-level layer. The first controller defines a reference for the engine torque, while the second establishes the gear selection policy. Also, for simplification, $\alpha_{\text{fuel}} = 1$, $\alpha_{\text{emi}} = 0$ and $Q_{gear} = 1.5 \times 10^{-4}$ kg are used in (1.1), hence penalizing both the fuel consumption and number of gearshifts.

The gear selection parametric controller is derived from the analysis of the optimal solution found using DP and recorded driving missions. The gear selection is made to stay close to a prescribed engine speed ω^*_{ice} observed to be proportional to the vehicle speed at each time k

$$\omega^*_{\text{ice}}(k) = \omega_0 + \theta_{1,1}(k)\, v_{\text{veh}}(k) \tag{1.2a}$$

with $\omega_0 = 90\,\mathrm{rad\,s^{-1}}$ identified form the optimal solution, and $\theta_{1,1}$ taking values in the range $[20, 27]\,\mathrm{rad\,m^{-1}}$ depending on the driving conditions. The gear selection controller triggers a gearshift whenever the current gear engaged could be modified to bring the engine speed closer to ω^*_{ice}. The required gear is therefore selected as the gear fulfilling system constraints in terms of speed and torque limits and minimizing the difference between the actual engine speed and the prescribed engine speed ω^*_{ice}

$$gear^*(k) = \arg \min_{\epsilon \in \overline{\mathbf{gear}}(k)} \mathrm{abs}\left(\omega_{\mathrm{ice}}(k, \epsilon) - \omega^*_{\mathrm{ice}}(k)\right) + \theta_{1,2}(k)\,\mathrm{abs}\left(\epsilon - gear(k)\right), \tag{1.2b}$$

with $\overline{\mathbf{gear}}(k)$ the set of feasible gears. The last term in (1.2b) penalizes a gearshift, with a relative fuel cost corresponding to the second parameter of the gear selection controller $\theta_{1,2}$. A gearshift is consequently triggered if necessary; that is

$$gear(k+1) = gear(k) + \Delta gear(k) \tag{1.2c}$$

$$\Delta gear(k) = gear^*(k) - gear(k)\,. \tag{1.2d}$$

A parametric controller for the torque split between the engine and the electric motor is directly formulated as an ECMS. Indeed, this controller has only one parameter θ_2 and is derived from optimal control, hence delivering the optimal solution to (1.1) with respect to T_{ice} and T_{em} associated with the provided gear selection policy.

The main idea of the ECMS method is to define an equivalent cost of electricity λ to penalize battery SoC deviation. Using an equivalent battery model, the SoC variations can be estimated

$$\Delta SoC = T_{\mathrm{s}} \frac{-U_{\mathrm{b}} + \sqrt{U_{\mathrm{b}}^2 - 4R_{\mathrm{b}}P_{\mathrm{b}}}}{2R_{\mathrm{b}}Q_{\mathrm{b}}} \tag{1.3a}$$

$$P_{\mathrm{b}} = \omega_{\mathrm{em}} T_{\mathrm{em}} \eta_{\mathrm{em}}\left(\omega_{\mathrm{em}} T_{\mathrm{em}}\right) \tag{1.3b}$$

with η_{em} the efficiency map of the electric motor depending on the electric motor torque and speed. The engine torque is consequently defined as the minimization of the total cost, including the equivalent cost of electricity,

$$T_{\mathrm{ice}}(k) = \arg \min_{T_{\mathrm{ice}}} \left(\dot{m}_{\mathrm{ice}}(T_{\mathrm{ice}}, k) + \lambda(k)\,\Delta SoC(T_{\mathrm{em}}, k)\right), \tag{1.4a}$$

with the electric motor torque providing the remaining demanded torque T_{gbx}

$$T_{\mathrm{em}} = T_{\mathrm{gbx}} - T_{\mathrm{ice}}. \tag{1.4b}$$

The equivalent cost of electricity λ varies with the battery SoC using a simple PI controller and the ECMS controller parameter θ_2

$$\lambda(k) = \theta_2(k) + K_{\mathrm{p}}\left(SoC(k) - SoC_{\mathrm{ref}}\right) + K_{\mathrm{i}} \sum_{k_i=1}^{k} \left(SoC(k_i) - SoC_{\mathrm{ref}}\right). \tag{1.4c}$$

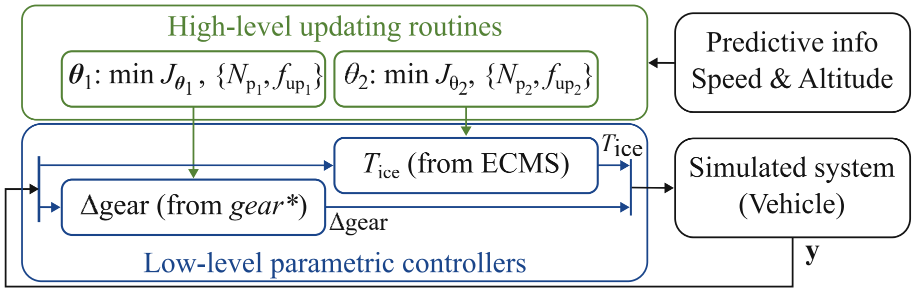

Figure 1.3: Cooperative multi-level EMS applied to the internal combustion HEV with a gearbox. (source: Publication A)

The update of the controller parameters, i.e., $\theta_{1,1}, \theta_{1,2}$, and θ_2, is realized by the updating routines in the high-level layer. Each updating routine is called independently with its own predictive horizon $N_{\mathrm{p}1}$ and $N_{\mathrm{p}2}$, and its own updating frequency rate $f_{\mathrm{up}1}$ and f_{up_2} respectively for the gear selection and torque split updating routine.

First, the gear selection updating routine updates the gear selection controller parameters by varying the value of the current parameters and estimating the following cost

$$J_{\boldsymbol{\theta}_1} = \sum_{k=k_i}^{k_i+N_{\mathrm{p}_1}} \left(\left(\dot{m}_{\mathrm{fuel}}\left(k\right)\right) T_{\mathrm{s}} + Q_{gear} \Delta gear\left(k\right)\right) + \lambda\left(k_i + N_{\mathrm{p}_1}\right)\left(SoC\left(k_{\mathrm{i}} + N_{\mathrm{p}_1}\right) - SoC_{\mathrm{current}}\right) \tag{1.5}$$

with SoC_{current} the SoC at the end of the prediction horizon if the parameters of the gear selection controller are kept unchanged. Indeed, the gear selection updating routine needs to consider the equivalent cost of modifying the SoC at the end of the prediction horizon to ensure cooperation with the torque split controller.

Second, the torque split controller parameter is updated by shooting different values of θ_1 to minimize

$$J_{\theta_2} = \sum_{k=k_i}^{k_i+N_{\mathrm{p}_2}} \left(\left(\dot{m}_{\mathrm{fuel}}\left(k\right)\right) T_{\mathrm{s}} + Q_{gear} \Delta gear\left(k\right)\right) + Q_{SoC}\left(SoC\left(k_{\mathrm{i}} + N_{\mathrm{p}_2}\right) - SoC_{\mathrm{ref}}\right)^2 \tag{1.6}$$

with $Q_{SoC} = 1 \times 10^3$ kg manually calibrated to ensure that over a driving mission, the SoC will always remain close to $SoC_{\mathrm{ref}} = 0.5$. This constant SoC reference maintains charging and discharging reserve in case of any non-predicted speed or road altitude variation. The torque split updating routine also cooperates with the gear selection controller by directly considering the equivalent cost of a gearshift thanks to the predictable behavior of the gear selection parametric controller.

The proposed multi-level cooperative EMS applied to the introduced vehicle is illustrated in Figure 1.3. The information exchanged between the high-level and the low-level layers is only the low-level controller parameters. The updating routines are executed in the background, while the low-level controllers independently control the powertrain. The component level has been ignored in this study due to the model's simplicity and to emphasize the need for cooperation between torque split and gear selection controllers. Selected simulation results are provided below, highlighting the benefits of components' cooperation and optimization using predictive information.

Selected results

The introduced multi-level EMS is applied to control a gasoline engine HEV. The passenger vehicle considered in the numerical study has a mass of 2000 kg, a six-speed gearbox, and a battery with a small capacity of 0.95 kW h. To emphasize the advantage of component cooperation, the proposed method is compared to an identical method, but where the gear selection updating routine does not cooperate with the torque split. Indeed, the non-cooperative method uses a gear selection updating routine minimizing (1.5) without the last term referring to an SoC variation at the end of the prediction horizon.

A specific section of a driving mission is illustrated in Figure 1.4 where the SoC for both EMSs is identical at the beginning and the end; therefore, the cost (1.1) can be directly compared. The non-cooperative gear selection strategy maximizes the number of gearshifts and the fuel consumption only. The gear is consequently kept constant, operating the engine in a low-efficiency region; therefore, the battery is used to reduce fuel consumption further. The issue with the lack of cooperation is that the battery is depleted, so the equivalent factor λ is decreased to force the regeneration of the battery. More significant variations of λ are associated with higher fuel consumption and lead to a relative cost increase of 3 % on this section only.

Table 1.1 presents the results of the cooperative and non-cooperative EMSs over the complete 27 h driving mission, consisting of the concatenation of various cycles. The cost is provided relative to the optimal solution found with DP. The first solution is from a standard EMS consisting of a fixed gear selection policy and the same predictive ECMS as the one proposed. When making a predictive update of the gear selection parameter selection without considering cooperation, the overall cost is higher than for a fixed gear selection policy. When the proposed cooperative EMS is proposed, the overall EMS cost is significantly reduced. This result emphasizes the need for component cooperation and the efficiency of the proposed solution.

The robustness of the proposed method concerning the prediction length, the predicted information accuracy, and the updating frequency are further provided in Publication A. Also, the proposed EMS is shown to be robust against update delays, which is necessary to execute the updating routine on the actual hardware.

Table 1.1: Cost of different control strategies over a complete driving mission.

Method	Cost relative to optimal in %
State-of-the-art ECMS	1.31
Non-cooperative	1.36
Cooperative	0.84

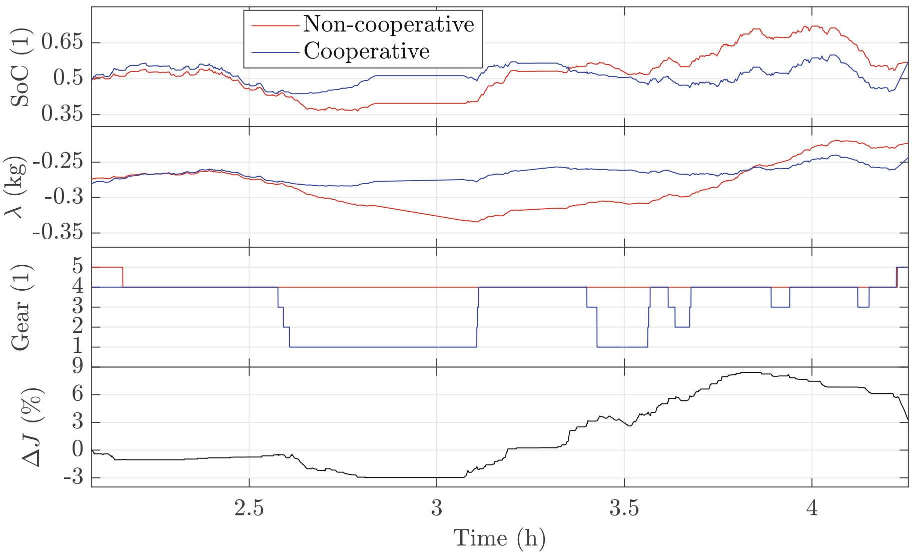

Figure 1.4: Gear selection updating routine with and without cooperation. (source: Publication A)

1.4.2 Optimization during transient operations

Whereas the fuel consumption of modern diesel engines mainly relies on torque and speed, the emissions are greatly affected by transient operations [24]. Taking advantage of hybridization, this thesis proposes to consider the engine transients when minimizing the emissions, hence using the electric motor to compensate for engine torque variations. The proposed optimization method relies on a functional representation of the input and shows large emissions reduction when applied to define the torque split of an HEV.

Main idea

The updating routines introduced in the proposed multi-level EMS, shown in Figure 1.2, need to minimize the EMS cost efficiently. The engine pollutant emissions necessitate the consideration of engine transient operations, hence explicitly considering the input variations. Standard methods exist to reduce the EMS cost over a predicted horizon (F-2). However, they usually don't consider input variations. A functional representation (F-3) of the system input is consequently proposed in this thesis so that the input variations are inherently considered when optimizing the EMS cost, leading to an efficient reduction of pollutant emissions.

The main idea proposed to consider transient operations is to explicitly account for the variations of the powertrain components input when optimizing (F-5) the parameters of the low-level controllers in the high-level updating routines. For that, the EMS cost minimized in (1.1) can be written in a general form for a single input u as

$$u = \arg\min \sum_{k \in \mathcal{C}} l \left(k, u\left(k\right), \left.\frac{\mathrm{d}u\left(t\right)}{\mathrm{d}t}\right|_{t=k} \right), \tag{1.7}$$

with $l\left(\bullet\right)$ representing the EMS instantaneous cost, for example, the fuel and pollutant emissions.

To minimize the cost (1.7) standard methods using a direct or indirect approach, or DP can be used but need a very fine temporal discretization to correctly approximate $\frac{\mathrm{d}u(t)}{\mathrm{d}t}|_{t=k}$ using a finite difference scheme. To make the updating routine applicable to the vehicle hardware, a functional approach is proposed, ensuring an accurate estimate of the input derivative for any arbitrary large time step.

Instead of directly looking for a sequence of control input $u\left(k\right)$, the input is parameterized using basis functions

$$u\left(k\right) = \boldsymbol{\varphi}\left(k\right)\boldsymbol{\gamma}_u \tag{1.8a}$$

$$\boldsymbol{\varphi}\left(k\right) = \begin{bmatrix}\varphi\left(k\right) & \cdots & \varphi_L\left(k\right)\end{bmatrix} \tag{1.8b}$$

with $\varphi_i, \forall i \in \{1, \cdots, L\}$ a set of independent basis functions. The key advantage of such a representation is the possibility to precisely evaluate the input derivative at any instant k

$$\left.\frac{\mathrm{d}u\left(t\right)}{\mathrm{d}t}\right|_{t=k} = \boldsymbol{\varphi}^{(1)}\left(k\right)\boldsymbol{\gamma}_u. \tag{1.9}$$

The minimization of the EMS cost (1.7) can be realized by varying $\boldsymbol{\gamma}_u$ to indirectly modify $\mathbf{u}$

$$\boldsymbol{\gamma}_u = \arg\min \sum_{k\in\mathcal{C}} l\left(k, \boldsymbol{\gamma}_u\right), \tag{1.10}$$

and can be solved efficiently with standard direct and indirect methods. This thesis proposes to use this functional representation of the input (1.9) to minimize the fuel and emissions of an internal combustion engine. Using a polynomial representation of the engine and battery behavior, computationally efficient direct and indirect methods are proposed and evaluated on a high-fidelity simulation platform.

Optimization of transient operations

The proposed functional representation of the input (1.9) is employed in this thesis to minimize the EMS cost (1.1), considering the *gear* as already defined. This coincides with the role of the torque split updating routine considering a fixed parameterization of the gear selection controller.

To efficiently estimate the engine torque minimizing the EMS cost, the fuel and pollutant emissions are approximated with polynomials

$$\dot{m}_{\mathrm{fuel}} = C_{\mathrm{f}}^0 + C_{\mathrm{f}}^1 u + C_{\mathrm{f}}^2 u^2 + o\left(u^3\right), \tag{1.11a}$$

$$\dot{m}_{\mathrm{emi}} = C_{\mathrm{e}}^0 + C_{\mathrm{e}}^1 u + C_{\mathrm{e}}^2 u^2 + C_{\mathrm{e}}^3 \dot{u}^2 + o\left(u^3, \dot{u}^3\right), \tag{1.11b}$$

with $u = T_{\mathrm{ice}}$ and the coefficients $C_{\{f,e\}}^{\{0,1,2,3\}}$ depending on the engine speed. The first derivative of the input is quadratically considered for modeling the emissions, as they tend to be higher during both positive and negative engine torque variations [25]. The equivalent battery model already proposed in (1.3) is also simplified using a second-order Taylor expansion. Expressing the electric motor torque from the gearbox demanded torque and the engine torque (1.4b), the battery SoC is represented by a polynomial expression of the input

$$S\dot{o}C = C_{\mathrm{s}}^0 + C_{\mathrm{s}}^1 u + C_{\mathrm{s}}^2 u^2 + o\left(u^3\right), \tag{1.11c}$$

with the coefficients $C_{\mathrm{s}}^{\{0,1,2\}}$ dependent on the engine speed and the torque demand.

The optimal control problem to be solved corresponds to finding the functional representation of the input (1.9), to minimize (1.7) using the polynomial models (1.11)

$$OCP: \begin{cases} \min\limits_{\gamma_u} \sum_{k\in\mathcal{C}} l\left(k, \boldsymbol{\gamma}_u\right) \\ l\left(k, \boldsymbol{\gamma}_u\right) = \alpha_{\text{fuel}} \dot{m}_{\text{fuel}} + \alpha_{\text{emi}} \dot{m}_{\text{emi}} \\ SoC \in \left[SoC_{\min}, SoC_{\max}\right] \\ u \in \left[u_{\min}, u_{\max}\right] \\ x\left(t_0\right) = x_0 \\ x\left(t_1\right) = x_0 \end{cases}, \tag{1.12}$$

with the conditions that the initial and final SoC are equal to x_0. This condition is employed to evaluate and compare the performance of the proposed algorithm on an entire driving mission. It can be replaced by a final cost, as proposed in the previous section, to ensure cooperation with the gear selection controller.

A direct approach can be used to solve the OCP (1.12). Indeed, using a linearization of the SoC dynamic (1.11), OCP can be efficiently solved using a standard quadratic programming (QP) algorithm. Further details are provided in Publication C.

An indirect approach can be efficiently used to solve OCP when directly considering the linear model (1.11). Using PMP, the indirect approach consists of finding λ, as introduced in the previous section, to meet the following necessary conditions for optimality

$$\dot{\lambda} = 0 \tag{1.13}$$

$$\boldsymbol{\gamma}_u = \arg\min_{\boldsymbol{\gamma}_u} H\left(\boldsymbol{\gamma}_u, \lambda\right), \tag{1.14}$$

where the so-called Hamiltonian $H = l\left(\boldsymbol{\gamma}_u\right) + \lambda \dot{SoC}\left(\boldsymbol{\gamma}_u\right)$ is minimized for the whole driving mission thanks to the functional representation of the input. The resolution of the indirect problem is achieved in two iterative steps, starting with an initial guess for λ:

1. The parameters $\boldsymbol{\gamma}_u$ are found by minimising H as in (1.14) and using the actual λ,
2. λ is updated using the secant method to meet $SoC\left(t_1\right) = x_0$,
3. Step 1 and 2 are repeated until $SoC\left(t_1\right) = x_0$ up to a provided tolerance.

The solution provided by the proposed indirect method accurately considers the variation of the input when evaluating the EMS cost. Moreover, the minimization of H is realized with a QP algorithm initialized from the solution found at the previous iteration of step 1. The algorithm's convergence is, therefore, fast even for a large driving mission, hence perfectly adapted to be employed in the updating routines presented in the previous section.

Table 1.2: Methods comparison using the high-fidelity simulation platform, all values are given relative to the PMP method. The fuel-to-emissions trade-off is as follow: $\alpha_{\text{fuel}} = 0.16$, $\alpha_{\text{emi}}\dot{m}_{\text{emi}} = 0.42\dot{m}_{\text{NO}_\text{x}} + 0.42\dot{m}_{\text{soot}}$.

Method	Δfuel %	ΔNO_x %	Δsoot %	ΔJ %	Δtime %
PMP smooth	0.58	-2.57	-4.60	-2.57	11
DP	3.40	-9.77	-6.46	-7.03	7267
Direct	3.68	-6.48	-13.44	-6.57	-60
Indirect	3.68	-7.48	-10.71	-6.56	-84

Selected results

A high-fidelity simulation platform of a heavy-duty diesel vehicle is used to demonstrate the performances of the proposed optimization method. The emissions to be minimized are the NO_x and soot. The simulation platform fully models the engine air path and uses a crank angle resolved engine model to accurately account for transient emissions.

State-of-the-art methods are employed to compare the efficiency of the proposed solution. First, the optimal solution is found using DP. Then, the PMP and a low-pass filtered version of the PMP solutions are constructed, representing the main options for reasonable calculation time. All these comparative methods directly use the nonlinear model of the engine and the equivalent battery model (1.3) instead of their polynomial approximation (1.11).

Table 1.2 summarizes the results obtained on the high-fidelity simulation platform for the proposed controller against the presented state-of-the-art controllers. The results are for an entire driving mission of around 12 minutes, corresponding to a short predictive horizon. In terms of fuel consumption, the PMP and PMP smooth achieve the best results, as they do not consider the transient emissions, focusing mainly on fuel consumption. Although, the PMP smooth reduces the NO_x and soot emissions; much more reduction is provided by the DP or the proposed direct and indirect methods. In the end, the PMP smooth achieves 2.5 % cost reduction, far from the optimality of DP achieving 7 % cost reduction. The proposed direct and indirect methods achieved almost as much cost reduction as the DP with around 6.6 % reduction. More noticeably, the DP is 72 times slower than the PMP method. In contrast, the proposed direct and indirect methods are even faster than the PMP method thanks to the polynomial model of the engine instead of a nonlinear model with lookup tables.

The proposed methods have been shown to efficiently consider the transient emissions, delivering almost the optimal solution with low computational requirements. The direct or indirect approach can consequently be employed in the high-level updating routines to consider transient operations of powertrain components. Moreover, the functional representation of the control variables can be reused for other powertrain components, in order to effectively minimize the EMS costs during transient operations.

1.4.3 Automated 2DoF controller design

The component references defined in the low-level control layer do not always coincide with the actuators. For example, for internal combustion engines, several controllers must be controlled to track an expected torque demand accurately. Furthermore, the realization of a specific torque is not necessarily unique, with different possibilities exhibiting different fuel consumption and pollutant emissions. This thesis proposes an automated feedforward controller design, and successfully applies it to control a diesel engine air path. Using a novel model structure, the method is shown to be robust to model order selection and provides accurate reference tracking with very low computational requirements.

Main idea

The component-level control layer is proposed to define actuators' trajectories to follow a desired reference. Rather than relying on feedback information, the actuators can more accurately track the desired reference, especially during transient operations. The fuel consumption, pollutant emissions, and all other EMS costs depending on transient behaviors can be efficiently minimized. The third contribution of this thesis is an automated feedforward controller design capable of defining the trajectory $\mathbf{u}$ of m actuators to follow the desired reference $\mathbf{y}$ of the m outputs of an arbitrary powertrain component (F-2).

The solution elaborated in this thesis aims to identify a feedforward controller directly from measurement data. Indeed, feedforward control is very advantageous as it provides an actuator trajectory to follow a component reference, guaranteeing accurate tracking during transient operations. The motivation for directly identifying a feedforward controller results from the need to invert a model $\Sigma(\boldsymbol{\theta})$ to realize feedforward control design using traditional methods. As such, problems such as lack of observability or unstable internal dynamics can be circumvented as no model is being identified, only the controller. Figure 1.5 schematically represents the traditional *indirect* method, where $\Sigma(\boldsymbol{\theta})$ is estimated by fitting the model output $\hat{\mathbf{y}}$, and then $\Sigma^{-1}(\boldsymbol{\theta})$ is found using model inversion. The proposed *direct* method, where $\Sigma^{-1}(\boldsymbol{\theta})$ is directly estimated by fitting the inverse model input $\hat{\mathbf{u}}$ is also depicted in Figure 1.5.

To realize successively the identification of the inverse model from measurement data and the design of a feedforward controller, a model structure is proposed

$$\left[\mathbf{dy}_1^{(r_1)}, \cdots, \mathbf{dy}_m^{(r_m)}\right] \boldsymbol{\theta}_y = \left[\mathbf{du}_1^{(r^*)}, \cdots, \mathbf{du}_m^{(r^*)}\right] \boldsymbol{\theta}_u \tag{1.15}$$

with the notation $\mathbf{dx}^{(k)} := \begin{bmatrix} x & x^{(1)} & \cdots & x^{(k)} \end{bmatrix}^{\mathrm{T}}$ and the model parameters $\boldsymbol{\theta}_y$ and $\boldsymbol{\theta}_u$ (F-4). The r_i first derivatives of each output signal i are weighted and equal to a weighted sum of the first r^* derivatives of each input. The second key idea developed in this thesis is to consider a functional approach (F-3) to model each input, output, and

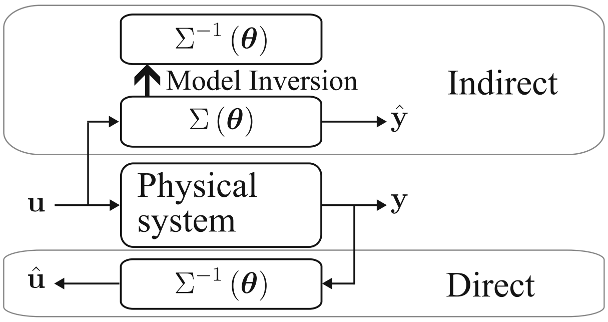

Figure 1.5: Indirect and direct approach for inverse model parameters identification. (source: Publication C)

their derivatives using basis functions. Each input and output signal is modeled using the same functional approach presented in (1.8) and their derivatives with (1.9). Each input u_i or output y_j and their derivatives are consequently described by the parameters $\boldsymbol{\gamma}_{u_i}$ and $\boldsymbol{\gamma}_{y_j}$ respectively.

The following of this section introduces succinctly the proposed identification method and how to use the proposed model structure (1.15) for feedforward control. Finally, numerical results are shown to control the engine air path of a diesel engine using a detailed and experimentally validated simulation platform.

Automated feedforward controller design

One of the advantages of the proposed model structure (1.15) is the linearity regarding the parameters $\boldsymbol{\theta}_y$ and $\boldsymbol{\theta}_u$. Using this linearity property, a total least squares is proposed in this thesis to identify the parameters, considering noise and inaccuracy in both the input and output signals and their derivatives.

After collecting measured input $\mathbf{u}$ and output $\mathbf{y}$ signals, their derivatives need to be found to identify the proposed model structure. To determine the time derivatives precisely, the input and output signals are first modeled with basis functions as in (1.8) using standard least squares regression. Knowing the modeled input and output signals as well as their derivatives the proposed model structure can be written as

$$\left[\mathbf{du}_1^{(r^*)}, \cdots, \mathbf{du}_m^{(r^*)}, \mathbf{dy}_1^{(r_1)}, \cdots, \mathbf{dy}_m^{(r_m)}\right] \begin{bmatrix} \boldsymbol{\theta}_u \\ -\boldsymbol{\theta}_y \end{bmatrix} = \mathbf{0}. \tag{1.16}$$

Applying the total least squares approach, the singular value decomposition (SVD) of the matrix containing the input and output signals and their derivative in (1.16) is numerically computed. From this SVD, the user can freely define a threshold that separates large from small singular values. The smallest singular values span the nullspace of the matrix built with the input and output signals and their derivatives. This nullspace is directly reused to define the model's parameters in (1.16). All the details and numerical results emphasizing the advantages of TLS for defining the number of derivatives needed for each input and output are exhaustively discussed in Publication C.

Once the proposed model structure (1.15) has been identified, a feedforward controller can be easily defined. Indeed, given the expected reference output $\mathbf{y}^*$ and their k-th derivatives $\mathbf{y}^{(k)}$ the inputs $\mathbf{u}$ realizing this reference trajectory can be efficiently estimated.

First, the inputs are once again parameterized with basis function as in (1.8), where $\gamma_\mathbf{u}$ are unknown parameters defining the input trajectories and consequently their derivatives. The proposed model structure (1.15) can be directly re-employed, and the unknown parameters $\gamma_\mathbf{u}$ can be directly identified using least squares. Also, to guarantee a realizable input trajectory in the case the system exhibits non-minimum phase behavior, regularization terms are employed

$$\gamma_\mathbf{u} = \left(\boldsymbol{\phi}_\mathbf{u}^\mathrm{T}\boldsymbol{\phi}_\mathbf{u} + \mathbf{C}_\mathrm{reg}^\mathrm{T}\mathbf{C}_\mathrm{reg}\right)^{-1}\boldsymbol{\phi}_\mathbf{u}^\mathrm{T}\boldsymbol{\phi}_\mathbf{y}, \tag{1.17}$$

with $\boldsymbol{\phi}_\mathbf{u}$ and $\boldsymbol{\phi}_\mathbf{y}$ matrices arranging the input, output, and their derivatives, using the identified model structure (1.15), all details being provided in Publication C. The matrix $\mathbf{C}_\mathrm{reg}$ is a block diagonal matrix, weighting each input and its derivatives independently

$$\mathbf{C}_\mathrm{reg} = \mathrm{diag}\left(\mathbf{C}_{\mathrm{reg},i}\right), \tag{1.18a}$$

$$\mathbf{C}_{\mathrm{reg},i} = c_\mathrm{i,k}\boldsymbol{\varphi}^{(k)^\mathrm{T}}, \tag{1.18b}$$

with the positive scalar $c_\mathrm{i,k}$ weighting the k-th derivative of the i-th input.

The last main advantage of the proposed model structure (1.15) is the possibility to merge different models to create a local model network. Indeed, different models can be identified at different operating points, defined by a so-called scheduling vector. Then, all these models can be combined into a single parameter-varying model using nonlinear activation functions defining the weighting interpolation of each model at a given operating point. The parameters $\boldsymbol{\theta}_\mathbf{u}$ and $\boldsymbol{\theta}_\mathbf{y}$ become functions of the scheduling vector. Thanks to this possibility, the proposed feedforward method can be employed for nonlinear models such as a diesel engine air path, described in the following selected results.

Selected results

The proposed feedforward controller has been applied to control the air path of a diesel engine. The goal is to find the trajectory of the variable geometry turbocharger (VGT) and the engine gas recirculation (EGR) valve to follow a reference exhaust manifold pressure P_exh and exhaust nitrogen oxides mass flow $\mathrm{NO_x}$.

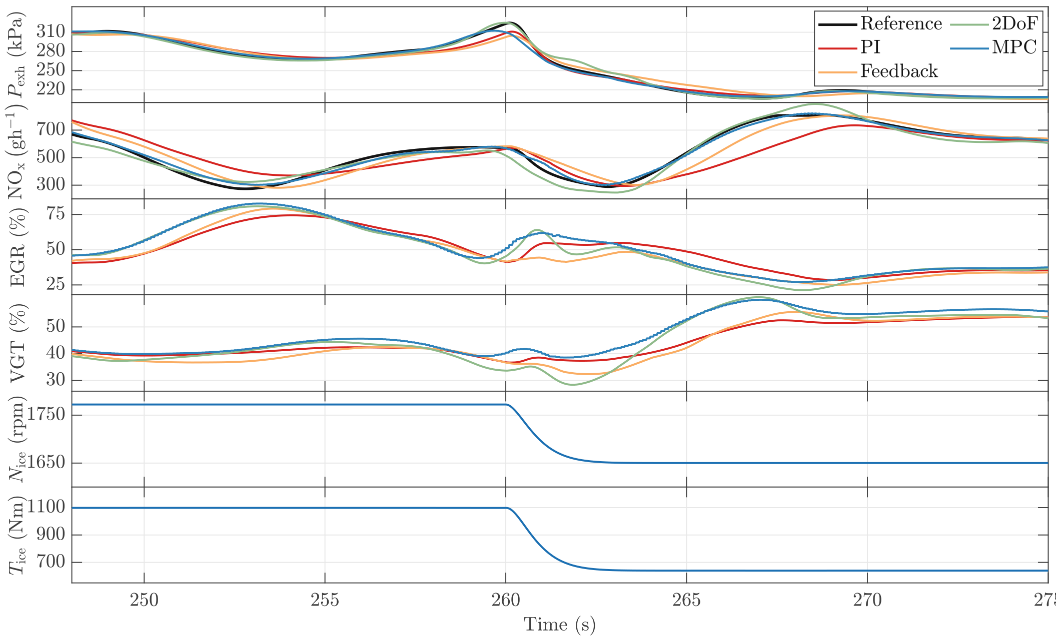

Figure 1.6: Reference following during transient engine operations using different control methods. (source: Publication C)

First, a collection of local models (1.15) are identified for various fixed values of the scheduling vector being composed of the engine speed N_{ice} and torque T_{ice}. Then, radial basis functions centered around each local model are identified to create an LMN, i.e., a model whose parameters are a function of the scheduling vector. Finally, the proposed feedforward controller synthesis is applied and demonstrated on a detailed and experimentally validated simulation platform.

A slow PI controller is added to remove any potential steady-state error due to model mismatch and disturbances. By adding a feedback loop, i.e., a PI controller, the proposed method results in a simple yet accurate 2-degrees-of-freedom (2DoF) controller. The proposed controller is compared to the PI controller only, a network of full-state feedback controllers with integration of the control error [26], and a flatness-based MPC as proposed in [27].

Figure 1.6 illustrate the reference following accuracy of the proposed method compared to the introduced state-of-the-art methods. The PI and feedback controller are by nature slow to react during transient reference following. The proposed 2DoF method tracks the output almost as accurately as the MPC. The main advantage of the 2DoF is its simplicity compared to an MPC. The proposed feedforward calibration and feedforward controller synthesis show encouraging tracking performances with low computational requirements, hence making it capable of performing in real-time on the vehicle hardware.

The proposed automated feedforward controller design method is of high value for designing a reference tracking controller in the component layer of the proposed multi-layer EMS.

1.5 Scientific contribution

This thesis provides several contributions regarding the EMS of HEVs to further reduce fuel consumption and pollutant emissions. Starting from a standard multi-level EMS, this thesis proposes solutions to systematically consider components' cooperation, minimize transient pollutant emissions, and control complex systems actuators to accurately follow a reference trajectory. Therefore, the several subordinate research questions proposed in Section 1.3.2 have been thoroughly answered, providing tangible solutions to (Q).

Contributions to "Components cooperation" (Q-1)→ Publication A

- Through the exchange of parameters between controllers, the proposed EMS ensures cooperation between all the powertrain components. Applied specifically to guarantee cooperation between the torque split and the gear selection controllers, further fuel reduction while mitigating the number of gearshifts has shown to be achievable.
- Thanks to the low-level control layer of independent controllers, the proposed EMS is real-time feasible. The parameters' updates are computed during uninterrupted operations of the low-level controllers, and the proposed method is robust to update time delays.
- The proposed cooperative EMS structure has been shown to be robust to inaccurate predictive information and varying predictive horizons.
- The proposed solution is highly modular. Additional powertrain components can be easily added thanks to the low-level layer consisting of independent controllers.

Contributions to "Transient pollutant emissions" (Q-2)→ Publication B

- A functional representation of the control variables with smooth basis functions is proposed and applied to the engine torque to directly consider transient pollution emissions.
- Both a direct and indirect method have been proposed with the introduced functional representation of the control variable and polynomial powertrain components model. In both cases, the fuel consumption and emissions reduction achieved are close to the optimal solution computed from DP, yet using only a fraction of its computational complexity.
- The proposed method can be directly re-used for a different system where transient behaviors must be considered. For example, battery degradation could be

reduced thanks to smoother battery transient operations.

Contributions to "Transient trajectory tracking" (Q-3)→ Publication C

- An automated feedforward controller design has been proposed for nonlinear multivariate systems. Thanks to its generic structure and the employed regularization, the proposed method can be applied to any system modeled by an LPV, even with unstable internal dynamics.
- A strength of the method is the possibility to identify a feedforward controller from measurement data directly. Also, the method has been shown to be robust to model order selection thanks to a total least squares identification algorithm.
- Using a model structure employing directly the input, output, and their derivatives, multiple controllers identified at various operating points can be easily merged to form a local model network.
- Implemented with a simple PI controller to remove steady-state tracking inaccuracy, the proposed method showed encouraging tracking performances for a diesel engine air path.
- With a simple least squares, the feedforward controller can be identified, consequently simplifying the calibration. The generation of the actuator trajectory to follow a desired output trajectory is directly obtained with a least squares algorithm, making the solution feasible in real-time.

1.6 Conclusion

This cumulative thesis provides three main contributions toward a further reduction of fuel consumption and pollutant emissions of HEVs with an internal combustion engine. Each contribution brings a solution to a specific challenge faced by state-of-the-art EMSs. The proposed contributions of this thesis are all formulated in a generic framework and are consequently applicable to different HEV configurations and component variants. The outcomes of each contribution of this thesis are investigated using specific examples, providing a detailed solution for dedicated EMS challenges.

First, a parametrization of the EMS controller is proposed to allow systematic components' cooperation. This solution has been employed to emphasize the need for cooperation between the torque split and the gear selection controller of an HEV, bringing substantial fuel reduction while mitigating the number of gearshifts. Second, a parameterization of the engine input with smooth basis functions is proposed to directly consider engine transient operations when minimizing pollutant emissions. A significant reduction of pollutant emissions has been achieved, and the solution could be re-employed to minimize powertrain component degradation during transient operations. Finally, a feedforward control structure has been identified to automatically design a feedforward controller from measurement data. Applied to control the air path of a diesel engine, the proposed method showed excellent robustness to model order selection and low computational requirements while guaranteeing accurate transient trajectory tracking.

The contributions of this thesis are control methods aimed at further reducing fuel consumption and pollutant emissions of HEVs. Indeed, using detailed simulation platforms, components cooperation, reduced transient emissions, and accurate trajectory following have been demonstrated. Using several technical properties, the outcomes of this thesis are generic methods employable for various HEV configurations and component variants. The main outlook of this PhD thesis resides in the adaptation and implementation of the proposed methods to actual vehicles.

Bibliography

[1] Euro 7: Council adopts new rules on emission limits for cars, vans and trucks. available online: https://www.consilium.europa.eu/en/press/press-releases/2024/04/12/euro-7-council-adopts-new-rules-on-emission-limits-for-cars-vans-and-trucks/ (accessed on 7 june 2024).

[2] Clara Marina Martinez and Dongpu Cao. 2 - integrated energy management for electrified vehicles. In Clara Marina Martinez and Dongpu Cao, editors, *Ihorizon-Enabled Energy Management for Electrified Vehicles*, pages 15–75. Butterworth-Heinemann, 2019.

[3] Lino Guzzella and Antonio Sciarretta. *Vehicle Propulsion Systems: Introduction to Modeling and Optimization*. Springer, Berlin, Heidelberg, 01 2007.

[4] Antonio Sciarretta and Lino Guzzella. Control of hybrid electric vehicles. *IEEE Control Systems Magazine*, 27(2):60–70, 2007.

[5] Pemmareddy Saiteja and B. Ashok. Critical review on structural architecture, energy control strategies and development process towards optimal energy management in hybrid vehicles. *Renewable and Sustainable Energy Reviews*, 157:112038, 2022.

[6] Guido Ricardo Guercioni, Enrico Galvagno, Antonio Tota, and Alessandro Vigliani. Adaptive equivalent consumption minimization strategy with rule-based gear selection for the energy management of hybrid electric vehicles equipped with dual clutch transmissions. *IEEE Access*, 8:190017–190038, 2020.

[7] Viet Ngo, Theo Hofman, Maarten Steinbuch, and Alex Serrarens. Optimal control of the gearshift command for hybrid electric vehicles. *IEEE Transactions on Vehicular Technology*, 61(8):3531–3543, 2012.

[8] E. G. Giakoumis and A. I. Alafouzos. Study of diesel engine performance and emissions during a Transient Cycle applying an engine mapping-based methodology. *Applied Energy*, 87(4):1358–1365, 2010.

[9] Yu Wang, Hu Zhang, and Zongxuan Sun. Optimal control of the transient emissions and the fuel efficiency of a diesel hybrid electric vehicle. *Proceedings of the Institution of Mechanical Engineers, Part D: Journal of Automobile Engineering*, 227(11):1546–1561, 2013.

[10] E. G. Giakoumis and S. C. Lioutas. Diesel-engined vehicle nitric oxide and soot emissions during the European light-duty driving cycle using a transient map-

ping approach. *Transportation Research Part D: Transport and Environment*, 15(3):134–143, 2010.

[11] Tobias Nüesch, Mu Wang, Pascal Isenegger, Christopher H. Onder, Rüdiger Steiner, Pedro Macri-Lassus, and Lino Guzzella. Optimal energy management for a diesel hybrid electric vehicle considering transient PM and quasi-static NOx emissions. *Control Engineering Practice*, 29:266–276, 2014.

[12] Tobias Nüesch, Mu Wang, Pascal Isenegger, Christopher H. Onder, Rüdiger Steiner, Pedro Macri-Lassus, and Lino Guzzella. Optimal energy management for a diesel hybrid electric vehicle considering transient pm and quasi-static nox emissions. *Control Engineering Practice*, 29:266–276, 2014.

[13] Roman Schmied, Stephan Stadlbauer, Harald Waschl, and Luigi del Re. Improving the transient emission performance of a diesel engine by input shaping techniques. In *2015 54th Annual Conference of the Society of Instrument and Control Engineers of Japan (SICE)*, pages 1287–1292, 2015.

[14] Fengqi Zhang, Xiaosong Hu, Reza Langari, and Dongpu Cao. Energy management strategies of connected hevs and phevs: Recent progress and outlook. *Progress in Energy and Combustion Science*, 73:235–256, 2019.

[15] Xueqin Lü, Siwei Li, XiangHuan He, Chengzhi Xie, Songjie He, Yuzhe Xu, Jian Fang, Min Zhang, and Xingwu Yang. Hybrid electric vehicles: A review of energy management strategies based on model predictive control. *Journal of Energy Storage*, 56:106112, 2022.

[16] Maryam Razi, Nikolce Murgovski, Tomas McKelvey, and Torsten Wik. Predictive energy management of hybrid electric vehicles via multi-layer control. *IEEE Transactions on Vehicular Technology*, 70(7):6485–6499, 2021.

[17] Florian Meier and Frank Willems. Multi-level integrated energy and emission management for hevs cold start operation. In *2022 European Control Conference (ECC)*, pages 1198–1203, 2022.

[18] André Murilo, Mazen Alamir, and Daniel Alberer. A general NMPC framework for a diesel engine air path. *International Journal of Control*, 87(10):2194–2207, 2014.

[19] Mingxin Kang and Tielong Shen. Experimental comparisons between LQR and MPC for spark-ignition engine control problem. *Chinese Control Conference, CCC*, pages 2651–2656, 2017.

[20] Jiadi Zhang, Mohammad Reza Amini, Ilya Kolmanovsky, Munechika Tsutsumi, and Hayato Nakada. Benefits of feedforward for model predictive airpath control of diesel engines. *IFAC-PapersOnLine*, 55(25):181–186, 2022. 10th IFAC Symposium on Robust Control Design ROCOND 2022.

[21] Alexis Benaitier Ferdinand Krainer, Christoph Hametner. Verfahren zur identifizierung eines gesetzes zur vorwärtssteuerung eines steuerungsparameters eines antriebsstrangs aus messdaten. Patent number: DE102023111180.

[22] Alexis Benaitier Ferdinand Krainer, Christoph Hametner. Kontrollverfahren und kontrollsystem für einen hybridantriebsstrang. Austrian registration number: A50304/2022.

[23] Alexis Benaitier, Ferdinand Krainer, Stefan Jakubek, and Christoph Hametner. Robust physical quantities estimation for diesel engine emission reduction using sensor fusion. In *2022 IEEE Conference on Control Technology and Applications (CCTA)*, pages 1080–1086, 2022.

[24] C. D. Rakopoulos, A. M. Dimaratos, E. G. Giakoumis, and D. C. Rakopoulos. Study of turbocharged diesel engine operation, pollutant emissions and combustion noise radiation during starting with bio-diesel or n-butanol diesel fuel blends. *Applied Energy*, 88(11):3905–3916, 2011.

[25] M Lindgren and P Hansson. Effects of Transient Conditions on Exhaust Emissions from two Non-road Diesel Engines. *Biosystems Engineering*, 87:57–66, 2004.

[26] Gregor Gregorcic and Gordon Lightbody. Nonlinear model-based control of highly nonlinear processes. *Comput. Chem. Eng.*, 34:1268–1281, 2010.

[27] Nikolaus Euler-Rolle, Ferdinand Krainer, Stefan Jakubek, and Christoph Hametner. Automated synthesis of a local model network based nonlinear model predictive controller applied to the engine air path. *Control Engineering Practice*, 110(October 2019):104768, 2021.

Chapter 2

Publications

This chapter comprises the full-length journal papers constituting the main contributions of this cumulative thesis. The three journal papers corresponding to the three main contributions of this thesis are first listed and then given in full length. The author's contributions to each journal paper are also provided.

Publication A

Alexis Benaitier, Ferdinand Krainer, Stefan Jakubek and Christoph Hametner
A Modular Approach for Cooperative Energy Management of Hybrid Electric Vehicles Considering Predictive Information
IEEE Access, Vol. 12 (2024), page 60588 - 60600
DOI: 10.1109/ACCESS.2024.3395019

Publication B

Alexis Benaitier, Ferdinand Krainer, Stefan Jakubek and Christoph Hametner
Optimal energy management of hybrid electric vehicles considering pollutant emissions during transient operations
Applied Energy, Vol. 344 (2023), page 121267
DOI: 10.1016/j.apenergy.2023.121267

Publication C

Alexis Benaitier, Stefan Jakubek, Ferdinand Krainer and Christoph Hametner
Automated nonlinear feedforward controller identification applied to engine air path output tracking
International Journal of Control, Vol. 1 (2023), pages 1-12
DOI: 10.1080/00207179.2023.2227740

2.1 Publication A

Alexis Benaitier, Ferdinand Krainer, Stefan Jakubek and Christoph Hametner

A Modular Approach for Cooperative Energy Management of Hybrid Electric Vehicles Considering Predictive Information

IEEE Access, Vol. 12 (2024), page 60588 - 60600
DOI: 10.1109/ACCESS.2024.3395019

Authors' contribution †

- A. Benaitier: Conceptualization, Methodology, Software, Validation, Formal analysis, Investigation, Resources, Data Curation, Writing - Original Draft, Writing - Review & Editing, Visualization
- S. Jakubek: Supervision, Project administration, Funding acquisition
- F. Krainer: Validation, Investigation, Resources, Data Curation, Writing - Review & Editing
- C. Hametner: Investigation, Writing - Review & Editing, Supervision, Project administration, Funding acquisition

† According to Contributor Roles Taxonomy (CRediT)

IEEE Access
Multidisciplinary | Rapid Review | Open Access Journal

Received 19 March 2024, accepted 16 April 2024, date of publication 29 April 2024, date of current version 6 May 2024.
Digital Object Identifier 10.1109/ACCESS.2024.3395019

RESEARCH ARTICLE

A Modular Approach for Cooperative Energy Management of Hybrid Electric Vehicles Considering Predictive Information

ALEXIS BENAITIER[1], FERDINAND KRAINER[2], STEFAN JAKUBEK[3], AND CHRISTOPH HAMETNER[1]
[1]Christian Doppler Laboratory for Innovative Control and Monitoring of Automotive Powertrain Systems, TU Wien, 1040 Vienna, Austria
[2]AVL list GmbH, 8020 Graz, Austria
[3]Institute of Mechanics and Mechatronics, TU Wien, 1040 Vienna, Austria
Corresponding author: Alexis Benaitier (alexis.benaitier@tuwien.ac.at)

This work was supported by Austrian Federal Ministry for Digital and Economic Affairs, the National Foundation for Research, Technology and Development, the Christian Doppler Research Association, and AVL List GmbH, Austria.

ABSTRACT Energy management strategies (EMSs) for hybrid vehicles have been extensively studied to achieve high system efficiency. EMSs usually focus on the torque split between the electric motor and the main power source. Other powertrain components, such as the gearbox or battery management system, are optimized individually. However, the cooperation between different powertrain components has been studied for specific hybrid architectures and demonstrated to be highly beneficial. A modular EMS that ensures the cooperation of multiple components with different characteristics, shared constraints and objectives, while taking advantage of predictive information will be highly beneficial. To address this research gap, a modular cooperative EMS is proposed using parametric controllers with parameter updates realized in the background using available predictive information. The strategy emphasizes modularity, feasibility, and systematically takes advantage of any available predictive information to improve the overall vehicle objectives, hence considering all the components playing a role in the EMS. The proposed cooperative strategy is first detailed for a generic EMS and then demonstrated for the control of the torque split and gear selection of a hybrid electric vehicle. A numerical study is presented to compare the proposed method with the optimal strategy derived from dynamic programming. The results are detailed for different available predictive information, both in terms of quantity and quality. The proposed method is revealed to be robust against incomplete predictive information and guarantees feasibility with low computational effort, making it real-time capable.

INDEX TERMS Cooperative control, energy management strategy, gear selection, hybrid electric vehicle, multi-level control strategy, torque split.

I. INTRODUCTION

Hybrid Electric Vehicles (HEVs) are nowadays seen as an effective intermediate step toward emission-free transportation systems. Hybrid architectures indeed benefit from lower emissions and better efficiency thanks to an additional degree of freedom, splitting the energy demand between the fuel and the battery. The Energy Management Strategy (EMS) is specifically designed to take full advantage of the torque split capabilities toward reduction of the vehicle operating cost, i.e., fuel consumption, component degradation, comfort, performance, etc. Also, the EMS can take advantage of past and predictive information whenever available while remaining relatively simple to allow its implementation on vehicle hardware. This paper proposes a modular and real-time capable EMS that emphasizes the cooperation of powertrain components while taking advantage of available predictive information.

The associate editor coordinating the review of this manuscript and approving it for publication was Ricardo de Castro.

EMSs for hybrid electric vehicles have been continuously developed for the past 30 years. However, nowadays, powertrains consist of a growing number of components and associated controllers, e.g., battery management system [1], [2], after-treatment systems [3], ultra-capacitor [4], electronic stability program [5], etc. The growing number and interdependence of the powertrain components impose multiple constraints, and the resulting operational cost to minimize includes several costs related to fuel consumption, emissions, degradation, comfort, performance, etc. Ideally, the EMS coordinates and controls all the components contributing to these common objectives while ensuring feasibility and real-time capability [6], [7]. Controlling a powertrain's components, considering the interdependent constraints and objectives, renders a generic and centralized EMS challenging to design.

With the recent advancements in technology, predictive information such as the future speed of a vehicle or the altitude of the road ahead is now available [8]. This information can significantly benefit EMSs and has already shown positive results in specific examples such as torque split, battery recharging, and component degradation. Huang et al. demonstrated the potential of predictive information in torque split in [9], while Al-Ogaili et al. highlighted its importance in battery recharging in [10] and Swief et al. dealt with the uncertainties in the network during battery recharging in [11]. Alyakhni et al. discussed its significance in component degradation in [12]. However, the accuracy and quantity of information ahead can significantly vary from time to time. Robustness toward inaccurate or missing information, together with a cooperative real-time controller considering predictive information, is one of the main challenges of current EMSs [6].

Several methods have been used to control the torque split and reduce the operational cost of HEVs. Dynamic Programming (DP) or Pontryagin's Maximum Principle (PMP) have been widely employed as offline methods to deliver the optimal solution [13], which is practical as a benchmark for determining the optimal control strategy. However, these methods require precise knowledge of the entire drive cycle, making them impractical for real-time control. To overcome this limitation, numerous studies have successfully derived efficient rule-based controllers from the optimal policy, particularly for combinatorial problems such as gear selection [14], [15], [16]. These rule-based controllers have been successfully extracted from DP solutions and are practical for real-time control. Nevertheless, when additional components need to be considered in the powertrain, optimal methods are no longer available due to their high computational cost [17].

Extensive research has been done on controlling the torque split of hybrid vehicles without the full knowledge of the drive cycle. Derived from PMP, the Equivalent Consumption Minimization Strategy (ECMS) with an adaptation of the equivalent electricity cost is the most employed method [18]. Numerous variants exist to consider predictive information, such as in [19] using a rule-based approach or employing fuzzy logic as in [4] and [20]. Also, model predictive control is another common option [21], followed by multiple other techniques such as backstepping [22], sliding-mode [7], conic formulation [23], or Bounded Load Following Strategy [24]. More recently, artificial intelligence and self-learning algorithms have been employed to strengthen the modularity of the EMS, i.e., simplifying the calibration for different vehicles. A fuzzy logic controller identified from a neural network is, for example, presented in [25], and reinforcement learning based on Q-learning techniques has been employed in [26] and [27].

In parallel to the torque split controller, the control of other powertrain components, such as the gearbox, has also been investigated but is generally optimized separately. For example, the gear selection controller usually does not communicate with the torque split controller, resulting in a fixed gear selection policy, i.e., independent of the torque split strategy. Such decentralized strategies, where the gear selection is controlled independently, have been regularly designed with a torque split controller relying on a model predictive controller such as in [21] or a fuzzy-adaptive ECMS in [20]. However, [28] shows that optimizing the gear selection policy from DP along with an adaptive ECMS, is beneficial. Moreover, optimizing the torque split and the gear selection cooperatively is even more beneficial, as shown in [29], where an agreement is found between a DP solver used for the gear selection and a PMP routine for the torque split. This latest example emphasizes the need for cooperation between the different powertrain components but also the difficulty in using a common solver between components of various natures, e.g., actuators with continuous or discrete input.

Modern powertrains are complex due to several interconnected components, with different input types and optimization horizons. A real-time capable EMS, modular for various types of vehicles, and taking advantage of components cooperation as well as the available predicted information will be highly beneficial. As a result, a multi-level EMS, i.e., with a high-level and a low-level control, is commonly employed [30], [31], [32]. The high-level layer defines references for the low-level layer by minimizing the overall vehicle cost, hence ensuring cooperation between the powertrain components. On the other hand, the low-level layer comprises several controllers, one for each powertrain component. Each low-level controller tries to follow the high-level references while further minimizing individual components' costs [30], [31]. Such a multi-level strategy is more practical for implementation than a unique centralized controller. However, the structure of such a multi-level predictive controller, to ensure feasibility, real-time capability, and considering all the components' costs, has not yet been proposed for a generic HEV, i.e., modular and scalable to various hybrid architectures.

This paper introduces a modular EMS relying on a multi-level strategy and emphasizing powertrain components cooperation. First, a low-level parametric controller layer ensures feasibility and real-time capability. Second, a high-level updating routine layer takes advantage of past and predictive speed and altitude information to update each controller parameter to further approach the optimal behavior. The resulting strategy is modular and can be applied to different interacting powertrain components, with continuous and discontinuous control variables and different optimization horizons. The novelty of the modular EMS proposed in this paper is to employ parametric controllers in the low-level control layer to enable

- real-time control thanks to the low-level control layer,
- the optimization of the controllers' parameters in the background, i.e., high-level in parallel to low-level, and considering predictive information,
- cooperation between powertrain components during the parameters update thanks to the known structure of each parametric controller and
- reduced communication between the powertrain components controllers, exchanging only their control parameters.

The proposed cooperative EMS is first detailed in Section II. Then, Section III illustrates the proposed strategy through a practical application detailed for an HEV with a torque split and a gear selection controller. Section IV presents comprehensive numerical results, first emphasizing the benefits of cooperation between powertrain's components as well as considering predictive information, comparing the proposed cooperative strategy to the global optimum and studying the robustness to varying accuracy and availability of predictive information. Also, cooperation is confirmed to be a necessary concept for an efficient minimization of the vehicle's operational cost. Finally, Section V summarizes the proposed concept, the main results and observations, and provides an outlook regarding further usage of the proposed cooperative strategy.

II. PROPOSED COOPERATIVE EMS CONCEPT

This section proposes a modular EMS for hybrid electric vehicles, emphasizing the cooperation of powertrain components. The proposed strategy focuses on modularity, feasibility, and taking advantage of available predictive information. This section introduces the proposed cooperative EMS, which is applied to control the gearbox and torque split of an HEV in Section III as an example.

The proposed strategy relies on having a model of the powertrain and vehicle to predict the vehicle's behavior. The model has no specific requirements apart from being deterministic and consisting of inputs $\mathbf{u}$, corresponding to actuators such as battery power or gear engaged, and measurement $\mathbf{y}$ such as the current vehicle speed. Generally, the EMS's goal is to reduce energy losses while ensuring some level of performance, reducing component degradation, and fulfilling technical constraints. A metric depending on the control inputs $\mathbf{u}$ and called *cost* is defined and noted J.

An ideal EMS will find the optimal control inputs $\mathbf{u}^*$ that minimizes the cost J

$$\mathbf{u}^* = \arg\min_{\mathbf{u}} J\left(\mathbf{u}\right), \tag{1}$$

and guaranteeing a feasible input $\mathbf{u}$, i.e., fulfilling the actuators and system technical requirements. The cost J typically comprises fuel consumption, component degradation, or driver comfort. Such a centralized problem, i.e., defining all the inputs at once, is generally hard to solve and requires the knowledge of the entire cycle. Considering the centralized problem directly for an online implementation is impractical.

In this paper, the proposed strategy first defines n agents, each agent being a specific control strategy controlling one or several powertrain components. Each agent j is responsible for controlling inputs $\mathbf{u}_j \subset \mathbf{u}$. To avoid the need for consensus between agents [33], each input is controlled by only one agent, i.e., $\mathbf{u}_i \cap \mathbf{u}_j = \emptyset, \forall i \neq j$. For example, one agent can control the torque split between the engine and the battery while a second controls the gear selection, as demonstrated in Section III.

To be able to simplify the complexity of cooperation between agents, this paper proposes that each agent uses a parametric controller

$$\mathbf{u}_j = \mathbf{u}_j\left(\mathbf{y}, \boldsymbol{\theta}_j\right) \tag{2}$$

with $\boldsymbol{\theta}_j$ the parameters for the controller of agent j. With such a controller, each agent makes a decision independently of the other agents. Hence no real-time communication is needed, and conflicts between agents are inherently avoided. This first control layer, gathering independent agents with their parametric controller, corresponds to the low-level layer of the proposed strategy as depicted in Fig. 1.

A high-level layer is added in parallel to the low-level layer to render the proposed EMS adaptive and predictive. The high-level layer is composed of updating routines, with the role of updating the parameters of the agents of the low-level layer. Each updating routine updates only the parameters of a single agent; hence the design of the updating routine is simple and adapted to the dynamics and specificity of the powertrain components controlled by each agent. Additionally, the updating routines can consider past and any available predictive information to update the parameters of each agent's controller efficiently.

The key point of the proposed strategy is the ability of the updating routine of agent j to update the parameters $\boldsymbol{\theta}_j$ while considering the reaction of all the other agents. Indeed, the parametric controller of each agent i can be known from the updating routine of agent j. Therefore the reaction of the parametric controller of agent i can be estimated for any modification of $\boldsymbol{\theta}_j$. Considering the overall agents' behavior to a change of the parameters of a single agent inherently makes the proposed control strategy cooperative. Indeed, when updating the parameters of an agent j, the overall cost

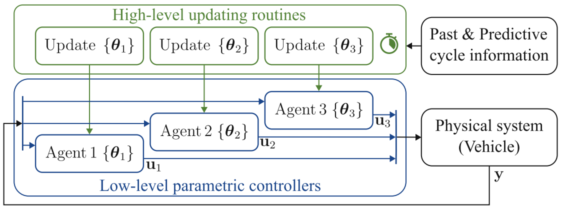

FIGURE 1. Overview of the proposed multi-level cooperative control strategy.

is accurately considered, depending on the inputs controlled by all the agents.

The proposed modular EMS is illustrated in Fig. 1, keeping the main advantage of a multi-layer EMS, dissociating real-time operation, low-level layer, and controller parameter updates, high-level layer. Additionally, the agents in the low-level control can be different, of various complexity, and easily modified, added, or removed. Indeed, there is no communication between the agents, simplifying the design of each agent's parametric controller.

The high-level layer has a crucial role in optimizing each agent's controller's parameters to minimize the cost (1). Once again, each parametric routine is different, using a dedicated optimization algorithm over a specific horizon that considers past and predictive information. Also, each updating routine can be executed in the *background*, i.e., in parallel to the low-level layer. The parameters of the agent j can be updated while agent j controls the inputs $\boldsymbol{u}_j$, allowing the updating routine j to employ an optimization algorithm without hindering real-time capability. Finally, each updating routine can be called using a different frequency, depending on the agent's needs and each component's dynamics.

The proposed cooperative EMS approach can be employed for various vehicle architectures. The requirements are easily fulfilled, consisting of a parametric controller for each agent and a method to update its parameters using predictive information and considering the whole vehicle cost. Real-time feasibility can be guaranteed by this EMS approach if the chosen parametric controllers and updating routines can be run in the hardware within their allocated computing time.

The following section applies the proposed cooperative strategy to control a gasoline HEV along with its gearbox. This example is considered, as it requires the control of two coupled elements, i.e., engine and gearbox, with shared constraints and objectives. Moreover, both controls have to be considered on different time scales for the optimization and are of different nature: the gear engaged is a discrete input, taking integer values, whereas the torque split is continuous, taking real values.

III. APPLICATION TO AN HEV WITH A GEARBOX

In this section, the cooperative EMS proposed in Section II is applied to control the gearbox and torque split of an HEV. A first agent is employed to control the gear selection, while a second agent controls the torque split between the engine and the electric motor.

TABLE 1. Vehicle mass and coastdown coefficients.

m	2000	kg
F_0	144.7	N
F_1	3.25	$\mathrm{N\,s\,m^{-1}}$
F_2	0.433	$\mathrm{N\,s^2\,m^{-2}}$

A. PROBLEM FORMULATION

A gasoline HEV is the vehicle considered for the demonstrative application of the proposed cooperative EMS. For this specific example, the EMS's goal is to minimize a cost, considering both fuel consumption and the number of gear shifts. To minimize this cost, a simplified vehicle model is employed, using both physical models and empirical laws calibrated from the real vehicle under investigation. All the models are expressed in discrete time, with a fixed sampling time $T_s = t(k+1) - t(k) = 1\,\mathrm{s}$.

A backward vehicle model is used to easily compare different controllers, while real measurement data are employed to account for various driving conditions and scenarios. Indeed, the impact of different drivers, traffic and weather conditions, speed limits, etc., are accurately represented using real-driving measurements. Multiple real driving cycles consisting of speed and road altitude recorded across Europe using equivalent vehicles are merged and used as a realistic representation of all the standard driving scenarios possibly encountered during the vehicle's lifetime.

From the vehicle speed v, the slope s derived from the altitude [34], and the acceleration a estimated using a finite difference scheme, the required vehicle force F_{req} is defined as

$$\begin{aligned} F_{\mathrm{req}}(k) &= \mathrm{m}a(k) + \mathrm{mg}\sin(s(k)) \\ &\quad + \cos(s(k))\left(\mathrm{F}_0 + \mathrm{F}_1 v(k) + \mathrm{F}_2 v^2(k)\right) \end{aligned} \tag{3}$$

with the vehicle parameters and coastdown coefficients measured from the actual vehicle and provided in Table 1, and g the constant of gravity.

Thanks to the backward vehicle model, the engine speed and powertrain torque are directly linked to the vehicle speed and road slope. The powertrain must provide the vehicle force through the driveline and a 6-speed gearbox. The engine's angular velocity is directly expressed depending on the vehicle speed and the current gear engaged $gear(k)$

$$\omega_{\mathrm{ice}}(k) = \frac{v_{\mathrm{veh}}(k)}{r_{\mathrm{i}}} r_{\mathrm{dr}} r_{\mathrm{gear}}(gear(k)) \tag{4}$$

with the driveline and gearbox transmission ratios, r_{dr} and $r_{\mathrm{gear}}(\bullet)$ shown in Table 2, and the rolling radius $r_{\mathrm{i}} = 0.3\,\mathrm{m}$. The required powertrain torque at the input of the gearbox is directly computed from the force applied at the wheels (3)

TABLE 2. Driveline and gearbox transmission ratios.

r_{dr}	4.7
$r_{\mathrm{gear}}(1)$	3.96
$r_{\mathrm{gear}}(2)$	2.11
$r_{\mathrm{gear}}(3)$	1.28
$r_{\mathrm{gear}}(4)$	0.87
$r_{\mathrm{gear}}(5)$	0.66
$r_{\mathrm{gear}}(6)$	0.51

and the current gear

$$T_{\mathrm{gbx}}(k) = \frac{F_{\mathrm{req}}(k)\, r_{\mathrm{i}}}{r_{\mathrm{dr}} r_{\mathrm{gear}}(gear(k))}. \tag{5}$$

The gearbox input torque demand (5) has to be fulfilled by the powertrain, i.e., engine, electric motor, and brakes, at all times. The engine is directly coupled to the gearbox to provide this torque, whereas the electric motor is coupled through a reduction gear $r_{\mathrm{em}} = 2.7$. The engine and electric motor torque should therefore verify

$$T_{\mathrm{req}}(k) = T_{\mathrm{brk}}(k) + T_{\mathrm{ice}}(k) + T_{\mathrm{em}}(k)\, r_{\mathrm{em}} \tag{6}$$

with T_{brk} the equivalent torque applied by the brakes at the gearbox input.

An accurate estimate of the electric motor efficiency, as well as the battery State of Charge (SoC) is required for the EMS to minimize fuel consumption. The electric motor efficiency is tabulated in a static efficiency map depending on the electric motor torque and speed. The inverter and power electronics losses are also included in the efficiency map η_{em} shown in Fig. 2.

An equivalent circuit model is employed to estimate the battery SoC accurately. The battery parameters are identified from the existing vehicle, with a capacity $Q_{\mathrm{bat}} = 0.95\,\mathrm{kW\,h}$, a maximum C-rate of four during charge and discharge, an open-circuit voltage $U_{\mathrm{bat}} = 47.6\,\mathrm{V}$ and a total internal resistance $R_{\mathrm{bat}} = 0.196\,\Omega$. The battery SoC dynamics is expressed

$$SoC(k+1) = SoC(k) + \Delta SoC(k), \tag{7a}$$

$$\Delta SoC(k) = T_{\mathrm{s}} \frac{-U_{\mathrm{bat}} + \sqrt{U_{\mathrm{bat}}^2 - 4R_{\mathrm{bat}}P_{\mathrm{bat}}(k)}}{2R_{\mathrm{bat}}Q_{\mathrm{bat}}} \tag{7b}$$

with the battery power P_{bat} computed from the electric engine speed and torque, and the electric motor static efficiency map

$$P_{\mathrm{bat}}(k) = \frac{\omega_{\mathrm{em}}(k)\, T_{\mathrm{em}}(k)}{\eta_{\mathrm{em}}(\omega_{\mathrm{em}}(k)\, 30/\pi, T_{\mathrm{em}}(k))}. \tag{7c}$$

The battery internal resistance and open-circuit voltage are considered constant as only a reduced SoC range is allowed in the vehicle for safety and degradation purposes [35], i.e., $\mathcal{X}_{\mathrm{SoC}} = [0.2, 0.8]$. The SoC is not considered in the EMS cost, but the EMS needs to keep the SoC within the allowed range $\mathcal{X}_{\mathrm{SoC}}$ at all times. Keeping the SoC within its allowable range becomes a key factor for the EMS, especially for the considered vehicle, which has a small battery capacity to reduce the vehicle price. Also, the simplified battery model

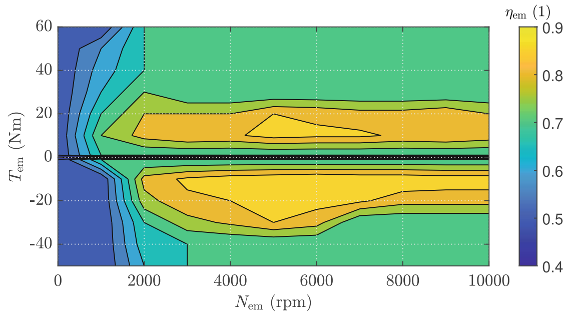

FIGURE 2. **Electric motor and inverter efficiency $\eta_{\mathrm{em}}(N_{\mathrm{em}}, T_{\mathrm{em}})$.**

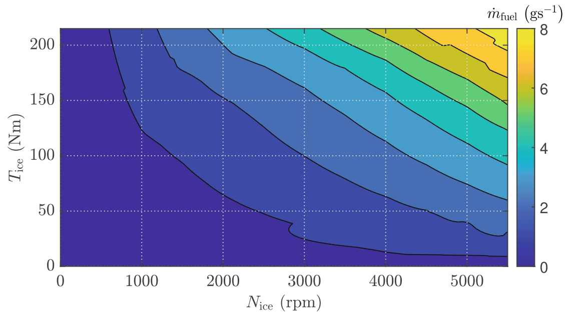

FIGURE 3. **Gasoline engine fuel consumption $\dot{m}_{\mathrm{fuel}}(N_{\mathrm{ice}}, T_{\mathrm{ice}})$.**

employed here for illustrating the proposed method can be replaced by any battery model fitting the actual vehicle technology.

The engine is a four-cylinder 1.2 L turbocharged gasoline engine. The EMS uses a static representation of the engine to accurately account for the fuel consumption during the cycle when evaluating the cost. The fuel consumption is indeed directly tabulated as a function of the engine speed and torque as shown in Fig. 3. The engine fuel map was derived from testbed measurements and validated by comparing transient cycle measurement and simulation.

Using the proposed models of the vehicle and powertrain components, the EMS can effectively estimate the cost over a cycle of N samples

$$J = \sum_{k=1}^{N} \left(\dot{m}_{\mathrm{fuel}}(k)\, T_{\mathrm{s}} + Q_{\Delta\mathrm{gear}} |\Delta\mathrm{gear}(k)| \right) \tag{8}$$

with $Q_{\Delta\mathrm{gear}} = 1.5 \times 10^{-4}\,\mathrm{kg}$ the equivalent costs in terms of fuel for each gear shift. Two control inputs are used to minimize the cost (8). The first input is defined as a modification of the current gear for the next sample $u_1(k) = \Delta\mathrm{gear}(k)$ leading to the gearbox dynamics

$$gear(k+1) = gear(k) + u_1(k). \tag{9}$$

Regarding the torque split, the engine torque is set as the second system input $u_2(k) = T_{\mathrm{ice}}(k)$.

Controlling the vehicle powertrain corresponds to finding $(u_1(k), u_2(k))\ \forall k \in [1, N]$ fulfilling (6) at each instant k and minimizing (8) while ensuring $SoC \in \mathcal{X}_{\mathrm{SoC}}$ and complying with the engine and electric maximum speed and torque limits.

B. PARAMETRIC CONTROLLERS

The EMS of the powertrain of the HEV introduced in the previous section is responsible for controlling the gearbox, the electric motor, and the engine. Therefore, two agents are employed, the first for the gear selection and the second for the torque split between the electric motor and the engine.

In the low-level layer depicted in Fig. 4, each agent is composed of a parametric controller and receives several measurements: the current gear engaged; the previous engine torque; as well as the current cycle requirements in terms of gearbox torque and speed

$$\mathbf{y}(k) = \left[gear(k), T_{\mathrm{ice}}(k-1), T_{\mathrm{gbx}}(k), \omega_{\mathrm{gbx}}(k)\right]. \quad (10)$$

The gear selection parametric control law is designed from the observation of the optimal gear selection behavior for various cycles, derived using DP with the SoC and the current gear as state variables. Indeed, the optimal engine speed appears to be linearly correlated to the cycle speed. A target engine speed ω^*_{ice} is accordingly formulated as a function of the gearbox output speed

$$\omega_{\mathrm{gbx,out}}(k) = v_{\mathrm{veh}}(k)\, r_{\mathrm{dr}} r_{\mathrm{i}}^{-1}, \quad (11a)$$

$$\omega^*_{\mathrm{ice}}(k) = \omega_0 + \theta_{1,1}(k)\, \omega_{\mathrm{gbx,out}}(k) \quad (11b)$$

with ω_0 identified as $90\,\mathrm{rad\,s^{-1}}$ and $\theta_{1,1}(k)$ a unitless parameter observed to be in $[1.3, 1.7]$ for all driving conditions. A control law is hence derived, such that a gear shift is triggered if a gear leading to an engine speed closer to the target engine speed is possible.

To approach the target engine speed, first, the feasible set of gear ratios $\overline{\mathbf{gear}}(k)$ is defined at each time such that the engine and motor torque speed limitations are fulfilled

$$\overline{\mathbf{gear}}(k) = \{gear \mid (11d) \wedge (11e) \wedge (11f)\}, \quad (11c)$$

$$gear \in \{1, 2, 3, 4, 5, 6\}, \quad (11d)$$

$$\omega_{\mathrm{ice}}(gear, k) \in \left[\omega^{\min}_{\mathrm{ice}}(k), \omega^{\max}_{\mathrm{ice}}(k)\right], \quad (11e)$$

$$T_{\mathrm{gbx}}(k) \le T^{\max}_{\mathrm{ice}}(gear) + r_{\mathrm{em}} T^{\max}_{\mathrm{em}}(gear). \quad (11f)$$

From the feasible set of gear ratios $\overline{\mathbf{gear}}(k)$, the optimal gear is chosen as the one leading to the engine speed closest to ω^*_{ice}

$$gear^*(k) = \arg \min_{\epsilon \in \overline{\mathbf{gear}}(k)} \mathrm{abs}\left(\omega_{\mathrm{ice}}(\epsilon, k) - \omega^*_{\mathrm{ice}}(k)\right) + \theta_{1,2}(k)\, \mathrm{abs}\left(\epsilon - gear(k)\right) \quad (11g)$$

with $\theta_{1,2}(k)$ in $\mathrm{rad\,s^{-1}}$ a parameter penalizing a change of the current gear engaged. This parameter allows the consideration of the trade-off between a gear shift cost, i.e., Δgear in (8), and the benefit of changing a gear in terms of fuel consumption. A gear shift is consequently triggered to follow $gear^*(k)$

$$u_1(k) = gear^*(k) - gear(k) \quad (11h)$$

leading to a gear shift at the next iteration according to the gearbox dynamics (9).

The torque split controller is a modified version of a standard PI ECMS initially proposed in [18]. This method results in minimizing, at each time, the fuel consumption as well as a change of battery SoC weighted by an equivalent fuel cost for using the battery energy. The proposed predictive ECMS conserves the PI structure of a standard ECMS but with a variable offset $\lambda_0(k)$ as the parameter of the controller, i.e., $\lambda_0(k) = \theta_2(k)$. The engine torque is defined to minimize at each time step

$$u_2(k) = \arg \min_{T_{\mathrm{ice}}} (\dot{m}(T_{\mathrm{ice}}) + \lambda(k)\, \Delta SoC(T_{\mathrm{ice}}, k)) \quad (12a)$$

with the ECMS PI correction of λ

$$\lambda(k) = \theta_2(k) + K_{\mathrm{p}}(SoC(k) - SoC_{\mathrm{ref}}) + K_{\mathrm{i}} \sum_{k_{\mathrm{i}}=1}^{k} (SoC(k_{\mathrm{i}}) - SoC_{\mathrm{ref}})\, T_{\mathrm{s}}. \quad (12b)$$

The reference SoC, i.e., SoC_{ref}, is considered constant and taken as 0.5 for this study. This value corresponds to the SoC average expectation to always guarantee both recharging and depleting capabilities. Indeed, in the case of no predictive information, depending on the cycle, the battery may need to be depleted if the power demand is high or recharged if the power demand is negative. Keeping the SoC at 0.5 is consequently a standard strategy for non-predictive EMS [6]. For practical implementation, to avoid computing the sum in (12b), λ is updated based on its previous value

$$\lambda(k) = \lambda(k-1) + \theta_2(k) - \theta_2(k-1) + K_{\mathrm{p}}(SoC(k) - SoC(k-1)) + K_{\mathrm{i}}(SoC(k) - SoC_{\mathrm{ref}})\, T_{\mathrm{s}}. \quad (12c)$$

The PI parameters of the ECMS are fixed for this study with $K_{\mathrm{p}} = 0.144\,\mathrm{kg}$ and $K_{\mathrm{i}} = 2.4 \times 10^{-4}\,\mathrm{kg\,s^{-1}}$, and their calibration is discussed in Section IV.

The parameters of the gear selection controller

$$\boldsymbol{\theta}_1(k) = \left[\theta_{1,1}(k), \theta_{1,2}(k)\right]^{\mathrm{T}}, \quad (13)$$

and the predictive ECMS parameter $\theta_2(k)$ can be optimized during the vehicle operation using available predictive information. In the next section, a routine is defined for each agent to update respectively $\boldsymbol{\theta}_1$ and θ_2 in the background and considering all the terms in the cost (8).

C. UPDATING ROUTINES

The parametric controllers of the low-level layer defined in the previous section ensure feasible operations as well as a simple controller implementation. Nevertheless, their respective parameters $\boldsymbol{\theta}_1$ and θ_2 need to be accordingly updated to efficiently reduce the cost (8). For this reason, an updating routine is designed for each agent in the high-level updating routine layer as shown in Fig. 4. Each routine is called individually and can be evaluated in parallel to the low-level controllers to guarantee the real-time capability of the EMS. For this study, predictive information is used by the updating routine, consisting of estimated vehicle speed and road slope. Also, the length of the predicted horizon and the quality of the estimate is studied in the numerical study in Section IV.

The routine associated with the gear selection controller will ideally minimize J from (8) with respect to $\boldsymbol{\theta}_1$ only over the remaining of the drive cycle. For practical implementation, considering predictive information only available over a bounded horizon and to ensure low computational effort for an update, the metric J is only minimized over the horizon N_{p_1}. A penalty term is necessarily added to account for any modification of the second agent policy. Indeed, the SoC reached at the end of the prediction horizon should stay close to the one that would be reached without updating the gear selection parameters, i.e., SoC_{current}. Taking the modification of the SoC at the end of the horizon while changing the gear selection parameterization is necessary to ensure cooperation, hence minimizing the cost (8).

Consequently, a modified cost function as introduced in [29] is employed, using the equivalent fuel cost for the electric energy λ to account for a change in the predicted SoC at the end of the prediction horizon

$$J_{\boldsymbol{\theta}_1} = \sum_{k_{\mathrm{i}}=k}^{N_{\mathrm{p}1}} \left(\dot{m}_{\mathrm{fuel}}\left(k_{\mathrm{i}}\right) T_{\mathrm{s}} + Q_{\Delta\mathrm{gear}} \left|\Delta\mathrm{gear}\left(k_{\mathrm{i}}\right)\right|\right) + \lambda\left(N_{\mathrm{p}1}\right)\left(SoC\left(N_{\mathrm{p}1}\right) - SoC_{\mathrm{current}}\right). \tag{14}$$

For practical implementation and to envision fast computation time, the minimization of (14) is done by evaluating the cost $J_{\boldsymbol{\theta}_1}$ with predefined local variations of $\boldsymbol{\theta}_1$. For this study, nine variations are considered, plus or minus 0.08 for $\theta_{1,1}$ and plus or minus 8 rad s^{-1} for $\theta_{1,2}$ around the current value of $\boldsymbol{\theta}_1$. This type of local search has the advantage of being scalable to the available computational power, i.e., changing the number of fixed variations, and only allows the parameters to change within predefined limits and with a maximum rate of change at each iteration defined by the fixed variations themselves.

The proposed updating routine for the gear selection controller cooperates with the torque split, as the torque split reaction to a parameter change of the gear selection controller is explicitly considered when evaluating the predicted cost. Indeed, the torque split controller is known, and the current parameter θ_2 can be provided to the gear selection updating routine. While minimizing $J_{\boldsymbol{\theta}_1}$, the gear selection updating routine directly considers the torque split controller as being part of the vehicle dynamics, and consequently the cost (8) can be accurately predicted over the prediction horizon. The optimization of $\boldsymbol{\theta}_1$ is done directly considering (8), hence efficiently going into the direction of a reduction of the vehicle operational cost.

As for the gear selection updating routine, the torque split updating routine needs to minimize the cost (8). Also, the torque split updating routine minimizes J only over the available prediction horizon of length N_{p_2}. The SoC at the end of the prediction horizon is consequently penalized when not following the reference SoC set at 0.5. This adaptation is made to implicitly consider the remaining of the cycle after the prediction horizon to keep the possibility of depleting or charging the battery after the prediction horizon, depending on the power demand. The adapted cost for the torque split updating routine is consequently formulated

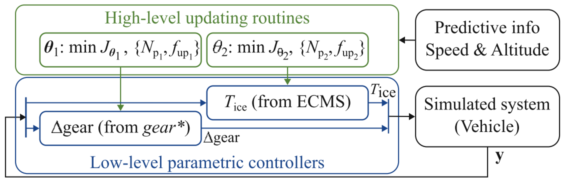

FIGURE 4. Cooperative EMS for the gasoline hybrid electric vehicle.

$$J_{\theta_2} = \sum_{k_{\mathrm{i}}=k}^{N_{\mathrm{p}2}} \left(\dot{m}_{\mathrm{fuel}}\left(k_{\mathrm{i}}\right) T_{\mathrm{s}} + Q_{\Delta\mathrm{gear}} \left|\Delta\mathrm{gear}\left(k_{\mathrm{i}}\right)\right|\right) + Q_{\mathrm{SoC},2}\left(SoC\left(N_{\mathrm{p}2}\right) - SoC_{\mathrm{ref}}\right)^2 \tag{15}$$

with $Q_{\mathrm{SoC},2} = 1 \times 10^3$ kg manually calibrated to make sure that the SoC stays close enough to the reference while maintaining a high system efficiency. Indeed, maintaining the SoC close to its reference at the end of the prediction horizon is necessary to stay away from the SoC constraints but can partially hinder optimality during regeneration periods or when the battery needs to be depleted.

The minimization of J_{θ_2} is done by shooting different values of θ_2 using a gradient method, defining a new testing point in the direction of the negative gradient of J_{θ_2}. To ensure fast computation time, the maximum number of testing points is set to ten for this study but could be varied to fit the available computational resources.

The torque split updating routine also cooperates with the gearbox, as the gear selection controller reaction to a change of θ_2 is directly considered when optimizing J over the horizon N_{p_2}. The gear selection controller is indeed known, and its parameters $\boldsymbol{\theta}_1$ are communicated to the torque split updating routine so that the gear selection controller reaction to a change of θ_2 is considered during the predicted horizon. As a result, the minimization (15) efficiently updates θ_2 considering all the terms of the cost (8), hence going in the direction of a reduction of J.

The gear selection and the torque split updating routine are called in parallel to the low-level control layer, ensuring real-time feasibility. Also, the updating frequency f_{up_1} and f_{up_2} for the gear selection and torque split updating routine can be chosen separately depending on the components' requirements and the availability of predictive information. A component with fast dynamics can be updated more often especially when its operating conditions are modified, e.g., by updating the gear selection controller parameters just before arriving at an intersection. Additionally, the gear

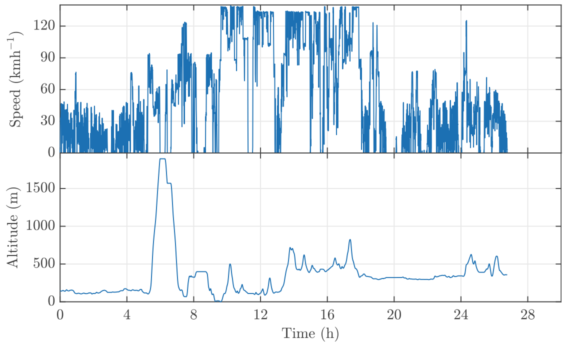

FIGURE 5. Concatenated cycles used for the numerical study.

selection routine minimizing (14) uses a sampling time of 1 s while the torque split routine minimizing (15) employs a sampling time of 30 s. This possibility of using different sampling times, adapted to each component is another strength of the proposed multi-level EMS toward a real-time implementation.

IV. NUMERICAL ANALYSIS

This section presents a numerical study emphasizing the benefits of cooperation and predictive information for controlling the presented HEV. The proposed cooperative strategy is compared to the performances of a standard non-predictive EMS as well as the optimal solution achievable when the whole cycle is known in advance. To achieve a comprehensive comparison, different driving conditions and various scenarios regarding the available predictive information are considered. All models ave been developed using MATLAB software, on a standard i7 with 16GB ram memory computer.

A. COMPARATIVE STUDY

Real-world driving data from multiple vehicles and drivers across Europe have been combined to analyze different EMS performances during various driving scenarios, such as navigating through crowded cities, driving on highways, and dealing with various weather conditions, road speed limitations, and terrains. This data provides a comprehensive view of the vehicle's behavior under different conditions. The resulting cycle, depicted in Fig. 5, represents more than 26 hours and 1300 km, with speed up to 140 km h^{-1} and a total positive elevation of 5900 m. Given the length of the used test cycle and the size of the battery, a variation of SoC at the end of the cycle will represent a marginal equivalent fuel consumption and, hence, will not be distinguishable in the cost (8).

The optimal gear selection and torque split for the proposed cycle are computed and used as a benchmark. A DP algorithm with two states, one for the SoC and one for the gear engaged is used to find the optimal control strategy, i.e., revealing the minimum cost for the proposed cycle. This minimum cost, associated with the optimal solution, is noted J^* throughout this section. Such an optimal solution can only be found when the exact speed and altitude profiles are known for the entire cycle, and will only be used as the target cost for the proposed EMS.

In the following, first, a predictive and non-predictive ECMS are compared to emphasize the benefits of predictive information. Second, the proposed cooperative EMS is employed, and the cooperation benefit is illustrated. Then, several sensitivity studies are conducted regarding the accuracy and length of the available predicted information, as well as the updating frequency and delay of the updating routines. The proposed cooperative scheme is shown to be robust to inaccurate predictive information, short prediction horizons, and different updating routine call frequencies and update delays.

B. EMS WITHOUT GEARBOX COOPERATION

The goal of this first study is to emphasize the benefit of having a predictive control for the torque split. Indeed, the SoC dynamics is slow, and the battery capacity is relatively small for a two-ton vehicle. A predictive control of the SoC brings opportunities for higher system efficiency while keeping the SoC further away from its minimum and maximum admissible values. The predictive ECMS (P-ECMS) proposed in (12) is compared to a non-predictive ECMS (ECMS), i.e., controller (12) with a fixed $\theta_2 = -0.25$ kg. The parameter θ_2 of the predictive ECMS is updated every ten minutes with a horizon of one hour, i.e., $f_{\mathrm{up}_2} = 6\,\mathrm{h}^{-1}$ and $N_{\mathrm{p}_2} = 1$ h. Both ECMSs have the same calibration for K_p and K_i as proposed in Section III.

The benefits of using a predictive ECMS are summarized in Table 3, for two different gear selection strategies. First, for directly reusing the gear profile from the optimal solution and then using the parametric gear selection controller proposed in (11) with fixed parameters $\theta_{1,1} = 1.5$ and $\theta_{1,2} = 35\,\mathrm{rad\,s}^{-1}$ optimized to get the best results with the non-predictive ECMS controller. The P-ECMS brings a lower cost compared to a non-predictive ECMS, being almost as efficient as the optimal solution when reusing the optimal gear profile. With a gear selection controller with fixed parameters, the P-ECMS is still better than the non-predictive ECMS but with a cost of more than one percent higher than the optimal solution.

The benefits of a predictive ECMS are illustrated in Fig. 6, where the SoC profile of the optimal solution is compared to the ECMS and P-ECMS SoC profiles. The equivalent cost of fuel for electricity, i.e., λ, is also depicted for the ECMS and the P-ECMS strategies. The P-ECMS is especially advantageous in avoiding SoC constraints during regeneration, depleting the SoC if necessary before a large regeneration period, as shown shortly after five hours in the cycle. Also, the P-ECMS is globally better than a non-predictive ECMS at keeping the SoC within its minimum and maximum admissible values. For the non-predictive ECMS, λ is slower and later to react than λ of the P-ECMS strategy, leading to SoC saturation during regeneration. Furthermore, the non-predictive ECMS also saturates the

TABLE 3. Cost with respect to the optimal cost for predictive and non-predictive torque split strategies.

Gear selection strategy	Torque split	ΔJ compared to J^* in %
From optimal solution	ECMS	0.69
From optimal solution	P-ECMS	0.09
Fixed $\boldsymbol{\theta}_1$ in (11)	ECMS	2.17
Fixed $\boldsymbol{\theta}_1$ in (11)	P-ECMS	1.31

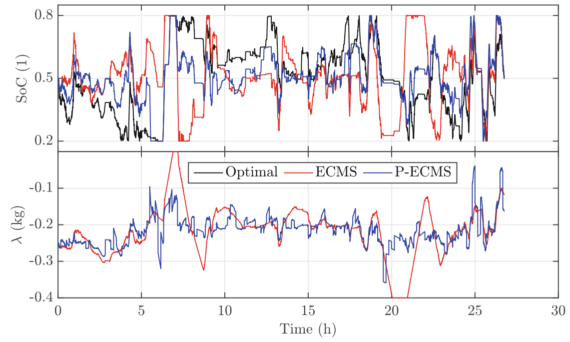

FIGURE 6. Non-predictive ECMS vs predictive ECMS using the gear selection profile of the optimal solution.

SoC at its minimum value after large regeneration periods, leading to blended powertrain operations, i.e., forced engine operations without the possibility of using the electric motors due to a low SoC.

The ECMS parameters, i.e., K_p and K_i, have been calibrated to reach the minimum cost for this cycle for the non-predictive ECMS strategy. Indeed, a less aggressive ECMS will engender more SoC saturation, and so less regeneration as well as more frequently blended operations where only the engine can be used. On the opposite, a more aggressive ECMS will engender more variations of λ, hindering further more optimality. The P-ECMS calibration could be adapted with a slightly less aggressive controller when the predictive information is often and accurately updated. In the following, the P-ECMS maintains the same ECMS calibration to achieve a straightforward and resilient controller, regardless of the accuracy and horizon of the predictive information.

The second crucial information of Table 3 is the gap between using the optimal gear profile and the non-adaptive gear selection strategy. This gap suggests that adapting the gear selection strategy parameters could be highly beneficial toward a reduced cost. The adaptation of the gear selection parameters using the proposed gear selection updating routine (14) is presented in the next section, where the cooperation between the gearbox and torque split is shown to be essential for effectively reducing the cost.

C. BENEFITS OF COMPONENTS COOPERATION

This section emphasizes the benefits of cooperation between the powertrain components, i.e., the gearbox, the engine, and the electric motor. The same ECMS and P-ECMS controllers as in the previous section are employed for controlling the torque split.

TABLE 4. Cost with respect to the optimal cost for cooperative and non-cooperative gearbox updating routine.

Gear selection updating routine	Torque split	ΔJ compared to J^* in %
Cooperative (14)	ECMS	1.90
Cooperative (14)	P-ECMS	0.84
Non-cooperative (16)	ECMS	2.20
Non-cooperative (16)	P-ECMS	1.36

Regarding the gear selection, the parametric controller (11) is employed with the parameters $\boldsymbol{\theta}_1$ optimized every minute with a predictive horizon of two minutes, i.e., $f_{\mathrm{up}_1} = 1\,\mathrm{min}^{-1}$ and $N_{\mathrm{p}_1} = 2\,\mathrm{min}$. To emphasize the benefits of a gear selection updating routine cooperating with the torque split, the cooperative updating routine updating $\boldsymbol{\theta}_1$ from (14) is compared to a non-cooperative gear selection updating routine. The non-cooperative gear selection updating routine optimizes $\boldsymbol{\theta}_1$ using a cost function alike (14) but without considering the SoC. Hence the non-cooperative gear selection updating routines minimizes

$$J_{\boldsymbol{\theta}_1,\text{no coop}} = \sum_{k_\mathrm{i}=k}^{N_{\mathrm{p}_1}} \left(\dot{m}_\mathrm{fuel}\left(k_\mathrm{i}\right) T_\mathrm{s} + Q_{\Delta\mathrm{gear}} \left|\Delta\mathrm{gear}\left(k_\mathrm{i}\right)\right|\right). \quad (16)$$

Indeed, the cooperation from the gear selection to the torque split is made possible through the consideration of the SoC at the end of the prediction horizon.

The results in terms of relative cost to J^* for the cooperative and the non-cooperative gear selection updating routine are presented in Table 4. As expected, the cooperative gear selection updating routine is able to greatly decrease the cost compared to the non-adaptive gear selection strategy presented in Table 3. For example, using a P-ECMS, the cost relative to the optimal solution is decreased from 1.31 % to 0.84 % when the gear selection updating routine is cooperating with the torque split controller. However, when the gear selection updating routine does not cooperate with the torque split, adapting the gear selection strategy parameters leads to a higher cost than when a non-adaptive gear selection strategy is employed.

To understand the difference between a cooperative and a non-cooperative gear selection updating routine, Fig. 7 depicts the SoC, λ, gear and cost difference for these two strategies. The figure depicts a specific section of the cycle, where both strategies start and end with the exact same SoC. For the non-cooperative gear selection updating routine, the gear is kept constant. Indeed, with the chosen gear selection parameters, the non-cooperative gear selection updating routine effectively minimizes the number of gear shifts, keeping the same gear and staying at a bad operating engine point efficiency such that the torque split favors battery depletion, hence also minimizing the fuel consumption. The problem with such a non-cooperative gear selection updating routine is that it results in a decreasing SoC. Therefore, the

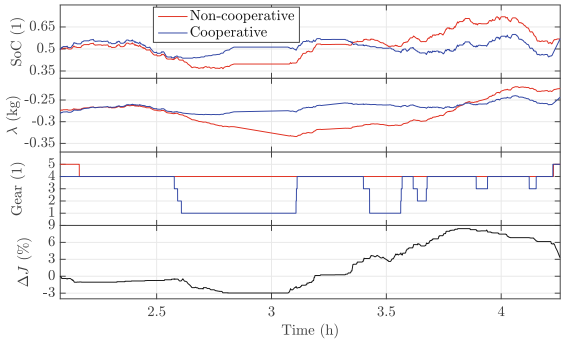

FIGURE 7. Gear selection updating routine with and without cooperation.

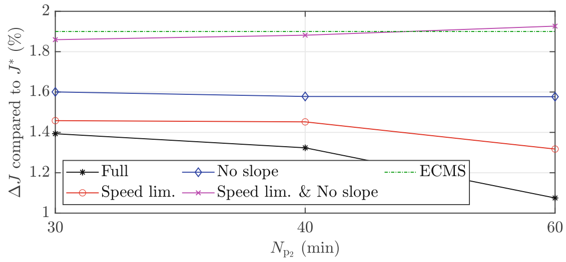

FIGURE 8. Variation of the torque split updating routine horizon and the available predicted information accuracy.

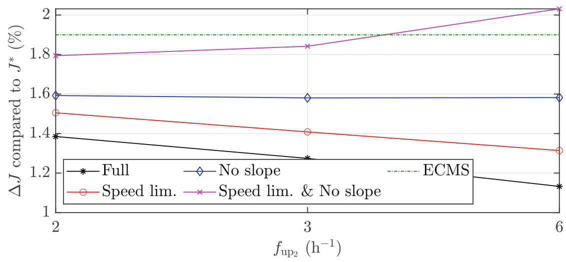

FIGURE 9. Variation of the torque split updating routine call frequency and the available predicted information accuracy.

ECMS needs to counteract to maintain the SoC close enough to the reference.

In the end, the value of λ shows more significant variations for the non-cooperative strategy to counteract the gear selection policy, resulting in a higher cost. The non-cooperative strategy appears to have a cost 3.2 % higher on the presented cycle section. The cooperation between the powertrain's components consequently brings crucial benefits toward effectively reducing the cost.

D. PREDICTIVE INFORMATION SENSITIVITY STUDY

For a practical application, the predictive information is available for a specific horizon and is not always accurate. This section investigates the sensitivity to predictive horizon length, predictive information accuracy, and updating routine call frequency.

Several scenarios are presented for the available predicted information. From full knowledge of the vehicle speed and road slope (exact) to knowing only the speed limits and road slope (speed lim.), knowing the exact speed but without the road slope (no slope) to knowing only the speed limits without the road slope (speed lim & no slope). The speed limits are estimated based on the vehicle speed, taking the closest speed to some predefined values $\{0, 30, 50, 90, 130\}\,\mathrm{km\,h^{-1}}$, and applying a low-pass filter to replicate plausible transients.

First, the predictive information is varied for the torque split updating routine. The gear selection updating routine parameters are set to $f_{\mathrm{up}_1} = 1\,\mathrm{min}^{-1}$ and $N_{\mathrm{p}_1} = 2\,\mathrm{min}$ and considering a perfect speed and slope knowledge. The relative cost to the optimal cost J^* for a varying horizon and quality of predictive information for the torque split updating routine is presented in Fig. 8. For each value of N_{p_2}, the average relative cost to the optimal cost using $f_{\mathrm{up}_2} \in \{2, 3, 6\}\,\mathrm{h}^{-1}$ is considered.

The first observation is that increasing the prediction horizon, i.e., N_{p_2}, is beneficial if the road slope is known. If the road slope is unknown, increasing N_{p_2} only brings a marginal cost improvement. If the road slope is not known and only the speed limits are known, the resulting P-ECMS cost can become higher than for a non-predictive ECMS. For that reason, the prediction horizon should be adapted to the accuracy of the predictive information. Whenever the predictive information is not accurate, a simple ECMS should be used instead to avoid undertaking counterproductive θ_2 updates. The proposed cooperative scheme could indeed integrate a decision rule regarding when to allow a θ_2 update based on the availability and accuracy of the predictive information.

The torque split updating routine call frequency is also significant, as it defines how often θ_2 is being updated using predictive information. In Fig. 9, the torque split updating routine call frequency is varied, and its resulting influence on the cost is depicted. Each point is the average cost difference to the optimal cost considering different prediction horizons $N_{\mathrm{p}_2} \in \{30, 40, 60\}\,\mathrm{min}$. The gear selection updating routine is kept identical as in Fig. 8.

A higher updating frequency is beneficial whenever the road slope is known, as it plays an important role in determining the equivalent fuel cost of electricity λ. Whenever the road slope is unknown, increasing the updating frequency does not lead to a lower cost and can even be counterproductive if only the speed limits are known further. Indeed, with speed limits and no road slope data, the P-ECMS has a higher cost than a non-predictive ECMS, as regular updates using inaccurate information may lead to a higher cost than a non-predictive strategy. Calling the torque split updating routine could, therefore, be arbitrated depending on the availability of the predictive information, avoiding unnecessary computation in case of inaccurate or missing information.

Second, the predictive information is varied for the gear selection updating routine. The torque split updating routine

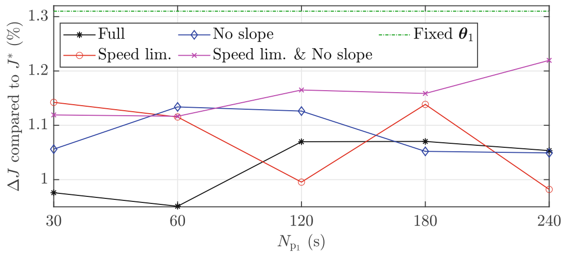

FIGURE 10. Variation of the gear selection updating routine horizon and the available predicted information accuracy.

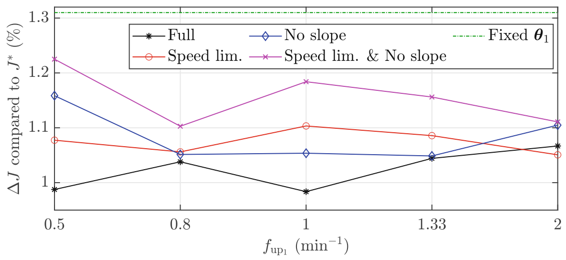

FIGURE 11. Variation of the gear selection updating routine call frequency and the available predicted information accuracy.

is parameterized taking $f_{\mathrm{up}_2} = 6\,\mathrm{h}^{-1}$ and $N_{\mathrm{p}_2} = 1\,\mathrm{h}$, and considering a perfect speed and slope knowledge. Fig. 10 presents the relative cost compared to the optimal cost for a varying prediction horizon length and accuracy, used by the gear selection updating routine. Each point is the average for various gear selection updating routine frequency $f_{\mathrm{up}_1} \in \{0.5, 0.8, 1, 1.33, 2\}\,\mathrm{min}^{-1}$. The proposed cooperative EMS has a relative cost to J^* always at least 0.2 % better than the non-adaptive, i.e., fixed $\boldsymbol{\theta}_1$, gear updating routine. Also, a small horizon is apparently more beneficial in ensuring robustness to inaccurate measurements. Indeed, with a long horizon, the update of $\boldsymbol{\theta}_1$ is not only optimizing the objective locally but for a large period, leading to a higher cost. It is consequently preferable to keep a smaller prediction horizon to allow the parameters of the gear selection controller to adapt faster to the current driving conditions.

The gear selection updating routine call frequency is analyzed in Fig. 11. For each point, the average relative cost to J^* using different prediction horizons is used $N_{\mathrm{p}_1} \in \{30, 60, 120, 180, 240\}\,\mathrm{s}$. The torque split updating routine used in Fig. 10 is kept unchanged. No trend toward a lower or higher updating frequency could be observed, however, the main aspect to emphasize is the robustness of the proposed method. Indeed, for any gear selection updating routine call frequency, the relative cost to J^* for the adaptive gear selection strategy is at least 0.2 % lower than for the non-adaptive strategy. Only a minimum updating frequency requirement can be observed. Indeed, updating the gear selection controller parameters less than 0.8 times per minute leads to higher costs whenever the prediction is not fully known. Reducing further the gear selection updating routine

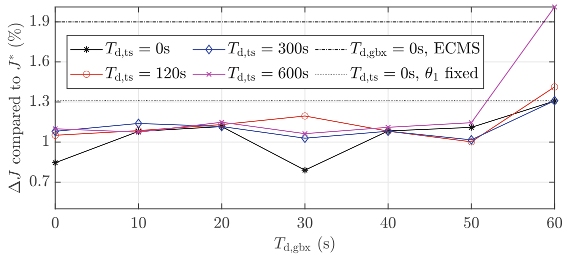

FIGURE 12. Variation of the gearbox and torque split updating routine delay $T_{\mathrm{d,gbx}}$ and $T_{\mathrm{d,ts}}$.

call frequency will eventually lead to the same cost as for the non-adaptive gear selection strategy, i.e., fixed $\boldsymbol{\theta}_1$.

E. UPDATING ROUTINE UPDATE DELAY

One of the main advantages of the proposed cooperative EMS is the ability to update the controller with predictive information while the low-level controller continues to control the powertrain. Obviously, an updating routine will need some processing time to update a controller's parameters, leading to a delay between the processing and the actual update. The time for an update depends on the hardware, the horizon length, and the updating routine algorithm employed. The updating routine delay is therefore variable, from a few seconds for systems with fast dynamics and a short prediction horizon to a few minutes for slower systems with a large prediction horizon.

In this last section of the numerical results, an artificial delay is added between the trigger of an updating routine and the actual modification of a controller's parameters. The gearbox and torque split dynamics have different time constants and optimization horizons. The delay added to each updating routine is varied from zero seconds to the maximum delay before another update. The delay associated with the gear selection updating routine and torque split updating routine is respectively noted $T_{\mathrm{d,gbx}}$ and $T_{\mathrm{d,ts}}$.

The results of the variation of $T_{\mathrm{d,gbx}}$ and $T_{\mathrm{d,ts}}$ is presented in Fig. 12. For this study, the gear selection updating routine has a horizon of $N_{\mathrm{p}_1} = 2\,\mathrm{min}$ and an update frequency $f_{\mathrm{up}_1} = 1\,\mathrm{min}^{-1}$, and the torque split updating routine uses a horizon of $N_{\mathrm{p}_2} = 1\,\mathrm{h}$ and is updated with the frequency $f_{\mathrm{up}_2} = 6\,\mathrm{h}^{-1}$. Both updating routines use perfect predictive information knowledge. Obviously, when adding a delay to the gear selection updating routine, the cost increases, still staying lower than for a non-predictive gear selection strategy. The only restriction is to keep the updating delay lower than the time between two updates. Otherwise, the updating routine is using the wrong assumption regarding the current controller parameters, resulting in a higher cost than for a non-predictive gear selection strategy. The torque split updating routine delay is almost not visible in the results, as the dynamics of λ is relatively slow. In summary, the proposed cooperative control strategy is shown to be robust against updating routine update delay and could, therefore, be easily implemented in real-time in the vehicle.

The influence of the predictive information on the torque split cannot be easily observed, as the employed adaptive ECMS is already robust to inaccurate or missing information. In the case of no predictive information at all, as illustrated in Fig. 6, the SoC profile without predictive information looks quite different from the one using predictive information. Still, both SoC profiles are almost identical in terms of local variations; only the long-term trend is different or when SoC constraints are active. As soon as predictive information is available, even if not accurate, the torque split arbitration is almost identical to the optimal one, up to a slight trend creating an SoC offset over time.

V. CONCLUSION

This paper proposes a modular EMS for HEVs, focusing on cooperation between the different powertrain components. A multi-layer approach is suggested, with a low-level layer consisting of agents controlling various powertrain components. Each agent is independent and uses a parametric controller to ensure feasibility and real-time capability. At the same time, a high-level layer utilizes predictive information to update the parameters of the low-level agents' controllers efficiently. Each agent's controller parameters are updated independently but take into account the other agent's reaction. This way, any agent update is made to decrease the overall cost effectively.

The proposed cooperative strategy is highly modular and can be adapted to guarantee cooperation between all the components of a HEV powertrain. The EMS can easily adapt to different powertrain components by adding an agent for each new component. The low-level layer's parametric controllers are independent and can use various algorithms and a suited sampling time. In the high-level layer, updating routines are also specifically designed for each agent and executed in parallel to the low-level layer, enabling higher complexity for the parameters update without compromising the EMS real-time capability.

The proposed cooperative EMS benefits from controlling the gearbox and torque split of a gasoline HEV are demonstrated numerically. The proposed method surpasses state-of-the-art real-time capable non-predictive and non-cooperative strategies and shows great robustness against inaccurate or missing predictive information. Indeed, predictive information and the cooperation between the gear selection and torque split strategy are shown to be necessary for effectively reducing the vehicle's operational cost. Finally, the length of the prediction horizon and frequency of updates of each controller are analyzed, demonstrating the robustness of the proposed EMS toward a practical implementation.

Further research is being conducted to implement more agents, such as speed planning, exhaust aftertreatment systems, and multiple electric motors. Additionally, validating the proposed EMS on an actual vehicle under real driving conditions is the next step toward implementing the proposed EMS concept in future vehicles.

REFERENCES

[1] R. R. Kumar, C. Bharatiraja, K. Udhayakumar, S. Devakirubakaran, K. S. Sekar, and L. Mihet-Popa, "Advances in batteries, battery modeling, battery management system, battery thermal management, SOC, SOH, and charge/discharge characteristics in EV applications," *IEEE Access*, vol. 11, pp. 105761–105809, 2023.

[2] S. S. G. Acharige, M. E. Haque, M. T. Arif, N. Hosseinzadeh, K. N. Hasan, and A. M. T. Oo, "Review of electric vehicle charging technologies, standards, architectures, and converter configurations," *IEEE Access*, vol. 11, pp. 41218–41255, 2023.

[3] W. Hong, I. Chakraborty, H. Wang, and G. Tao, "Co-optimization scheme for the powertrain and exhaust emission control system of hybrid electric vehicles using future speed prediction," *IEEE Trans. Intell. Vehicles*, vol. 6, no. 3, pp. 533–545, Sep. 2021.

[4] F. Tao, L. Zhu, Z. Fu, P. Si, and L. Sun, "Frequency decoupling-based energy management strategy for fuel cell/battery/ultracapacitor hybrid vehicle using fuzzy control method," *IEEE Access*, vol. 8, pp. 166491–166502, 2020.

[5] H. Jing, F. Jia, and Z. Liu, "Multi-objective optimal control allocation for an over-actuated electric vehicle," *IEEE Access*, vol. 6, pp. 4824–4833, 2018.

[6] P. Saiteja and B. Ashok, "Critical review on structural architecture, energy control strategies and development process towards optimal energy management in hybrid vehicles," *Renew. Sustain. Energy Rev.*, vol. 157, Apr. 2022, Art. no. 112038.

[7] C. M. Martinez and D. Cao, "Integrated energy management for electrified vehicles," in *Ihorizon-Enabled Energy Management for Electrified Vehicles*, C. M. Martínez and D. Cao, Eds. Oxford, U.K.: Butterworth-Heinemann, 2019, pp. 15–75.

[8] A. Alalewi, I. Dayoub, and S. Cherkaoui, "On 5G-V2X use cases and enabling technologies: A comprehensive survey," *IEEE Access*, vol. 9, pp. 107710–107737, 2021.

[9] Y. Huang, H. Wang, A. Khajepour, H. He, and J. Ji, "Model predictive control power management strategies for HEVs: A review," *J. Power Sources*, vol. 341, pp. 91–106, Feb. 2017.

[10] A. S. Al-Ogaili, T. J. T. Hashim, N. A. Rahmat, A. K. Ramasamy, M. B. Marsadek, M. Faisal, and M. A. Hannan, "Review on scheduling, clustering, and forecasting strategies for controlling electric vehicle charging: Challenges and recommendations," *IEEE Access*, vol. 7, pp. 128353–128371, 2019.

[11] R. A. Swief, N. H. El-Amary, and M. Z. Kamh, "Optimal energy management integrating plug in hybrid vehicle under load and renewable uncertainties," *IEEE Access*, vol. 8, pp. 176895–176904, 2020.

[12] A. Alyakhni, L. Boulon, J.-M. Vinassa, and O. Briat, "A comprehensive review on energy management strategies for electric vehicles considering degradation using aging models," *IEEE Access*, vol. 9, pp. 143922–143940, 2021.

[13] H. Waschl, I. Kolmanovsky, M. Steinbuch, and L. Re, *Optimization and Optimal Control in Automotive Systems*. Cham, Switzerland: Springer, Jan. 2014.

[14] C.-C. Lin, H. Peng, J. W. Grizzle, J. Liu, and M. Busdiecker, "Control system development for an advanced-technology medium-duty hybrid electric truck," in *Proc. SAE Tech. Paper Ser.*, Nov. 2003, p. 11.

[15] C.-C. Lin, H. Peng, J. W. Grizzle, and J.-M. Kang, "Power management strategy for a parallel hybrid electric truck," *IEEE Trans. Control Syst. Technol.*, vol. 11, no. 6, pp. 839–849, Nov. 2003.

[16] R. Finesso, E. Spessa, and M. Venditti, "An unsupervised machine-learning technique for the definition of a rule-based control strategy in a complex HEV," *SAE Int. J. Alternative Powertrains*, vol. 5, no. 2, pp. 308–327, Apr. 2016.

[17] Y. Zhang, C. Guo, G. Li, Y. Liu, and Z. Chen, "Cooperative control strategy for plug-in hybrid electric vehicles based on a hierarchical framework with fast calculation," *J. Cleaner Prod.*, vol. 251, Apr. 2020, Art. no. 119627.

[18] D. Ambuhl and L. Guzzella, "Predictive reference signal generator for hybrid electric vehicles," *IEEE Trans. Veh. Technol.*, vol. 58, no. 9, pp. 4730–4740, Nov. 2009.

[19] S. Han, F. Zhang, and J. Xi, "A real-time energy management strategy based on energy prediction for parallel hybrid electric vehicles," *IEEE Access*, vol. 6, pp. 70313–70323, 2018.

[20] S. Wang, X. Huang, J. M. López, X. Xu, and P. Dong, "Fuzzy adaptive-equivalent consumption minimization strategy for a parallel hybrid electric vehicle," *IEEE Access*, vol. 7, pp. 133290–133303, 2019.

[21] Y. Zhang, L. Chu, Y. Ding, N. Xu, C. Guo, Z. Fu, L. Xu, X. Tang, and Y. Liu, ''A hierarchical energy management strategy based on model predictive control for plug-in hybrid electric vehicles,'' *IEEE Access*, vol. 7, pp. 81612–81629, 2019.
[22] M. S. Khan, I. Ahmad, H. Armaghan, and N. Ali, ''Backstepping sliding mode control of FC-UC based hybrid electric vehicle,'' *IEEE Access*, vol. 6, pp. 77202–77211, 2018.
[23] R. S. Vadamalu and C. Beidl, ''Online MPC based PHEV energy management using conic interior-point methods,'' in *Proc. IEEE Intell. Vehicles Symp. (IV)*, Jun. 2016, pp. 466–471.
[24] M. Carignano, V. Roda, R. Costa-Castelló, L. Valiño, A. Lozano, and F. Barreras, ''Assessment of energy management in a fuel cell/battery hybrid vehicle,'' *IEEE Access*, vol. 7, pp. 16110–16122, 2019.
[25] M. Suhail, I. Akhtar, S. Kirmani, and M. Jameel, ''Development of progressive fuzzy logic and ANFIS control for energy management of plug-in hybrid electric vehicle,'' *IEEE Access*, vol. 9, pp. 62219–62231, 2021.
[26] H. Lee, C. Song, N. Kim, and S. W. Cha, ''Comparative analysis of energy management strategies for HEV: Dynamic programming and reinforcement learning,'' *IEEE Access*, vol. 8, pp. 67112–67123, 2020.
[27] H. Lee, C. Kang, Y.-I. Park, N. Kim, and S. W. Cha, ''Online data-driven energy management of a hybrid electric vehicle using model-based Q-learning,'' *IEEE Access*, vol. 8, pp. 84444–84454, 2020.
[28] G. R. Guercioni, E. Galvagno, A. Tota, and A. Vigliani, ''Adaptive equivalent consumption minimization strategy with rule-based gear selection for the energy management of hybrid electric vehicles equipped with dual clutch transmissions,'' *IEEE Access*, vol. 8, pp. 190017–190038, 2020.
[29] V. Ngo, T. Hofman, M. Steinbuch, and A. Serrarens, ''Optimal control of the gearshift command for hybrid electric vehicles,'' *IEEE Trans. Veh. Technol.*, vol. 61, no. 8, pp. 3531–3543, Oct. 2012.
[30] F. Meier and F. Willems, ''Multi-level integrated energy and emission management for HEVs cold start operation,'' in *Proc. Eur. Control Conf. (ECC)*, Jul. 2022, pp. 1198–1203.
[31] M. Razi, N. Murgovski, T. McKelvey, and T. Wik, ''Predictive energy management of hybrid electric vehicles via multi-layer control,'' *IEEE Trans. Veh. Technol.*, vol. 70, no. 7, pp. 6485–6499, Jul. 2021.
[32] Y. Wu, Y. Zhang, G. Li, J. Shen, Z. Chen, and Y. Liu, ''A predictive energy management strategy for multi-mode plug-in hybrid electric vehicles based on multi neural networks,'' *Energy*, vol. 208, Oct. 2020, Art. no. 118366.
[33] Y. Shang, D. Li, Z. Peng, A. Heydari, K. Turkoglu, and J. Thunberg, ''IEEE access special section editorial: Recent developments in consensus problems for complex networked systems,'' *IEEE Access*, vol. 6, pp. 60993–60995, 2018.
[34] L. Guzzella and A. Sciarretta, *Vehicle Propulsion Systems: Introduction to Modeling and Optimization*. Berlin, Germany: Springer, Jan. 2007.
[35] S. Pelletier, O. Jabali, G. Laporte, and M. Veneroni, ''Battery degradation and behaviour for electric vehicles: Review and numerical analyses of several models,'' *Transp. Res. B, Methodol.*, vol. 103, pp. 158–187, Sep. 2017.

ALEXIS BENAITIER received the Diplome d'Ingnieur (equivalent to M.Sc.) degree in mechanical engineering (energy, propulsion, electricity, and environment) from ISAT Nevers, France, in 2019.

Since 2020, he has been a Project Assistant with the Christian Doppler Laboratory for Innovative Control and Monitoring of Automotive Powertrain Systems, TU Wien. His current research interests include nonlinear system modeling, control, and optimization.

FERDINAND KRAINER received the Diploma (FH) degree in electronics and the M.Sc. degree in control system design, in 2004 and 2013, respectively.

Since 2004, he has been working on various automotive control areas, such as combustion engines, transmission systems, and hybrid powertrains and on a vehicle level with AVL List GmbH. Since 2018, he has been a Technical Expert on control system design focusing also on optimal nonlinear and predictive control topics.

STEFAN JAKUBEK received the M.Sc. degree in mechanical engineering, the Ph.D. degree in technical sciences, and the Habilitation (Professorial Qualification) degree in control theory and system dynamics from TU Wien, Vienna, Austria, in 1997, 2000, and 2007, respectively.

From 2006 to 2009, he was the Head of the Development for Hybrid Powertrain Calibration and Battery Testing Technology, AVL List GmbH, Graz, Austria (automotive industry company). He is currently a Professor and the Head of the Institute of Mechanics and Mechatronics, TU Wien. His research interests include fault diagnosis, nonlinear system identification, and simulation technology.

CHRISTOPH HAMETNER received the M.Sc. degree in mechanical engineering, the Ph.D. degree in technical sciences, and the Habilitation (Professorial Qualification) degree in control theory and system dynamics from TU Wien, Vienna, Austria, in 2005, 2007, and 2014, respectively.

He is currently the Head of the Christian Doppler Laboratory for Innovative Control and Monitoring of Automotive Powertrain Systems, TU Wien. His research interests include nonlinear system identification, modeling, and control.

2.2 Publication B

Alexis Benaitier, Ferdinand Krainer, Stefan Jakubek and Christoph Hametner
Optimal energy management of hybrid electric vehicles considering pollutant emissions during transient operations
Applied Energy, Vol. 344 (2023), page 121267
DOI: 10.1016/j.apenergy.2023.121267

Authors' contribution †

- A. Benaitier: Conceptualization, Methodology, Software, Validation, Formal analysis, Investigation, Resources, Data Curation, Writing - Original Draft, Writing - Review & Editing, Visualization
- F. Krainer: Validation, Investigation, Resources, Writing - Review & Editing, Visualization
- S. Jakubek: Review & Editing, Supervision, Project administration, Funding acquisition
- C. Hametner: Conceptualization, Validation, Review & Editing, Supervision, Project administration, Funding acquisition

† According to Contributor Roles Taxonomy (CRediT)

Applied Energy 344 (2023) 121267

Contents lists available at ScienceDirect

Applied Energy

journal homepage: www.elsevier.com/locate/apenergy

Optimal energy management of hybrid electric vehicles considering pollutant emissions during transient operations

Alexis Benaitier [a,*], Ferdinand Krainer [b], Stefan Jakubek [c], Christoph Hametner [a]

[a] Christian Doppler Laboratory for Innovative Control and Monitoring of Automotive Powertrain Systems, TU Wien, Getreidemarkt 9, 1060, Vienna, Austria
[b] AVL List GmbH, Hans-List-Platz 1, 8020, Graz, Austria
[c] Institute of Mechanics and Mechatronics, TU Wien, Getreidemarkt 9, 1060, Vienna, Austria

ARTICLE INFO

Keywords:
Energy management system
Hybrid electric vehicle
Optimal control
Pontryagin's maximum principle
Transient pollutant emissions

ABSTRACT

The reduction of fossil-fuel vehicles' pollutant emissions has been improved with exhaust aftertreatment systems and, more recently, with electric hybridization. Indeed, hybrid electric vehicles (HEVs) can shift engine operating points toward low fuel consumption and pollutant emissions regions. Also, engine transient operations have already been shown to impact pollutant emissions negatively. As a result, the electric motor can be additionally used to reduce the engine transient operations. The engine optimal control, i.e., minimizing fuel consumption and pollutant emissions, must consequently consider the engine transient dynamics. Therefore, this paper introduces a parametric approximation of the optimal engine control variable based on a weighted sum of smooth basis functions to directly consider transient engine dynamics and guarantee smooth engine operations. Two approaches are presented and compared to find the parametric approximation of the engine control, minimizing fuel consumption and pollutant emissions. The proposed direct and indirect approaches rely on polynomial approximations of the vehicle components' models, leading to efficient quadratic programming algorithms. In this paper, a high-fidelity simulation platform of a heavy-duty HEV is employed to calibrate the controller model and then compare it to classical control methods. The results from the proposed minimization approaches are shown to be close to the dynamic programming optimality, yet being much faster alternatives.

1. Introduction

Hybrid electric vehicles (HEVs) are currently the preferred solution to reduce on-road vehicles' fuel consumption and pollutant emissions [1]. In combination with aftertreatment systems that have continuously improved for several decades, modern vehicles already achieve the current emissions target but need further improvement to comply with future targets. Also, alternative fuels are now considered to partially replace conventional diesel, but lead to higher CO and NO_x pollutant emissions [2] as well as particle number [3], especially during transient engine operations [4]. In order to further decrease the pollutant emissions of HEVs without complexifying their hybrid or aftertreatment architecture, the engine needs to be precisely controlled.

Hybridization of fossil fuel vehicles adds a degree of freedom corresponding to splitting the power demand between fossil and electric sources. Therefore, the engine operating points can be shifted to low fuel and emissions regions, and the engine transient operations can be reduced. As such, a large battery and a powerful electric motor are beneficial to avoid transient engine operations but are inherently heavy and expensive. As a result, modern vehicles use a small battery and an electric motor that cannot guarantee electric-only operations during large accelerations, leading to more dynamic engine operations [5]. This paper proposes to use a smooth parametric approximation of the engine control to efficiently reduce the engine transient operations toward fewer pollutant emissions while guaranteeing low fuel consumption.

The engine-out emissions depend primarily on the engine operating point, i.e., engine speed and load, but also on the variation of the engine operating point. Indeed, for turbocharged diesel engine, the turbo lag makes the air fuel ratio difficult to control during transient engine operations, leading to high NO_x [4] as well as soot emissions [6,7]. As measured by [8] on a turbocharged diesel engine, the NO_x and particulate emissions increase when the driver load demand jumps from minimum to maximum. Multiple other authors made the same observation, that the NO_x, particulate, and soot emissions are higher during fast variations of the engine operating point [7] or during engine restart [9], and study the impact of considering these transient

* Corresponding author.
E-mail address: alexis.benaitier@tuwien.ac.at (A. Benaitier).

https://doi.org/10.1016/j.apenergy.2023.121267
Received 19 December 2022; Received in revised form 16 March 2023; Accepted 9 May 2023
Available online 19 May 2023

phases [10]. As a consequence, transient engine operations need to be considered when estimating pollutant emissions as they represent a large part of the overall cumulative emissions. Mera et al. [11] measured a possible NO_x reduction in the range of 30 to 80 %. Also, using machine learning [12] or a semi empirical model [13], both considering NO_x transient emissions has been shown to be more accurate than standard quasi-static emissions models.

Several models have already been proposed to capture the engine-out emissions during transient engine operations. A classical method is to add a correction to a quasi-static emissions model during transient engine operations [14]. The air-fuel equivalence ratio is, for example, used by [15,16] to correct the quasi-static estimate of several pollutant emissions, with transient emissions being up to 50 % higher than the quasi-static estimate [15]. More recently, [17] created a neurofuzzy modeling tree using the estimated emissions at the previous time step to estimate the current emissions.

Using experimental data, [18] observed that the derivative of the engine torque engenders a quasi-linear increment in the emissions of NO_x and unburned hydrocarbons. Also, [3] measured that the particulate emissions are increased during varying engine torque, and are higher for alternative fuels than for regular diesel. To accurately predict transient pollutant emissions a transient emissions correction to a quasi-static emissions model has been proposed with a weighting factor depending on the engine speed derivative and torque derivative [6] or the engine power derivative [7]. Approximating the engine torque derivative with the torque increment results in a precise estimation of the transient emissions and therefore should to be considered for optimal engine control [19].

Although multiple methods exist to minimize fuel consumption and quasi-static emissions, they must be modified to consider transient engine operations. For example, the Pontryagin's maximum principle (PMP) [20] is classically employed to minimize the fuel and quasi-static emissions [21], but cannot directly account for the transient emissions. Indeed, for a dynamic engine model, e.g., considering the engine torque derivative, the PMP solution will need to be computed with at least one additional state and states' constraints. Directly reusing a classical PMP formulation with a dynamic engine model is not straightforward and has yet to be documented.

The concept of *input smoothing* proposed by [22,23] can be used to filter the PMP solution, i.e., without directly considering the engine torque derivative. The engine torque variations from the PMP can be reduced with a simple filter or an advanced rule-based method. Also, the smoothing algorithm needs to fulfill the engine torque constraints and keep the battery state of charge close to the PMP reference. In that sense, [24] uses PMP for fuel optimality and a rule-based controller to reduce the soot emissions further.

Dynamic programming (DP) [25] is another method for HEV control. Always leading to an optimal control policy, DP has already been employed to minimize fuel consumption and transient emissions [26,27]. DP can inherently consider states' constraints, making its implementation with a dynamic engine model straightforward. For example, [19] showed that using DP with a transient soot emissions model based on the engine torque derivative leads to a better fuel economy for the same amount of emissions compared to a strategy considering only quasi-static emissions. Similarly, [17] showed the advantages of using DP and a neurofuzzy modeling tree to estimate the transient emissions, to minimize the fuel, the NO_x and the soot emissions.

The main difficulty with DP lies in its computational complexity. First, a state must be added to consider the engine dynamic. And second, the sampling time must be kept small enough to capture the engine torque derivative accurately. In that sense, [10] used DP only with a quasi-static map for fuel efficiency and then locally implemented a linear quadratic regulator [25] to consider transient emissions.

Engine transient operations need to be considered to estimate pollutant emissions accurately. Nevertheless, efficiently considering a dynamic engine model for fuel consumption and emissions minimization

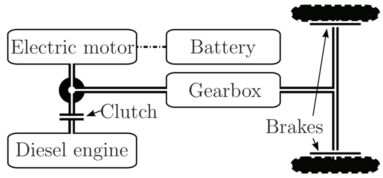

Fig. 1. Diagram of the hybrid electric vehicle powertrain and driveline.

is still challenging. Rule-based methods can be employed but do not guarantee optimality. And DP leads to optimal control but at a very high computational cost hindering a practical implementation. A control method leading to low fuel consumption and smooth engine operations to minimize transient emissions would constitute an appreciable step toward cleaner HEVs. Additionally, the proposed algorithm should remain simple enough to allow synergies with the components-level controllers and the route-planning strategy.

This paper proposes a parametric approximation of the engine control using a weighted sum of smooth basis functions, to jointly minimize the fuel consumption and the pollutant emissions of an HEV during transient engine operations. With such a smooth representation of the engine control, two approaches are proposed and compared to minimize the fuel consumption, the NO_x, and the soot emissions; first using a direct approach and, second, adapting the standard PMP algorithm. These approaches rely on efficient quadratic programming techniques shown to achieve near DP optimality while being much faster alternatives, allowing large-scale study analysis [28,29].

A heavy-duty HEV employing a turbocharged diesel engine and a battery as main power sources is used to emphasize the proposed approaches' efficiency and low computational requirements. A high-fidelity simulation platform of the HEV is used to verify the modeling assumptions and show how close the results using the proposed approaches are to the DP results. This high-fidelity simulation platform is built using the AVL CRUISE™ M software [30] and calibrated from measurement data. The simulation platform employs a physical air path and a crank angle resolved engine model to accurately estimate fuel consumption and transient pollutant emissions.

Section 2 proposes a controller model relying on a dynamic engine model to accurately capture the transient emissions while ensuring a convenient model structure for the controller. The model estimated pollutant emissions is calibrated and validated using the high-fidelity simulation platform. A parametric approximation of the engine torque with smooth basis functions is introduced in Section 3. Also, two different approaches are proposed to estimate the parametric approximation minimizing fuel consumption and pollutant emissions. Both proposed approaches are shown to be close to DP optimality with only a fraction of its complexity in Section 4. The proposed method is also compared to DP using the high-fidelity simulation platform, showing that it is also robust against model inaccuracies.

2. Control-oriented model

A control-oriented model is proposed in this section and calibrated using the high-fidelity simulation platform to capture the fuel and emissions, especially during transient engine operations. The proposed nonlinear engine controller model and its polynomial counterpart directly consider the engine torque derivative to inherently account for the emissions during transient engine operations. The resulting control-oriented model is shown to be appropriate for an efficient control algorithm proposed in Section 3 and accurate enough to achieve almost optimal results in Section 4.

Table 1
Vehicle model parameters.

Coastdown coefficient	c_v^0	1413.42	N
Coastdown coefficient	c_v^1	3.24	N s m^{-1}
Coastdown coefficient	c_v^2	0.27	N s^2 m^{-2}
Vehicle mass	m_{veh}	30 100	kg

2.1. Vehicle model

In this paper, the investigated HEV configuration is depicted in Fig. 1, with the engine mechanically coupled to an automatic gearbox and to the electric motor with a reduction gear $r_{em} = 2$. The gear ratio is defined with a standard automatic gearbox scheduling algorithm based on the vehicle speed and required load to replicate feasible and coherent gearbox operations. The clutch is used to disconnect the engine from the transmission whenever the engine torque request is zero, hence for electric-only operations.

A backward approach is used to estimate the resulting force acting on the vehicle, considering that the vehicle follows a prescribed speed trajectory v_{veh}. The vehicle longitudinal force F_{veh} is therefore directly estimated from the vehicle speed and the road slope α_r,

$$F_{veh} = c_v^0 + m_{veh}\, g \sin(\alpha_r) + c_v^1 v_{veh} + c_v^2 v_{veh}^2 + m_{veh} \dot{v}_{veh}, \tag{1}$$

with the vehicle parameters detailed in Table 1 and g the gravitational constant.

The required gearbox torque, knowing the gearbox ratio r_{gbx}, is directly derived from the vehicle longitudinal force,

$$T_{gbx} = F_{veh} \frac{D_w}{2 r_{gbx}}, \tag{2}$$

with D_w the wheel diameter.

The engine torque T_{ice} combined with the electric motor torque T_{em}, needs to provide the desired gearbox torque from (2) at each instant,

$$T_{gbx} = T_{ice} + T_{em} r_{em} + T_{brk}. \tag{3}$$

The braking torque $T_{brk} \le 0$ is manually set to the torque difference between the gearbox required torque and the lowest possible electric motor torque to maximize the recuperated energy during deceleration.

2.2. Battery model

An accurate model of the battery dynamics and internal losses is necessary to evaluate the vehicle's energetic performance. The battery state of charge is therefore modeled as a first-order dynamic model based on an equivalent circuit approach that considers the battery internal resistance [31],

$$\dot{\xi} = -\frac{1}{2 R_0 Q_0} \left(U_0 - \sqrt{U_0^2 - 4 R_0 P_{bat}} \right), \tag{4}$$

with ξ the state of charge of the battery, $R_0 = 100\,\mathrm{m\Omega}$ its internal resistance, $Q_0 = 50\,\mathrm{A\,h}$ its capacity and $U_0 = 350\,\mathrm{V}$ the open circuit voltage. The battery power P_{bat} is a function of the electric motor torque and speed,

$$P_{bat} = \omega_{em} T_{em} \eta_{em} \left(N_{em}, T_{em} \right), \tag{5}$$

with the electric motor efficiency map $\eta_{em}\left(N_{em}, T_{em}\right)$.

For control purposes, the nonlinear battery model (4) is approximated by its second-order Taylor expansion around $P_{bat} = 0$,

$$\dot{\xi} = -\frac{1}{U_0 Q_0} P_{bat} - \frac{R_0}{U_0^3 Q_0} P_{bat}^2 + o(P_{bat}^3), \tag{6}$$

when the solver requires a quadratic model. Also, the battery state of charge dynamics is expressed as a function of the engine torque, as this variable will be selected as the control variable in Section 3.1. Using relation (3) the electric motor torque is a function of the gearbox and the engine torque, and the engine speed. Also, substituting (5) in (6), the battery state of charge dynamics is directly modeled from the engine torque,

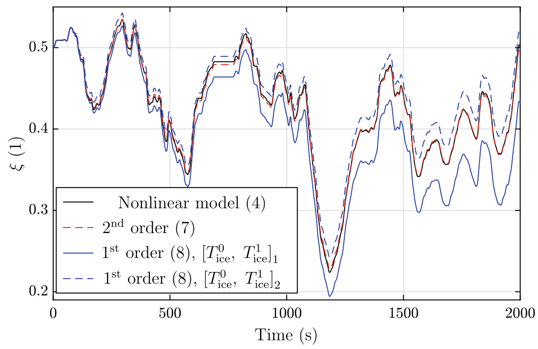

Fig. 2. State of charge estimation from polynomials of order one and two compared to the nonlinear battery model. With $[T_{ice}^0, T_{ice}^1]_1 = [0, 1500]\,\mathrm{Nm}$ and $[T_{ice}^0, T_{ice}^1]_2 = [350, 530]\,\mathrm{Nm}$.

$$\dot{\xi} = C_2^0 + C_2^1 T_{ice} + C_2^2 T_{ice}^2 + o\left(T_{ice}^3\right), \tag{7}$$

where C_2^0, C_2^1 and C_2^2 are parameters varying with the engine speed and the desired gearbox torque.

Additionally, the battery state of charge dynamics (4) can be estimated by fitting a linear model to (7), using the least-squares method on an interval $[T_{ice}^0, T_{ice}^1]$,

$$\dot{\xi} = C_1^0 + C_1^1 T_{ice} + o\left(T_{ice}^2\right), \tag{8}$$

where C_1^0 and C_1^1 vary with the engine speed and the desired gearbox torque. This linearization can be quite inaccurate if the interval $[T_{ice}^0, T_{ice}^1]$ is large or if the battery capacity is small in comparison to the admissible battery power. Although the accuracy of the linearized battery state of charge dynamics is not very accurate, it will be shown in Section 3 to be convenient for efficient control algorithms.

For the considered heavy-duty vehicle, the state of charge linearization with a second-order polynomial (7) is sufficiently accurate as shown in Fig. 2. A first-order approximation considering the full engine load range is, however, not accurate enough to reach a predefined target state of charge. As illustrated in Fig. 2, the linearization range $[T_{ice}^0, T_{ice}^1]$ can be narrowed around the most used engine torque range, i.e., $[T_{ice}^0, T_{ice}^1]_2 = [350, 530]\,\mathrm{Nm}$, resulting in a better estimate but with a low accuracy outside of this engine operating region.

2.3. Engine model

The engine fuel consumption and pollutant emissions must be sufficiently well approximated to precisely control the engine torque. The engine fuel map depends on the engine speed N_{ice} and torque T_{ice},

$$\dot{m}_{fuel} = \Psi_{fuel}\left(N_{ice}, T_{ice}\right), \tag{9}$$

and is calibrated using results data from stationary operating points in the high-fidelity simulation platform.

The engine pollutant emissions are also modeled with maps depending on the engine speed and torque, but further consider the derivative of the engine torque to capture the transient behaviors of the engine,

$$\dot{m}_{emi} = \Psi_{emi}\left(N_{ice}, T_{ice}\right)\left(1 + K_{emi} \dot{T}_{ice}^2\right), \tag{10}$$

where $K_{emi} \ge 0$ depends on the engine speed.

To apply efficient algorithmic techniques, i.e., quadratic programming (QP), the fuel consumption (9) and the pollutant emissions (10) need to be expressed as second-order polynomials of the input and

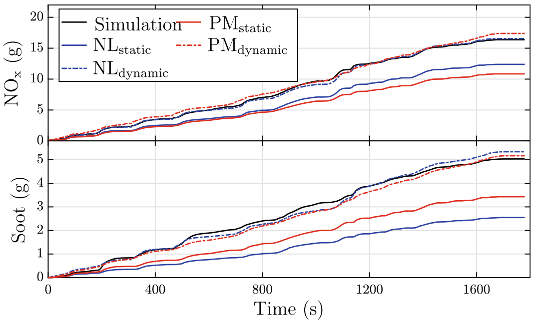

Fig. 3. Cumulative emissions using the high-fidelity simulation platform, and estimated by the nonlinear (NL) and polynomial (PM) models with and without transient correction.

its derivative. The static fuel map Ψ_{fuel} is therefore expressed as a second-order polynomial of the engine torque,

$$\dot{m}_{\text{fuel}} = C^0_{\text{fuel}} + C^1_{\text{fuel}} T_{\text{ice}} + C^2_{\text{fuel}} T^2_{\text{ice}} + o(T^3_{\text{ice}}), \tag{11}$$

with the parameters C^0_{fuel}, C^1_{fuel} and C^2_{fuel} function of the engine speed. The emissions from (10) are also approximated with a second-order polynomial model of the input but further include its first derivative,

$$\dot{m}_{\text{emi}} = C^0_{\text{emi}} + C^1_{\text{emi}} T_{\text{ice}} + C^2_{\text{emi}} T^2_{\text{ice}} + C^3_{\text{emi}} \dot{T}^2_{\text{ice}} + o(T^3_{\text{ice}}, \dot{T}^3_{\text{ice}}). \tag{12}$$

The first derivative is only considered in a quadratic form, as the emissions tend to be higher during both positive and negative engine torque variations [18].

The nonlinear (10) and polynomial (12) emissions models need to be further filtered to capture the instantaneous transient emissions. A first-order linear filter with a time delay $\tau > 0$ is therefore employed to reproduce the instantaneous emissions correctly,

$$\Gamma(s) = \frac{\omega}{s+\omega} e^{-\tau s}, \tag{13}$$

in the frequency domain where s represents the Laplace variable and with $\omega > 0$.

The filtered nonlinear (10) and polynomial (12) emissions models and their respective filter (13) parameters are calibrated using results from the high-fidelity simulation platform. Although the identified filter (13) is needed for calibrating (10) and (12), it is not convenient for the controller due to its additional dynamics, and not useful for estimating the cumulative emissions. Indeed, the cumulative emissions estimated with or without the filter (13) are identical as detailed in Appendix. The filter is considered in this section for model calibration, but will not be used by the controller as only the cumulative emissions are of interest.

The filter (13) and the coefficients related to the input derivative in (10) and (12) are calibrated to match the transient results obtained from the high-fidelity simulation platform. Compared to the static estimation, i.e., without considering the engine torque derivative, the dynamic estimation is more accurately captured. The resulting cumulative emissions shown in Fig. 3 over a transient vehicle trajectory are considerably higher when considering the input derivative and much closer to the actual high-fidelity simulation platform results. The proposed model cannot exactly match the high-fidelity simulation platform emissions but is able to accurately predict the cumulative emissions; which is of interest for an efficient controller.

To summarize, the nonlinear engine model corresponds to the fuel (9) and the emissions (10) models. And the polynomial model consists of second-order engine torque polynomials and its first derivative for the fuel (11) and emissions (12) estimate. Both of these models are calibrated using results from the high-fidelity simulation platform.

3. Optimal control with a parametric input approximation

This section details the optimal control problem (OCP) associated with the minimization of the fuel consumption and the pollutant emissions of the HEV detailed in Section 2. Also, a parametric approximation of the input as a linear sum of smooth basis functions is proposed so that the derivative of the engine torque is directly considered by the solver when estimating pollutant emissions. Two approaches are presented to find a solution to the OCP using the parametric approximation, i.e., a direct and an indirect approach, both relying on iterative QP algorithms. The proposed method is shown in Section 4 to be very close to DP optimality while needing to solve only a few QP algorithms.

3.1. Optimal control problem

The OCP associated with the HEV Fig. 1, corresponds to finding the optimal engine torque so that the fuel consumption and the pollutant emissions are minimized. In the following, the OCP is described using the standard formalism of control theory.

The battery state of charge is the only state

$$x(t) = \xi(t), \tag{14}$$

and the engine torque is selected as the input

$$u(t) = T_{\text{ice}}(t), \tag{15}$$

both being function of the time $t \in [t_0, t_1]$.

The state dynamics described in (4) is written as

$$\dot{x}(t) = \mathrm{f}(x(t), u(t)). \tag{16}$$

Additionally, the battery state of charge needs to remain within a predefined operating range

$$x(t) \in [x_{\min}, x_{\max}], \tag{17}$$

and the final state of charge should converge to a predefined value $\bar{\xi}$, to allow a straightforward comparison between controllers,

$$x(t_1) = \bar{\xi}. \tag{18}$$

The input is constrained by time-varying lower and upper bounds to account for the engine and electric motor torque limitations, and given that (3) must hold at each time,

$$u(t) \in [u_{\min}(t), u_{\max}(t)]. \tag{19}$$

The objective function corresponds to a linear weighting of the fuel and the emissions

$$J(x(t), u(t)) = \int_{t_0}^{t_1} l(x(t), u(t))\, \mathrm{d}t, \tag{20}$$

$$\begin{aligned} l(x(t), u(t)) = {} & (1-\beta_1)(1-\beta_2)\, \dot{m}_{\text{fuel}}(x(t), u(t)) + \\ & \beta_1 (1-\beta_2/2)\, \dot{m}_{\text{NO}_x}(x(t), u(t)) + \\ & (1-\beta_1/2)\, \beta_2 \dot{m}_{\text{soot}}(x(t), u(t)), \end{aligned} \tag{21}$$

with the fuel-to-NO$_x$ and fuel-to-soot trade-off parameters $\beta_1 \in [0,1]$ and $\beta_2 \in [0,1]$.

The OCP is summarized as

$$\text{OCP}: \begin{cases} \min\limits_{u(t)} J(x(t), u(t)) \\ u(t) \in [u_{\min}(t), u_{\max}(t)] \\ x(t) \in [x_{\min}, x_{\max}] \\ \dot{x}(t) = \mathrm{f}(x(t), u(t)) \\ x(t_1) = \bar{\xi} \end{cases}, \tag{22}$$

where the control task is to find u, i.e., the engine torque trajectory minimizing the objective function J.

Dynamic programming can be used to solve the OCP (22) with a finite difference scheme to estimate the input derivative for the selected emissions model (10) or (12). The resulting DP algorithm requires a fine time discretization, implying a large number of input control actions to be determined, leading to a high computational cost, as shown in Section 4.

The following section proposes a parametric approximation of the input u as a weighted sum of smooth basis functions to solve the OCP (22). The resulting input is, therefore, *smooth*, i.e., infinitely differentiable, and the input derivative is directly known from the basis functions derivatives.

3.2. Parametric input approximation with basis functions

The OCP (22) is not only a function of the input but also its first time derivative. Even though different numerical methods exist to approximate the derivative of a signal, the time discretization needs to be chosen sufficiently small to provide an accurate estimate of the input derivative.

Furthermore, most optimization algorithms, dynamic programming, PMP, or nonlinear programming are usually employed in discrete time with a large enough sampling time to reduce the computational complexity. The resulting input trajectory needs to be re-sampled with methods such as spline interpolation. The obtained re-sampled input sometimes exhibits a derivative quite different from the one initially estimated by the solver, yet leading to non-optimal behaviors.

To circumvent all the numerical difficulties associated with estimating the input derivative and re-sampling the input, a parametrization with smooth basis functions is proposed. The input is expressed as a weighted sum of basis functions

$$u = \boldsymbol{\varphi}\boldsymbol{\theta} \tag{23}$$

with $\boldsymbol{\theta} \in \mathbb{R}^N$ the parametrization of the input trajectory approximation and N linearly independent functions

$$\boldsymbol{\varphi} = \left[\varphi_1, \dots, \varphi_N\right], \tag{24a}$$

$$\varphi_i : \mathbb{R} \to \mathbb{R}, \forall i \in \{1, 2, \dots, N\}. \tag{24b}$$

The parametric approximation (23) is advantageous as any kth derivative of the input u is expressed as

$$u^{(k)} = \boldsymbol{\varphi}^{(k)}\boldsymbol{\theta},\ \forall k \in \mathbb{N}^*, \tag{25}$$

where $\boldsymbol{\varphi}^{(k)}$ contains the kth derivative of each function φ_i defined in (24). Finding the optimal engine torque is now equivalent to finding the coefficients $\boldsymbol{\theta}$ weighting the basis functions $\varphi_k, \forall k \in \{1, \dots, N\}$.

The solver can consider a sampled version of the parametric approximation (23), with a time increment Δt. Collecting the values of each basis function at the sampling point $k\Delta t$ in a matrix $\hat{\boldsymbol{\varphi}}_k$, where the input at $k\Delta t$ is written as

$$u(k\Delta t) = \hat{\boldsymbol{\varphi}}_k\boldsymbol{\theta}. \tag{26}$$

The discrete parameterized approximation of the input (26) is also convenient when the input has to be re-sampled afterward. Indeed, knowing the parameter $\boldsymbol{\theta}$, the basis functions $\boldsymbol{\varphi}$ can be evaluated at any time t to recover $u(t)$ using (23).

In order to solve the OCP (22) with the discrete parametric input approximation (26), i.e., find the parameter vector $\boldsymbol{\theta}$, a direct or an indirect approach can be used. The direct approach has the advantage of providing sufficient conditions for optimality but its realization results in a nonlinear programming problem. The indirect approach only provides necessary conditions for optimality but with the advantage of resulting in a nonlinear programming algorithm with only a single decision variable. This paper compares both approaches, the implementation of the direct approach being detailed in Section 3.3 while the implementation of the indirect approach is described in Section 3.4.

3.3. Direct approach

In this section, the OCP (22) is proposed to be solved with a direct approach, using the parametric input approximation introduced in (26). This direct approach consists in directly trying to find the input parametrization $\boldsymbol{\theta}$ that minimizes the objective function (20) while fulfilling the constraints defined in (22). A polynomial approximation of the objective function and a linearization of all the constraints is proposed in this section so that a computationally efficient QP method is used instead of a generic nonlinear optimization method.

Considering the polynomial models for the fuel (11) and the emissions (12), the integrand of the objective function (21) is approximated around $t = k\Delta t$ resulting in the following quadratic approximation

$$l_k(\boldsymbol{\theta}) = \boldsymbol{\theta}^{\mathrm{T}}\boldsymbol{H}_k\boldsymbol{\theta} + \boldsymbol{g}_k^{\mathrm{T}}\boldsymbol{\theta} + h_k, \tag{27}$$

with $\boldsymbol{H}_k \in \mathbb{R}^{N\times N}$ being semi-positive definite, $\boldsymbol{g}_k \in \mathbb{R}^N$ and $h_k \in \mathbb{R}$. The objective function (20) is approximated applying a zero-order hold to l_k,

$$\hat{J}(\boldsymbol{\theta}) = \sum_k l_k(\boldsymbol{\theta})\,\Delta t. \tag{28}$$

The input constraints (19) are linearly dependent on the input and so on the variable $\boldsymbol{\theta}$. Using the first-order polynomial (7) to estimate the state of charge dynamic, the final state constraint (18) becomes a linear constraint with respect to $\boldsymbol{\theta}$. Both the input and final state constraints are written as

$$\mathbf{A}_1\boldsymbol{\theta} \le \mathbf{B}_1. \tag{29}$$

The OCP (22), assuming that no state constraint violation happens (17), and described with the parametric input approximation (26), is expressed as the following quadratic programming

$$\mathrm{OCP1}: \begin{cases} \min\limits_{(\boldsymbol{\theta})} \hat{J}(\boldsymbol{\theta}) \\ \mathbf{A}_1\boldsymbol{\theta} \le \mathbf{B}_1. \end{cases} \tag{30}$$

The assumption that the state ξ stays between the lower and upper bound defined in (17) is generally verified when the initial and final states are far away from the constraints.

To avoid a large state of charge deviation at the end due to the linearization of the state of charge dynamics (8), an iterative QP algorithm is proposed in Algorithm 1. First, the initial QP problem (30) is solved with the expected $\bar{\xi}$ in (32a) and using an initial heuristic solution estimated from the minimum and maximum allowable input torque

$$\boldsymbol{\theta}_{\mathrm{i}} = \left(\hat{\boldsymbol{\varphi}}_k^{\mathrm{T}}\hat{\boldsymbol{\varphi}}_k\right)^{-1}\hat{\boldsymbol{\varphi}}_k^{\mathrm{T}}\left(\frac{T_{\mathrm{ice}}^{\max}(k\Delta t) + T_{\mathrm{ice}}^{\min}(k\Delta t)}{2}\right). \tag{31}$$

Finally, the corresponding state of charge trajectory is computed with the resulting parametric input approximation, i.e., ψ in (32b) is defined from (26), (3), (5) and (4).

Based on the current deviation of the final state of charge, the boundary constraint $\bar{\xi}$ is artificially updated to define a virtual target for the final state of charge $\bar{\xi}^*$ (32c). Iteratively updating the QP solution with the new $\bar{\xi}^*$, this algorithm should converge to the expected boundary condition $\bar{\xi}$, up to a tolerance ξ_{tol}. To further reduce the computational time, the previous QP solution is reused as a guess for the current iteration (32d).

3.4. Indirect approach

A second approach is considered in this section to solve the OCP (22) using the parametric input approximation (26). This indirect approach is derived from the PMP, and contrary to the direct approach,

Algorithm 1 Iterative QP optimization for state of charge boundary satisfaction.

$\bar{\xi}^* \leftarrow \bar{\xi}$

$$\theta_{k=0} \leftarrow \mathrm{QP}\left(\bar{\xi}^*, \theta_\mathrm{i}\right) \tag{32a}$$

$$\xi_{k=0} \leftarrow \psi\left(\theta_{k=0}\right) \tag{32b}$$

$k \leftarrow 1$

While $\|\xi_{k-1}\left(t_1\right) - \bar{\xi}\| \geq \xi_\mathrm{tol}$

$$\bar{\xi}^* \leftarrow \bar{\xi}^* - \left(\xi_{k-1}\left(t_1\right) - \bar{\xi}\right) \tag{32c}$$

$$\theta_k \leftarrow \mathrm{QP}\left(\bar{\xi}^*, \theta_{k-1}\right) \tag{32d}$$

$$\xi_k \leftarrow \psi\left(\theta_k\right) \tag{32e}$$

$k \leftarrow k+1$

End While

it directly considers a second-order polynomial model for the state of charge (7) to satisfy (18).

The PMP consists of a set of necessary conditions for optimality. Fulfilling these conditions is usually enough to provide the optimal solution for vehicle energy management under the assumption that strong duality holds, e.g., when the Hamiltonian is a convex function of the input [21].

The parametric input approximation (26) is used again to ensure a smooth engine torque and to get an accurate estimate of its derivative. The objective function is discretized as in (28) and the linear input constraints (19) is written in the form

$$\mathbf{A}_2\theta \leq \mathbf{B}_2. \tag{33}$$

A so-called costate $\lambda(t) \in \mathbb{R}$ and the scalar-valued Hamiltonian H are introduced as follows

$$H(\theta, t) = l(\theta) + \lambda(t) f(\theta). \tag{34}$$

The costate dynamics is directly given as the partial differentiation of the Hamiltonian with respect to the state ξ,

$$\dot{\lambda} = -\nabla_\xi H. \tag{35}$$

Also, because the state ξ does not appear in the Hamiltonian, the costate is constant $\lambda(t) := \lambda$, hence H defined in (34) becomes a function of θ and λ only.

A solution to the OCP (22) needs to fulfill the PMP conditions, corresponding to the minimization of the Hamiltonian with a final boundary constraint on the state ξ,

$$\mathrm{OCP2}: \begin{cases} \min\limits_{(\theta,\lambda)} H(\theta, \lambda) \\ \mathbf{A}_2\theta \leq \mathbf{B}_2, \\ \xi\left(t_1\right) = \bar{\xi}. \end{cases} \tag{36}$$

To find a candidate solution, i.e., meeting the PMP necessary conditions (36), a shooting method is employed as shown in Algorithm 2. The *while* loop is used to find a value of λ such that the final state of charge is equal to $\bar{\xi}$, up to a tolerance ξ_tol. Within this loop, the secant method is used to update λ based on the state of charge difference between the end and the beginning of the cycle, refer to f_λ in (37d).

Thanks to the functional representation of the input (26), the minimization of the Hamiltonian is done for the entire trajectory with a QP algorithm (37e) corresponding to the minimization of (34) under the linear constraints (33). Furthermore, using an active-set method to solve the QP (37e), the parameters θ and the active constraints from the previous iteration Ω_{k-1} are reused to speed up the computation [32]. Indeed, for a small modification of the costate initial value, the QP optimal solution has almost the same set of active constraints and nearly identical optimal variables θ.

The initialization of the algorithm is of great importance for its fast convergence. The initial costate value λ_0 in (37a) is defined based on previous knowledge of the system and is therefore calibrated manually. The initial parametric input approximation θ_i in (37b) is estimated as for the direct approach, that is using the heuristic initial candidate solution (31). Also, initially, the set of active constraints is defined as empty in (37c), based on the assumption that θ_0 defines a feasible solution.

Algorithm 2 Shooting method for the PMP with basis functions.

$$\lambda_{k=0} \leftarrow \lambda_0 \tag{37a}$$

$$\theta_{k=0} \leftarrow \theta_\mathrm{i} \tag{37b}$$

$$\Omega_{k=0} \leftarrow \{\emptyset\} \tag{37c}$$

$k \leftarrow 1$

While $\|\xi_{k-1}\left(t_1\right) - \bar{\xi}\| \geq \xi_\mathrm{tol}$

$$\lambda_k \leftarrow \mathrm{f}_\lambda\left(\xi_{\{0,\dots,k-1\}}\left(t_1\right), \lambda_{\{0,\dots,k-1\}}, \bar{\xi}\right) \tag{37d}$$

$$\left\{\theta_k, \Omega_k\right\} = \mathrm{QP}\left(\bar{\xi}, \theta_{k-1}, \Omega_{k-1}\right) \tag{37e}$$

$k \leftarrow k+1$

End While

4. Simulation results

This section provides a detailed numerical analysis of the presented method, relying on a smooth engine torque parametrization, to minimize the fuel consumption and pollutant emissions of the considered HEV. The direct and indirect approaches detailed in Sections 3.3 and 3.4 are used to find the optimal input parametrization and are compared to the following classical methods to solve the OCP (22):

1. A standard PMP method, i.e., without considering transient emissions;
2. A filtered version of the PMP method referred to as PMP smooth, where the engine torque is filtered so that the engine torque transients are dampened;
3. A DP method with a second state added to estimate the engine torque derivative using a backward finite difference scheme (38a). Also, the transient emissions are evaluated with a discretized version of (10), where the current engine torque is evaluated from the current and past control variable (38b) to avoid unpenalized torque transient when the current input $T_\mathrm{ice}(k)$ is set to zero in (38c). And with $\hat{\psi}_\mathrm{emi}$ being whether the nonlinear (10) or the polynomial (12) emissions model.

$$\Delta T_\mathrm{ice}(k) = \frac{1}{\Delta t}\left(T_\mathrm{ice}(k) - T_\mathrm{ice}(k-1)\right) \tag{38a}$$

$$\overline{T_\mathrm{ice}}(k) = 0.5\left(T_\mathrm{ice}(k-1) + T_\mathrm{ice}(k)\right) \tag{38b}$$

$$\dot{m}_\mathrm{emi,DP}(k) = \hat{\psi}_\mathrm{emi}\left(N_\mathrm{ice}(k), \overline{T_\mathrm{ice}}(k), \Delta T_\mathrm{ice}(k)\right) \tag{38c}$$

For the numerical study, a cycle recorded on a passenger vehicle and corresponding to urban and extra-urban driving conditions is chosen, where transient emissions are usually high compared to a cycle with stabilized speed. The corresponding reference speed and altitude profile are shown in Fig. 4. Also, the emissions weighting coefficients defined in (21) are arbitrarily set to $\beta_1 = 0.6$ and $\beta_2 = 0.6$ to penalize the

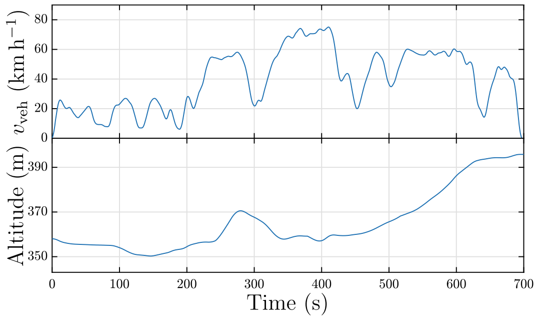

Fig. 4. Reference velocity and altitude profile of the considered cycle.

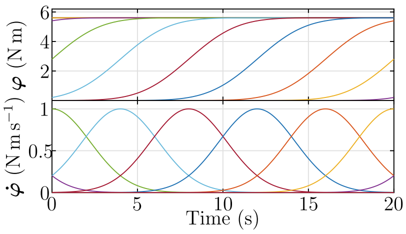

Fig. 5. Basis functions and their derivative, centered every 4 s, used for the first 20 s of the cycle Fig. 4.

fuel consumption, the NO_x, and the soot emissions concurrently. In Section 4.3, the weighting coefficients β_1 and β_2 are varying from 0 to 1 to emphasize the proposed method's consistency over various emissions weighting.

The method using a parameterized input approximation introduced in Section 3 is implemented with the direct and indirect approaches and compared to DP in Section 4.1 using the polynomial engine model described in Section 2. Then all the control methods are compared in Section 4.2 using the nonlinear engine model introduced in Section 2. The high-fidelity simulation platform is adapted in Section 4.4 to follow the reference of the different control methods. The results using this platform are presented and compared for all the control methods in Section 4.5.

4.1. Optimality analysis with the polynomial engine model

The practical implementation of the direct and indirect approaches proposed in Section 3 necessitates a choice of basis functions to represent the input, i.e., the engine torque. Integrated Gaussian functions, referred to as radial basis functions, are used in this study and shown in Fig. 5 along with their first derivative. The width of each basis function is manually defined to capture the highest engine torque dynamic, while the spacing between consecutive basis functions is manually calibrated to achieve a trade-off between optimality and complexity.

The DP and the direct and indirect approaches are compared in Fig. 6 using the polynomial engine model. The optimality of both proposed approaches is less than two percent higher than the DP optimality for a wide range of basis functions spacing, see ΔJ in Fig. 6. Nevertheless, the spacing between basis functions should not be too small to avoid numerical difficulties nor too large to prevent a lack of optimality. The basis functions will be spaced by 4 s for the rest of this study. The DP used in the comparison is sampled at 0.5 s, hence needs eight times more decision variables, resulting in a computational time around 100 times larger.

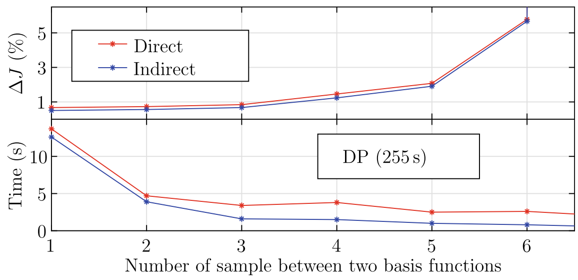

Fig. 6. Direct and indirect approach optimality and computational time compared to dynamic programming.

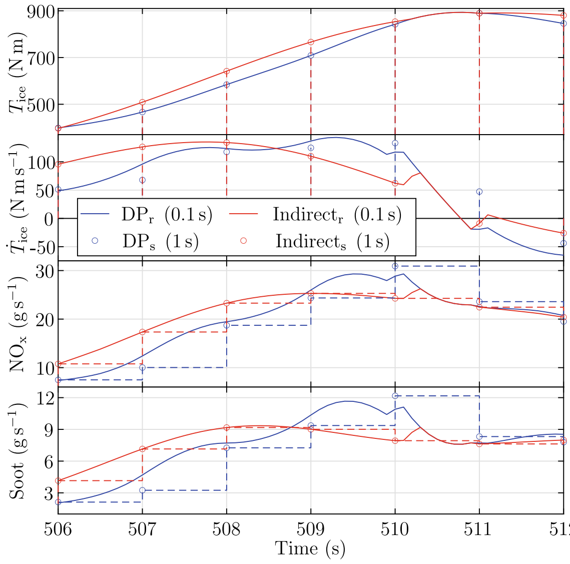

Fig. 7. Input derivative and emissions estimates; signals with subscript r represented with a solid line refer to re-sampled solutions, while the solvers estimate, with subscript s, are plotted at each iteration with a $\circ$. The dash line with a zero-order hold represents the solver estimated emissions.

The main advantage of the direct or indirect approach is the accurate estimation of the input derivative. Indeed, by comparison, when the DP sampling time is set to 1 s, the final objective increases by 2.5 %. Especially when the reference trajectory is re-sampled with a spline interpolation method to deliver a smooth trajectory, the DP estimated input derivative and the predicted emissions are no longer accurate. Fig. 7 emphasizes the DP inaccuracy, with a sampling time of 1 s, compared to the robust estimation of the input derivative when using the indirect approach.

The methods using basis functions to parameterize the input evaluate the exact input derivative at any evaluation point because the re-sampling is not done with an interpolation method but directly from the re-sampled basis functions. As shown in Fig. 7, even with a basis function centered every four sampling points, i.e., 4 s, the indirect approach provides a more accurate estimate of the emissions than the DP for the same sampling time of 1 s.

4.2. Results using the nonlinear engine model

In this section, the direct and indirect approaches are compared to the PMP, PMP smooth, and DP methods using the nonlinear engine model, i.e., the fuel (9) and the emissions (10) model. The engine torque from each method is re-sampled at 0.1 s using spline interpolation or using the re-sampled basis functions when applicable. The goal of this comparison is the analysis of the behavior of each method, especially with respect to DP that provides an optimal solution.

The results of the comparison of the different methods are synthetically given in Table 2; all the values are expressed relative to the PMP method. For example, smoothing the PMP reference contributes to reducing the emissions by a factor of almost two while keeping the same fuel consumption. This result is to be expected with the simple nonlinear engine model, as the PMP solution exhibits large torque transients.

Also, the nonlinear emissions model (10) is calibrated for realistic engine torque signal, i.e., the engine torque derivative is physically limited for a real engine. This study emphasizes the importance of generating a smooth engine torque trajectory, yet as discussed in Section 4.5, the engine torque from PMP will in any case be smoothed due to the engine inertia and its actuators dynamics. However, a more complex rule-based filtering of the PMP engine torque trajectory needs to be employed to always ensure that the expected final state of charge is reached. The filter parameters of the PMP smooth method are set for this example to achieve a trade-off between optimality and state of charge deviation from the expected final value.

The DP method is employed with a sampling time of 0.5 s to ensure an accurate estimate of the engine torque derivative, hence providing the optimal solution for this nonlinear engine model. Compared to the PMP smooth algorithm, the DP solution brings an additional 13 % improvement, with fewer emissions for slightly more fuel consumption. The main drawback of using a DP method is the significantly higher computational time compared to the PMP method, i.e., DP is more than 70 times slower than PMP.

Even though the polynomial engine model is slightly less accurate that the nonlinear engine model, the direct and indirect approaches exhibits the same objective function reduction as the DP method. Moreover, the main advantage of the direct or indirect approach is the reduced required computational effort compared to DP, still delivering results very close to the DP optimality. A reduced number of decision variables is possible thanks to the smooth representation of the input in (23). The DP needs a very fine sampling time to achieve the same smoothness of the engine operations, that is required for low pollutant emissions.

The proposed direct and indirect approaches both rely on an iterative QP algorithm; they are consequently very fast at approximating the optimal engine torque trajectory. The direct approach is already almost twice as fast as the PMP method. Indeed this approach converges within four QP iterations of around 0.3 s each, refer to Table 3. Adding the time to correct the nonlinear state of charge between each iteration, i.e., with Eq. (32e), the overall time is of 3.8 s. In comparison the PMP method needs around 9.5 s to meet the final conditions with the same tolerance. The PMP is slower mainly because it considers the nonlinear engine model, and it requires almost 20 iterations because a small modification of the costate initial value can engender a non-negligible modification of the state of charge at the end of the cycle due to the lack of smoothness of the solution.

The indirect approach is even faster, only requiring 1.5 s, because it relies only on the polynomial engine model and the second-order polynomial approximation of the state of charge. Additionally, the indirect approach requires only five QP iterations, as shown in Table 3, each iteration lasting 0.3 s initially but then only 0.02 s when the costate value is already close to the optimal one. These very fast QP iterations are made possible by providing the QP solver with the solution and the active set of constraints from the previous iteration, and because a small change in the costate only creates a small modification of the solution thanks to the smooth representation of the input.

Multiple model nonlinearities are not considered in the controller model, such as engine restart or the driver dynamic. Also, the controller model tends to exaggerate the transient engine torque influence on the

Table 2
Methods comparison evaluated with the nonlinear engine model, all values are given relative to the PMP method.

Method	Δfuel %	ΔNO_x %	Δsoot %	ΔJ %	Δtime %
PMP smooth	0.27	−41.55	−54.15	−40.91	10.7
DP	0.82	−54.19	−69.77	−53.07	7266.8
Indirect	1.40	−53.60	−68.90	−52.40	−84.2
Direct	1.09	−53.34	−69.01	−52.31	−60.0

Table 3
Timing in seconds of each iteration of Algorithms 1 and 2.

Iteration	1	2	3	4	5
Direct	0.31	0.33	0.31	0.32	
Indirect	0.29	0.37	0.24	0.02	0.02

emissions, as a real engine will always naturally produce a smoother torque than the one requested during strong transients. For these reasons, the different methods are tested on the high-fidelity simulation platform in the following sections.

4.3. Emissions weighting variations

The same simulation study as in Section 4.4 is conducted in this section, but with varying emissions' weighting. The weighting coefficients β_1 and β_2 are varied between 0 and 1 to respectively add more emphasis on the NO_x and the soot emissions. Fig. 8 shows the objective function improvement relative to the smooth PMP approach for the indirect and DP strategies.

The proposed indirect approach gives results very close to the DP optimality and, in most cases, much better than the PMP smooth strategy. The indirect approach fails to achieve the optimal strategy for small values of both β_1 and β_2. This specific case corresponds to almost no emissions weighting but only fuel consumption. In such a scenario, the optimal engine torque provided by PMP or DP is not continuous and exhibits large jumps. The proposed indirect approach works as expected whenever the emissions are considered; a standard PMP approach should be used instead for fuel-only optimization.

4.4. Reference following using the high-fidelity simulation platform

In the following sections, the same comparison as in Section 4.2 is realized but using the high-fidelity simulation platform. First, each method, i.e., PMP, PMP with smoothing, DP, direct and indirect approach from Section 3, is employed to create a reference engine torque T_{ice}^{ref} and a battery state of charge ξ^{ref} trajectory. Then these trajectories are followed in the high-fidelity simulation platform to evaluate the fuel consumption and pollutant emissions realistically.

A two-degree-of-freedom controller is employed to apply the reference engine torque while staying close to the reference battery state of charge. A slow feedback loop is used so that the engine torque and its derivative are only slightly modified to track the reference state of charge,

$$T_{ice} = T_{ice}^{ref}\left(1 - K\left(\xi - \xi^{ref}\right)\right), \tag{39}$$

with the manually calibrated parameter $K = 30$.

Additionally, the electric load is saturated to meet the electric motor's physical constraints, and the engine torque is consequently modified so that the total load request from the driver is always fulfilled. This controller is intentionally left simple to emphasize the robustness of the reference trajectory against the chosen modeling assumptions and allow additional rule-based controllers to locally modify this control law, e.g., coupling with the braking system.

The PMP reference defines the baseline as most current optimization methods only consider a quasi-static engine model. To penalize a state of charge difference with the prescribed boundary condition $\bar{\xi} = 0.5$, the

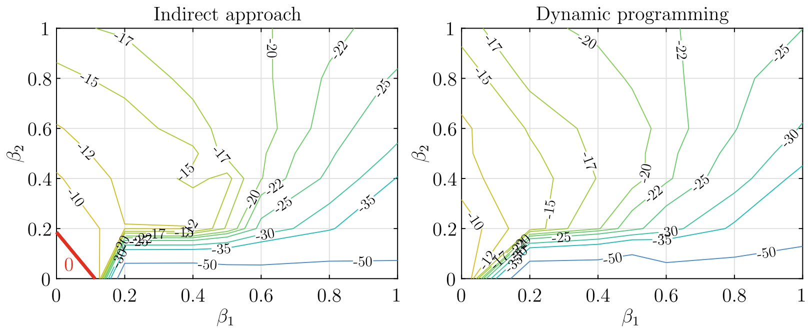

Fig. 8. Objective function improvement in % compared to PMP smooth method for various emissions weighting.

costate from the PMP method is used to correct the fuel consumption heuristically,

$$\dot{m}_{\text{fuel,corrected}} = \dot{m}_{\text{fuel}} + \lambda_{\text{PMP}} \left(\xi \left(t_1 \right) - \bar{\xi} \right). \quad (40)$$

4.5. Controller comparison using the high-fidelity simulation platform

Compared to the controller model with the nonlinear engine model, using the high-fidelity simulation platform, large variations of the reference engine torque cannot be followed. Indeed, the reference engine torque cannot always be immediately fulfilled because of the engine inertia and the physical limitations of the actuators. The simulation platform exhibits a low-pass filtering behavior, smoothing the reference torque input during strong transients. As a result, the PMP method is less impacted by transient emissions compared to the results using the nonlinear engine model (9) and (10), yet PMP is still far from optimality.

The performances of each controller on the cycle shown in Fig. 4 are provided in terms of deviation from the PMP results in Table 4. The most widely encountered method in literature corresponds to the PMP smooth method, which already achieves respectively 2.5 % and 4.6 % less NO_x and soot emissions for only 0.58 % fuel increase. The resulting objective, i.e., J, of the PMP method is decreased by 2.57 % only by using a low-pass filter on the reference trajectory. This result confirms the influence of the engine torque transients on pollutant emissions formation. The disadvantages of this method are, first the limiting smoothing possibilities because of input constraints and, second the lack of optimality.

Indeed, the DP solution reduces the objective by 7 % compared to the PMP method, which is more than twice as much as the smoothing method. Also, the DP has a large fuel over-consumption of 3.4 % but even larger NO_x and soot reduction of 9.8 % and 6.5 % respectively. The PMP method is indeed focusing too much effort on fuel reduction only. Without considering the engine torque derivative directly, the PMP smooth method lacks optimality due to excessive soot and NO_x formation during large engine torque fluctuations.

The proposed direct and indirect approaches, relying on a parametric input approximation with smooth basis functions, lead to nearly identical results. The same fuel consumption is reached, with slightly more NO_x and less soot for the direct approach compared to the indirect approach. Interestingly, the direct and indirect approaches achieve almost the same objective value as the DP but with more reduction of the soot emissions and less NO_x. These differences can be explained by the fact that the DP uses the nonlinear engine model, whereas the direct and indirect approaches are using the polynomial engine model. Therefore, the DP is able to take advantage of more precise engine operating points to reach local minima in the NO_x engine map. However, the DP reference torque trajectory, re-sampled with spline interpolation, is slightly less smooth than the direct and indirect approaches, leading to slightly higher soot emissions during transient operations.

Table 4
Methods comparison using the high-fidelity simulation platform, all values are given relative to the PMP method.

Method	Δfuel %	ΔNO_x %	Δsoot %	ΔJ %
PMP smooth	0.58	−2.57	−4.60	−2.57
DP (0.5 s)	3.40	−9.77	−6.46	−7.03
Indirect	3.68	−7.48	−10.71	−6.56
Direct	3.68	−6.48	−13.44	−6.57

The transient emissions are particularly high when the engine is restarted and under transient torque in a high torque region. As shown in Fig. 9, the NO_x emissions are much higher for the PMP and PMP smooth methods after each engine restart, e.g., around 825 m or 880 m. The soot emissions are not significantly impacted by the restart of the engine but are more pronounced when the engine torque is high and exhibits large fluctuations. This phenomenon is visible around 850 m and 900 m, where the soot emissions using the PMP reference are large and where the PMP smooth cannot efficiently reduce the engine torque variations.

Additionally, the reference trajectories have to be sufficiently smooth to be followed accurately in the high-fidelity simulation platform. In Fig. 9 the direct and indirect approaches, and the DP method, lead to a lower state of charge deviation than the PMP or the PMP smooth methods. Indeed, a non-smooth torque reference cannot be followed accurately due to engine time delay and inertia, resulting in a higher deviation from the reference battery state of charge.

The main advantage of the proposed method, based on a parametric input approximation, is the smoothness of the engine torque and battery state of charge trajectories. Also, the two proposed approaches relying on this smooth parametrization are computationally effective as they rely on simple polynomial fuel and emissions models. In the end, the fuel consumption and the pollutant emissions are shown to be very close to the DP results, yet using only a fraction of the time used by the DP algorithm.

5. Conclusion and outlook

In this paper, the engine torque is parameterized as a sum of radial basis functions such that its derivative is intrinsically considered to capture the transient emissions accurately. On the first hand, such a representation guarantees the input signal to be smooth. On the other hand, the input derivative is known analytically using the basis functions derivatives, and the input can be re-sampled without changing its derivative.

This paper proposes to find the optimal input parametrization with two different approaches to achieve minimal fuel consumption while reducing pollutant emissions. The proposed direct and indirect approaches benefit from iterative QP algorithms that are shown to be computationally efficient compared to more complex methods such as

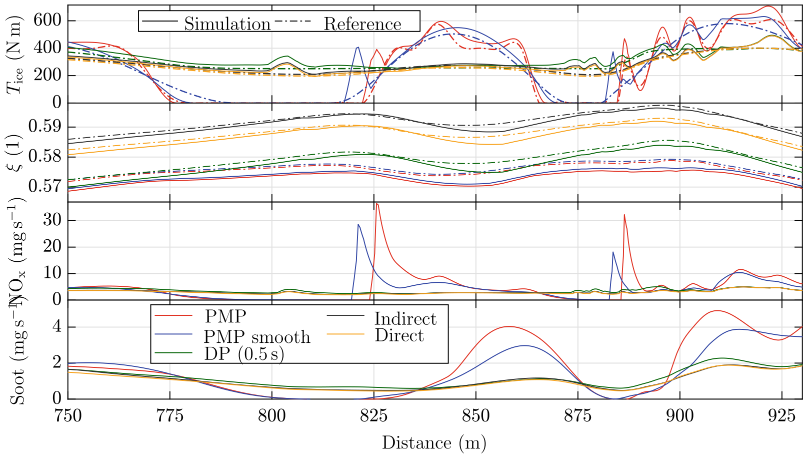

Fig. 9. Controller comparison using the high-fidelity simulation platform.

dynamic programming. Relying on a polynomial engine model, these methods are shown to achieve almost the same optimality as a dynamic programming algorithm, yet are much faster to compute as the number of decision variables is greatly reduced.

Further work is currently considered to combine the proposed methodology with the component controllers operating at a faster sampling rate. Indeed, the proposed controller creates reference signals that need to be followed by the electric machine and the engine. A hierarchical strategy could therefore be considered, where the component controllers could send feedback to the proposed strategy to account for system constraints and nonlinearities. The second point of future investigation is the beneficial synergy of the proposed method with ADAS systems and vehicle networking possibilities, as already demonstrated in [33,34]. Indeed, the proposed direct and indirect methods need an accurate prediction of future vehicle speed. In that sense, onboard sensors and vehicle-to-vehicle or vehicle-to-infrastructure communication will be highly beneficial to update predictive information. The proposed method has the further advantage of being very fast to update the optimal strategy whenever new predictive information is available.

CRediT authorship contribution statement

Alexis Benaitier: Conceptualization, Methodology, Software, Formal analysis, Investigation, Data curation, Writing – original draft. **Ferdinand Krainer:** Software, Validation, Investigation, Resources, Data curation, Writing – review & editing. **Stefan Jakubek:** Writing – review & editing, Project administration, Funding acquisition. **Christoph Hametner:** Validation, Resources, Writing – review & editing, Supervision, Project administration, Funding acquisition.

Declaration of competing interest

The authors declare that they have no known competing financial interests or personal relationships that could have appeared to influence the work reported in this paper.

Data availability

The authors do not have permission to share data.

Acknowledgments

The financial support by the Austrian Federal Ministry for Digital and Economic Affairs, the National Foundation for Research, Technology and Development, the Christian Doppler Research Association as well as AVL List GmbH, Austria is gratefully acknowledged.

Appendix. Integration of filtered emissions

This appendix shows that the cumulative modeled emissions m_{emi} from either (10) or (12), are unchanged when the modeled emissions are filtered with (13). For the simplicity of notation, the modeled emissions are renamed $f := \dot{m}_{\text{emi}}$.

Given that the modeled emissions are zero when the engine is stopped after some time $T > 0$,

$$f(t >= T) = 0, \tag{A.1}$$

the integration of $f(t)$ over the interval $I = [0, T]$ consequently verifies

$$\int_0^T f(t)\,\mathrm{d}t = \int_0^\infty f(t)\,\mathrm{d}t. \tag{A.2}$$

The integration of the emissions over an infinite time is given in the Laplace domain using the final value theorem,

$$\int_0^\infty f(t)\,\mathrm{d}t = \lim_{s\to 0}\left\{s\frac{1}{s}F(s)\right\}. \tag{A.3}$$

Using relation (A.2), the cumulative emissions are given as

$$\int_0^T f(t)\,\mathrm{d}t = F(s=0). \tag{A.4}$$

A first-order linear filter with a static gain of one and a delay $\tau \geq 0$ as expressed in (13) with $\omega > 0$, is used to filter the modeled emissions and is noted $\gamma(f(t))$ in the time domain.

Considering a time T^* such that $T^* \geq T + \tau$, the integral of the filtered modeled emissions can be decomposed into

$$\int_0^\infty \gamma(f(t))\,\mathrm{d}t = \int_0^{T^*} \gamma(f(t))\,\mathrm{d}t + \int_{T^*}^\infty \gamma(f(t))\,\mathrm{d}t. \tag{A.5}$$

Also, the integral on the left-hand side of (A.5) can be expressed in the s-domain, and using the final value theorem

$$\int_0^\infty \gamma(f(t))\,\mathrm{d}t = \lim_{s\to 0}\left\{s\frac{1}{s}\Gamma(s)F(s)\right\}. \tag{A.6}$$

Using the property that the filter γ has a static gain of one, the integral (A.6) becomes,

$$\int_0^\infty \gamma(f(t))\,\mathrm{d}t = F(s=0). \tag{A.7}$$

The initial claim can consequently be formulated for any $T^* \geq T + \tau$,

$$\int_0^T f(t)\,\mathrm{d}t = \int_0^{T^*} \gamma(f(t))\,\mathrm{d}t + \epsilon, \tag{A.8}$$

with

$$\epsilon = \int_{T^*}^{\infty} \gamma\,(f\,(t))\,\mathrm{d}t. \tag{A.9}$$

Also, from the filter definition (13) with $\omega > 0$, the filter is exponentially stable and the term ϵ in (A.8) can be expressed as a function of T^*

$$\epsilon = \frac{1}{\omega}\gamma\,(f\,(T+\tau))\exp^{-\omega(T^*-T-\tau)}. \tag{A.10}$$

As a conclusion, integrating the filtered modeled emissions $\gamma\,(f\,(T))$ over an interval $[0, T^*]$ is equal to the integral of the modeled emissions $f\,(t)$ over the interval I for high enough value T^*. Also, the difference between these two integrals, i.e., ϵ, is exponentially decaying with respect to T^* as shown in (A.10). It is therefore sufficient to set T^* to a few seconds after the engine is shut down.

References

[1] Conway G, Joshi A, Leach F, García A, Senecal PK. A review of current and future powertrain technologies and trends in 2020. Transp Eng 2021;5:100080. http://dx.doi.org/10.1016/j.treng.2021.100080.

[2] van Niekerk AS, Drew B, Larsen N, Kay PJ. Influence of blends of diesel and renewable fuels on compression ignition engine emissions over transient engine conditions. Appl Energy 2019;255:113890. http://dx.doi.org/10.1016/j.apenergy.2019.113890.

[3] Tan PQ, Ruan SS, Hu ZY, Lou DM, Li H. Particle number emissions from a light-duty diesel engine with biodiesel fuels under transient-state operating conditions. Appl Energy 2014;113:22–31. http://dx.doi.org/10.1016/j.apenergy.2013.07.009.

[4] Rakopoulos CD, Dimaratos AM, Giakoumis EG, Rakopoulos DC. Study of turbocharged diesel engine operation, pollutant emissions and combustion noise radiation during starting with bio-diesel or n-butanol diesel fuel blends. Appl Energy 2011;88:3905–16. http://dx.doi.org/10.1016/j.apenergy.2011.03.051.

[5] Huang Y, Wang H, Khajepour A, Li B, Ji J, Zhao K, et al. A review of power management strategies and component sizing methods for hybrid vehicles. Renew Sustain Energy Rev 2018;96:132–44. http://dx.doi.org/10.1016/j.rser.2018.07.020.

[6] Giakoumis EG, Lioutas SC. Diesel-engined vehicle nitric oxide and soot emissions during the European light-duty driving cycle using a transient mapping approach. Transp Res D 2010;15:134–43. http://dx.doi.org/10.1016/j.trd.2009.12.003.

[7] Giakoumis EG, Alafouzos AI. Study of diesel engine performance and emissions during a transient cycle applying an engine mapping-based methodology. Appl Energy 2010;87:1358–65. http://dx.doi.org/10.1016/j.apenergy.2009.09.003.

[8] Hagena JR, Filipi ZS, Assanis DN. Transient diesel emissions: Analysis of engine operation during a tip-in. SAE Tech Pap 2006 2006. http://dx.doi.org/10.4271/2006-01-1151.

[9] Rakopoulos C, Dimaratos A, Giakoumis E, Peckham M. Experimental assessment of turbocharged diesel engine transient emissions during acceleration, load change and starting. SAE Tech Pap 2010. http://dx.doi.org/10.4271/2010-01-1287.

[10] Wang Y, Zhang H, Sun Z. Optimal control of the transient emissions and the fuel efficiency of a diesel hybrid electric vehicle. Proc Inst Mech Eng D 2013;227:1546–61. http://dx.doi.org/10.1177/0954407013500661.

[11] Mera Z, Fonseca N, López JM, Casanova J. Analysis of the high instantaneous NOx emissions from euro 6 diesel passenger cars under real driving conditions. Appl Energy 2019;242:1074–89. http://dx.doi.org/10.1016/j.apenergy.2019.03.120.

[12] Maroto Estrada P, de Lima D, Bauer PH, Mammetti M, Bruno JC. Deep learning in the development of energy management strategies of hybrid electric vehicles: A hybrid modeling approach. Appl Energy 2023;329:120231. http://dx.doi.org/10.1016/j.apenergy.2022.120231.

[13] D'Ambrosio S, Finesso R, Fu L, Mittica A, Spessa E. A control-oriented real-time semi-empirical model for the prediction of NOx emissions in diesel engines. Appl Energy 2014;130:265–79. http://dx.doi.org/10.1016/j.apenergy.2014.05.046.

[14] Hausberger MS Ivanisin, Riemersma IJ. Modelling of transient influences on HDV emissions. SAE Tech Pap 2001. http://dx.doi.org/10.4271/2001-24-0076.

[15] Ericson C, Westerberg B, Egnell R. Transient emission predictions with quasi stationary models. SAE Tech Pap 2005. http://dx.doi.org/10.4271/2005-01-3852.

[16] Rakopoulos CD, Giakoumis EG. Diesel engine transient operation. London: Springer; 2009, p. 305–52. http://dx.doi.org/10.1007/978-1-84882-375-4.

[17] Johri R, Filipi Z. Optimal energy management of a series hybrid vehicle with combined fuel economy and low-emission objectives. Proc Inst Mech Eng D 2014;228:1424–39. http://dx.doi.org/10.1177/0954407014522444.

[18] Lindgren M, Hansson P. Effects of transient conditions on exhaust emissions from two non-road diesel engines. Biosyst Eng 2004;87:57–66. http://dx.doi.org/10.1016/j.biosystemseng.2003.10.001.

[19] Nüesch T, Wang M, Isenegger P, Onder CH, Steiner R, Macri-Lassus P, et al. Optimal energy management for a diesel hybrid electric vehicle considering transient PM and quasi-static NOx emissions. Control Eng Pract 2014;29:266–76. http://dx.doi.org/10.1016/j.conengprac.2014.01.020.

[20] L. P. Mishchenko R Gamkrelidze, EF, Pontryagin LS. Selected works volume 4. In: The mathematical theory of optimal processes, vol. 4. The mathematical theory of optimal processes, New York, London: Interscience Publishers John Wiley & Sons Inc.; 1962, http://dx.doi.org/10.1201/9780203749319.

[21] Kim N, Cha S, Peng H. Optimal control of hybrid electric vehicles based on Pontryagin's minimum principle. IEEE Trans Control Syst Technol 2011;19:1279–87. http://dx.doi.org/10.1109/TCST.2010.2061232.

[22] Schmied R, Stadlbauer S, Waschl H, Del Re L. Improving the transient emission performance of a diesel engine by input shaping techniques. In: 2015 54th A nnual conference of the society of instrument and control engineers of Japan. 2015, p. 1287–92. http://dx.doi.org/10.1109/SICE.2015.7285459.

[23] Grondin O, Thibault L, Quérel C. Energy management strategies for diesel hybrid electric vehicle. Oil Gas Sci Technol 2015;70:125–41. http://dx.doi.org/10.2516/ogst/2013215.

[24] Tribioli L, Bella G. Reduction of particulate emissions in diesel hybrid electric vehicles with a PMP-based control strategy. Energy Procedia 2018;148:994–1001. http://dx.doi.org/10.1016/j.egypro.2018.08.062.

[25] Naidu DS, Dorf RC. Optimal control systems. 1st ed. Boca Raton: CRC Press; 2003, http://dx.doi.org/10.1201/9781315214429.

[26] Serrao L, Sciarretta A, Grondin O, Chasse A, Creff Y, Di Domenico D, et al. Open issues in supervisory control of hybrid electric vehicles: A unified approach using optimal control methods. Oil Gas Sci Technol 2013;68:23–33. http://dx.doi.org/10.2516/ogst/2012080.

[27] Xie S, Hu X, Xin Z, Brighton J. Pontryagin's minimum principle based model predictive control of energy management for a plug-in hybrid electric bus. Appl Energy 2019;236:893–905. http://dx.doi.org/10.1016/j.apenergy.2018.12.032.

[28] Ritter A, Widmer F, Duhr P, Onder CH. Long-term stochastic model predictive control for the energy management of hybrid electric vehicles using Pontryagin's minimum principle and scenario-based optimization. Appl Energy 2022;322. http://dx.doi.org/10.1016/j.apenergy.2022.119192.

[29] Anselma PG. Computationally efficient evaluation of fuel and electrical energy economy of plug-in hybrid electric vehicles with smooth driving constraints. Appl Energy 2022;307:118247. http://dx.doi.org/10.1016/j.apenergy.2021.118247.

[30] AVL. AVL CRUISE™ M. 2022, https://www.avl.com/cruise-m. [Accessed 16 December 2022].

[31] Guzzella L, Sciarretta A. Vehicle propulsion systems: Introduction to modeling and optimization. Springer, Berlin, Heidelberg; 2007, http://dx.doi.org/10.1007/978-3-642-35913-2.

[32] Ferreau HJ, Kirches C, Potschka A, Bock HG, Diehl M. qpOASES: A parametric active-set algorithm for quadratic programming. Math Program Comput 2014;6:327–63. http://dx.doi.org/10.1007/s12532-014-0071-1.

[33] Chen Z, Wu S, Shen S, Liu Y, Guo F, Zhang Y. Co-optimization of velocity planning and energy management for autonomous plug-in hybrid electric vehicles in urban driving scenarios. Energy 2023;263:126060. http://dx.doi.org/10.1016/j.energy.2022.126060, https://www.sciencedirect.com/science/article/pii/S0360544222029462.

[34] Chen B, Evangelou SA, Lot R. Hybrid electric vehicle two-step fuel efficiency optimization with decoupled energy management and speed control. IEEE Trans Veh Technol 2019;68:11492–504. http://dx.doi.org/10.1109/TVT.2019.2948192.

2.3 Publication C

Alexis Benaitier, Stefan Jakubek, Ferdinand Krainer and Christoph Hametner

Automated nonlinear feedforward controller identification applied to engine air path output tracking

International Journal of Control, Vol. 1 (2023), pages 1-12
DOI: 10.1080/00207179.2023.2227740

Authors' contribution †

- A. Benaitier: Conceptualization, Methodology, Software, Validation, Formal analysis, Investigation, Data Curation, Writing - Original Draft, Writing - Review & Editing, Visualization
- S. Jakubek: Conceptualization, Validation, Writing - Review & Editing, Supervision, Funding acquisition
- F. Krainer: Validation, Formal analysis, Resources, Writing - Review & Editing
- C. Hametner: Conceptualization, Validation, Writing - Review & Editing, Supervision, Project administration, Funding acquisition

†According to Contributor Roles Taxonomy (CRediT)

International Journal of Control

ISSN: (Print) (Online) Journal homepage: www.tandfonline.com/journals/tcon20

Automated nonlinear feedforward controller identification applied to engine air path output tracking

Alexis Benaitier, Stefan Jakubek, Ferdinand Krainer & Christoph Hametner

To cite this article: Alexis Benaitier, Stefan Jakubek, Ferdinand Krainer & Christoph Hametner (27 Jun 2023): Automated nonlinear feedforward controller identification applied to engine air path output tracking, International Journal of Control, DOI: 10.1080/00207179.2023.2227740

To link to this article: https://doi.org/10.1080/00207179.2023.2227740

Published online: 27 Jun 2023.

INTERNATIONAL JOURNAL OF CONTROL
https://doi.org/10.1080/00207179.2023.2227740

Taylor & Francis
Taylor & Francis Group

OPEN ACCESS Check for updates

Automated nonlinear feedforward controller identification applied to engine air path output tracking

Alexis Benaitier [a], Stefan Jakubek[b], Ferdinand Krainer[c] and Christoph Hametner[a]

[a]Christian Doppler Laboratory for Innovative Control and Monitoring of Automotive Powertrain Systems, TU Wien Vienna, Vienna, Austria; [b]Institute of Mechanics and Mechatronics, TU Wien Vienna, Vienna, Austria; [c]AVL list GmbH, Graz, Austria

ABSTRACT
This paper introduces a feedforward control method for physical systems that can be described with linear parameter-varying (LPV) models. The proposed feedforward controller structure is consequently derived from a generic LPV representation and is shown to be identifiable directly from noisy measurement data. The identified structure is advantageous for feedforward control, as using a simple least squares algorithm allows to parameterise basis functions representing the required input trajectory to follow a given output trajectory. Also, with the proposed regularisation, the input trajectory remains bounded even when the physical system exhibits non-minimum phase behaviour. Additionally, the proposed controller structure does not possess states but only considers the inputs and outputs signals and their derivatives, leading to a unique physical interpretation of each controller's parameter. Multiple feedforward controllers identified at various operating points can therefore be directly merged to create a parameter-varying controller. A nonlinear and locally non-minimum phase system is considered in this study, i.e. an engine air path, to evaluate the performances of the proposed feedforward strategy. The controller parameters are first identified from noisy measurement data, and then the proposed feedforward controller is implemented with a feedback controller to track the exhaust pressure and NO_x concentration. Using a detailed physical simulation of the engine air path, the proposed feedforward strategy showed encouraging output tracking performances compared to state-of-the-art control methods. The presented feedforward method is shown to be straightforward to identify and calibrate while guaranteeing a contained computational complexity and being applicable to many physical systems thanks to its modularity.

ARTICLE HISTORY
Received 29 August 2022
Accepted 9 June 2023

KEYWORDS
Nonlinear feedforward; output tracking; predictive control; multivariate engine control

1. Introduction

Feedforward control is a classical and efficient method to enhance the performances of a feedback controller (Jean-Francois et al., 2009; Poe & Mokhatab, 2017; Zhang et al., 2022). However, no general method exists to identify a feedforward controller of an arbitrary nonlinear physical system. This paper proposes a controller structure that can be easily identified from measurement data and applied to any physical system that can be modelled as a linear parameter-varying (LPV) multi-input multi-output (MIMO) model. A diesel engine air path is taken as an example throughout this paper as multiple studies already successfully identified LPV MIMO models to capture its dynamics (Euler-Rolle et al., 2021; Kang & Shen, 2017; Ortner & Re, 2007; Zhang et al., 2022).

Physical systems potentially exhibit, without loss of generality, nonlinear dynamics, coupling behaviour and non-minimum phase behaviours (John Hauser & Sastry, 1992; Qiu & Davison, 1993). For many fields of applications, simple rule-based and map-based controllers are still predominantly employed. The necessary calibration efforts and the determination of an appropriate control structure nevertheless limit the resulting performance of such controllers. Different systems or systems configurations usually necessitate distinct control strategies, leading to high development costs and efforts. A modular controller structure with an automated identification from measurement data would therefore be highly beneficial in terms of calibration effort and modularity.

Numerous advanced control methods are currently using a hierarchical control framework. It consists of a first control layer defining setpoints for measured signals to achieve optimality with respect to a given metric, e.g. cost, time, reference tracking, etc. These setpoints, or desired trajectories, are usually map-based as in Plianos and Stobart (2011) or result from a static optimisation using a simplified model of the system (Jiang & Shen, 2019). Hierarchical control frameworks typically comprise a second control layer responsible for controlling the actuators to achieve accurate output setpoints or trajectories tracking.

This second control layer has already been investigated to realise an accurate output tracking of the reference. Initially consisting of a single adaptive feedback controller as in Plianos and Stobart (2011), a recent study emphasises the importance of a feedforward control for accurate transient output tracking (Zhang et al., 2022). Indeed, predictive control methods, i.e. when the output trajectory from the first layer is known beforehand for a given horizon, considerably increase the tracking

CONTACT Alexis Benaitier alexis.benaitier@tuwien.ac.at

accuracy if the horizon is long enough (Euler-Rolle et al., 2021; Kang & Shen, 2017). The main bottleneck of model predictive controllers is their inherent computational complexity, given the limited capabilities of control hardware devices especially for mobile applications. Even considering simplified algorithms such as an explicit model predictive controller as in Ortner and Re (2007) or a parametrisation of the input for a reduced dimensionality of a nonlinear predictive controller as proposed in Murilo et al. (2014), more straightforward methods are highly desired regarding a forthcoming hardware implementation.

Feedforward control is an interesting candidate to realise accurate output tracking with computationally limited requirements. Indeed, for a specific simplified model of the system, a nonlinear feedforward controller may be developed based on the inverse characteristics of the model (Hirata et al., 2019). Such controllers benefit from reduced computational complexity but still suffer from calibration efforts and a lack of modularity. To achieve a modular feedforward controller, i.e. reusable for different systems or systems configurations, a black-box local model network (LMN) can be of great interest. Especially if each local model is a linear time-invariant (LTI) model, linear control theory can be used to derive a control law for perfect output tracking.

Necessary conditions for the inversion of an LTI model to achieve perfect output tracking have been formulated by Silverman (1969) at the beginning of the seventies. However, since then, no such conditions for the inversion of a multi-input multi-output (MIMO) nonlinear model have been formulated. As a result, various feedforward methods rely on the differential flatness property introduced by Fliess et al. (1995). Flatness-based control designs are of great interest, especially with the concept of flat input (Waldherr & Zeitz, 2008, 2010). Indeed, a flat input can always be found when the system is observable, and the trajectory of the flat input can be directly known from the desired output trajectory. The physical input can thereafter be recovered from the flat input using a differential parametrisation referred to as a dynamic compensator (Jean-Francois et al., 2009).

The main difficulty when using the concept of flat input with a dynamic compensator is the potential non-minimum phase behaviour of the considered system, i.e. unstable zero dynamics. Indeed, non-minimum phase behaviour can appear in numerous physical systems (John Hauser & Sastry, 1992; Sira-Ramírez & Agrawal, 2004). For a system exhibiting a non-minimum phase behaviour, a dynamic compensator method may create an unbounded control input to realise a perfect output tracking (Isidori, 1995). Nevertheless, perfect output tracking of a non-minimum phase system is still possible with a bounded control input if the controller knows the trajectory beforehand, i.e. with a non-causal controller (Chen & Paden, 1996).

A decomposition-based algorithm can also be employed to identify a feedforward controller (Harris McClamroch & Al-Hiddabi, 1998; Spirito & Marconi, 2022). Splitting the system into a minimum phase system and a non-minimum phase system, the idea is to trivially invert the minimum phase part of the original system while compensating in steady-state conditions for the non-minimum phase part. This method can provide acceptable results, but requires knowledge of control

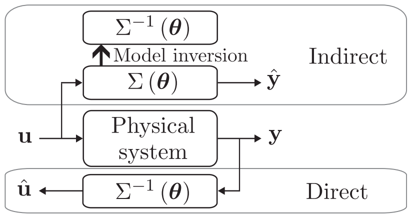

Figure 1. Indirect and direct approach for inverse model parameters identification.

engineering, and cannot be applied in full generality for an arbitrary nonlinear system.

In order to avoid difficulties when inverting a model to identify a feedforward controller, a direct identification method can be employed. Schenkendorf and Mangold (2014) indeed proposed two methods to identify the parameters $\boldsymbol{\theta}$ of an inverse model Σ^{-1}. Classically, an indirect method is used, inverting a model previously identified by fitting a reconstructed output $\hat{\mathbf{y}}$ to the measured output $\mathbf{y}$ given the measured input $\mathbf{u}$, as depicted in Figure 1. Alternatively, a direct method can be considered, where the inverse model is directly identified by fitting the reconstructed input $\hat{\mathbf{u}}$ to the measured input $\mathbf{u}$ given the measured output $\mathbf{y}$, also illustrated in Figure 1. The main advantage of the direct method is that no inversion is necessary, hence no numerical difficulties.

This paper proposes a feedforward controller structure directly identified from measurement data, i.e. direct identification as shown in Figure 1, to ensure robustness against model order selection and applicability to non-minimum phase systems. Additionally, the proposed feedforward controller structure offers the possibility to merge local controllers identified at various operating points to create a single parameter-varying controller. The proposed feedforward method can be applied to a large class of physical systems which can be modelled with an LPV model. The system must be open-loop stable, and the output reference trajectory known and smooth, i.e.sufficiently many times differentiable. Also, the input saturation is not explicitly considered by this method but can be indirectly considered by modifying the output reference, usually limiting the output rate of change. Finally, measurement data have to be available and fulfil persistency of excitation, i.e. all frequencies in the operating range of interest have to be excited.

In this paper, a nonlinear and locally non-minimum phase system is taken as an example; the control of an engine air path. The control inputs are the exhaust gas recirculation valve (EGR) and the variable geometry turbocharger (VGT), controlled to follow a prescribed exhaust manifold pressure P_{exh} and exhaust nitrogen oxides mass flow NO_x (Murilo et al., 2014; Plianos & Stobart, 2011; Shi & Shen, 2021). Engine air paths are nonlinear systems that are open-loop stable and exhibit strong output coupling (Kang & Shen, 2017; Murilo et al., 2014). This paper mainly focuses on reference output trajectories followable without input saturation. The case where the input is saturated is presented at the end of Section 5, where the output is not perfectly followed, to emphasise the robustness of the proposed method.

The remainder of this paper describes an automated feedforward controller identification method implemented to realise the output tracking of any stable non-linear system. Section 2 details the implementation of the feedforward controller within a classical hierarchical strategy. The proposed control algorithm to generate an input trajectory to track a prescribed output trajectory is presented in Section 3. The identification of the feedforward controller parameters is discussed in Section 4. Finally, the proposed feedforward controller is implemented in combination with a simple feedback controller to track the NO_x and P_{exh} of a diesel engine. Using a detailed simulation platform, the proposed feedforward controller is compared to different classical controllers in Section 5 for fixed and variable engine operating points.

2. Control concept

A new feedforward method is proposed in this paper, with a straightforward identification of its parameters and low computational requirements. The controller structure is derived from a generic LPV model; hence it can be used for many physical systems. This section first provides background information regarding feedforward control within a hierarchical control strategy. Then the controller structure is introduced as a transformation of a generic LPV model.

2.1 Hierarchichal control strategy

The proposed feedforward control strategy necessitates output reference to be followed and is therefore proposed to be employed in a hierarchical control framework as depicted in Figure 2. The high-level controller generates the desired output trajectory based on the known operating point trajectory of the system. Then a low-level controller designs the required input trajectory to follow the reference output trajectory from the high-level controller. Additionally, the low-level controller can consider feedback from the plant, i.e. the measured physical output, to compensate for model inaccuracies and disturbances.

The reference output trajectory is expected to be smooth in the sense that the reference can be differentiated. Indeed, for many physical systems, the output trajectory essentially consists of smooth transitions between predefined output setpoints and is generated anytime a transition to a new output setpoint is necessary. Additionally, a non-differentiable trajectory, i.e. step, can always be approximated by a smooth trajectory using some filtering techniques. This requirement comes from the fact that most physical systems cannot follow a non-differentiable output reference without an unbounded input unless they exhibit

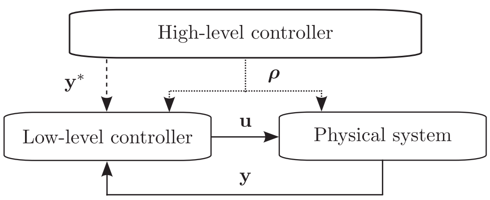

Figure 2. Diagram of the low-level controller implementation within the hierarchical control strategy.

a direct feedthrough. To keep the feedforward method general enough, differentiability of the output reference is therefore required.

This paper focuses only on the design of the low-level controller. More specifically, an automated method for feedforward controller identification is proposed and tested. Eventually, a feedback controller is added to the feedforward controller to further study the accuracy and advantages of the proposed feedforward controller. The high-level controller is not considered in this paper, i.e. the desired output trajectory, written with the star superscript $\bullet^*$, is considered perfectly known for the remainder of this paper.

The main assumption of this paper for the design of a feedforward controller is that the physical system can be accurately modelled as an LPV MIMO model for control purposes. The scheduling vector $\boldsymbol{\rho}$, defining the operating point at each instant, is usually taken as the engine speed N_{ice} and the engine torque T_{ice} for an engine air path (Euler-Rolle et al., 2021; Kang & Shen, 2017; Ortner & Re, 2007; Zhang et al., 2022). Without loss of generality, an LPV model can be built as a nonlinear aggregation of LTI models Σ_j identified at fixed operating points $\boldsymbol{\rho}_j$

$$\Sigma_j : \begin{cases} \dot{\mathbf{x}}^j = \mathbf{A}^j\mathbf{x}^j + \mathbf{B}^j\mathbf{u} \\ \mathbf{y} = \mathbf{C}^j\mathbf{x}^j + \mathbf{D}^j\mathbf{u} \end{cases}, \tag{1}$$

with $\mathbf{x}^j \in \mathbb{R}^n, \mathbf{y} \in \mathbb{R}^m, \mathbf{u} \in \mathbb{R}^m$ and the matrices $\mathbf{A}^j, \mathbf{B}^j, \mathbf{C}^j$ and $\mathbf{D}^j$ for each local model. The states $\mathbf{x}^j$ have no physical meaning when the system is identified from black-box identification methods, i.e. when no a-priori knowledge of the system dynamics is known. The states have therefore a different physical meaning at different operating points $\boldsymbol{\rho}_j$ and so different state space parameters cannot be directly merged, i.e. it is not possible to directly interpolate between the matrices $\mathbf{A}^j, \mathbf{B}^j, \mathbf{C}^j$ and $\mathbf{D}^j$. The following section proposes a feedforward controller structure where the controllers' parameters at different operating points can be merged directly.

2.2 Feedforward controller structure

A generic feedforward controller structure is proposed in this section, assuming that the physical system can be modelled as an LPV MIMO system. Local controllers are identified at various operating points, with the particularity of all sharing the same parameters' physical interpretation making the design of a parameter-varying controller straightforward.

First, the proposed feedforward structure is introduced at a fixed operating point $\boldsymbol{\rho}_j$, where it is inherited from the linear time-invariant model Σ_j defined by the matrices $\mathbf{A}, \mathbf{B}, \mathbf{C}$ and $\mathbf{D}$, the index j being omitted for the ease of notation. Without loss of generality, Σ_j is assumed to be state observable, with the states noted $\mathbf{x}$. The observability matrix can therefore be built blockwise with a relative degree $r_i \geq 1$ associated with each output and fulfilling $\sum_{i=1}^{m} r_i = n$ (Brunovský, 1970)

$$\mathcal{Q} = \begin{bmatrix} \mathcal{Q}_1 \\ \mathcal{Q}_2 \\ \cdots \\ \mathcal{Q}_m \end{bmatrix}, \quad \mathcal{Q}_i = \begin{bmatrix} \mathbf{c}_i \\ \mathbf{c}_i\mathbf{A} \\ \vdots \\ \mathbf{c}_i\mathbf{A}^{r_i-1} \end{bmatrix}, \quad \forall i \in \{1, \ldots, m\}, \tag{2a}$$

where $\mathbf{c}_i$ represents the ith row of the matrix $\mathbf{C}$.

A linear state transformation using the observability matrix is possible and can be expressed as $\hat{\mathbf{x}} = \mathcal{Q}\mathbf{x}$ leading to the new state space representation

$$\hat{\Sigma}_j : \begin{cases} \dot{\hat{\mathbf{x}}} = \hat{\mathbf{A}}\hat{\mathbf{x}} + \hat{\mathbf{B}}\mathbf{u} \\ \mathbf{y} = \hat{\mathbf{C}}\hat{\mathbf{x}} + \mathbf{D}\mathbf{u} \end{cases}, \tag{3a}$$

$$\hat{\mathbf{A}} = \begin{bmatrix} \hat{\mathbf{A}}_1 & \mathbf{0} & \mathbf{0} & \cdots & \mathbf{0} \\ [\text{———} & & \boldsymbol{\Psi}_1^x & & \text{———}] \\ \mathbf{0} & \hat{\mathbf{A}}_2 & \mathbf{0} & \cdots & \mathbf{0} \\ [\text{———} & & \boldsymbol{\Psi}_2^x & & \text{———}] \\ & & \vdots & & \\ \mathbf{0} & \mathbf{0} & \mathbf{0} & \cdots & \hat{\mathbf{A}}_m \\ [\text{———} & & \boldsymbol{\Psi}_m^x & & \text{———}] \end{bmatrix}, \tag{3b}$$

with $\boldsymbol{\Psi}_j^x \in \mathbb{R}^{1\times n}, \forall j \in \{1,\dots,m\}$. Each $\boldsymbol{\Psi}_j^x$ is a row vector corresponding to the highest output derivative dynamics of each physical output j. The obtained model $\hat{\Sigma}_j$ consists of m chains of integrators $\hat{\mathbf{A}}_i$, one associated with each output. Yet, for an arbitrary system Σ_j, the inputs can still have a direct impact on all the states $\hat{\mathbf{x}}$, because $\hat{\mathbf{B}}$ and $\mathbf{D}$ have no particular structure. For example, the first r_1 states correspond to the first output and verify

$$\hat{x}_k = y_1^{(k-1)} - \mathbf{d}_1\mathbf{u}^{(k-1)} - \sum_{l=1}^{k-1} \hat{\mathbf{b}}_l\mathbf{u}^{(k-l-1)}, \quad \forall k \in \{1,\dots,r_1\}, \tag{4a}$$

with the last state dynamics

$$\frac{\mathrm{d}}{\mathrm{d}t}\hat{x}_{r_1} = \boldsymbol{\Psi}_1^x\hat{\mathbf{x}} + \hat{\mathbf{b}}_{r_1}\mathbf{u}. \tag{4b}$$

The states associated with each output can be transformed so that the new states become the outputs and their derivatives. For example, for the first output, using relation (4a), new states $\mathbf{z}$ are defined as

$$z_k = \hat{x}_k + \mathbf{d}_1\mathbf{u}^{(k-1)} + \sum_{l=1}^{k-1} \hat{\mathbf{b}}_l\mathbf{u}^{(k-l-1)}, \quad \forall k \in \{1,\dots,r_1\}, \tag{5}$$

such that $z_k = y_1^{(k-1)}$ holds.

The highest output dynamics can be found by derivating z_{r_1} using (5) and the derivative of x_k given in (4b)

$$\frac{\mathrm{d}}{\mathrm{d}t}\hat{z}_{r_1} = \boldsymbol{\Psi}_1^x\hat{\mathbf{x}} + \hat{\mathbf{b}}_{r_1}\mathbf{u} + \mathbf{d}_1\mathbf{u}^{(r_1)} + \sum_{l=1}^{r_1-1} \hat{\mathbf{b}}_l\mathbf{u}^{(r_1-l)}. \tag{6}$$

Finally, $\hat{\mathbf{x}}$ can be expressed as a function of $\mathbf{z}$ and the input and its derivatives in (5) and then replaced in (6) to find

$$\frac{\mathrm{d}}{\mathrm{d}t}\hat{z}_{r_1} = \boldsymbol{\Psi}_1^x\mathbf{z} + \sum_{l=0}^{r_1} \Psi_{1,l}^u\mathbf{u}^{(l)}, \tag{7}$$

with $\Psi_{1,l}^u \in \mathbb{R}^{1\times m}$.

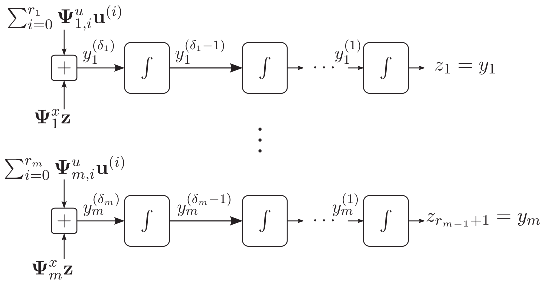

Figure 3. Representation of $\tilde{\Sigma}_j$ with m chains of integrators.

This transformation can be done for each output and leads to the new representation presented in Figure 3, where each state corresponds to an output or one of its derivatives

$$\mathbf{z} = \begin{bmatrix} y_1 & y_1^{(1)} & \cdots & y_1^{(r_1-1)} & y_2 & \cdots & y_m^{(r_m-1)} \end{bmatrix}^{\mathrm{T}}. \tag{8}$$

Collecting all the equations representing the highest derivative of each output, i.e. Equation (7) for each output, the following m ordinary differential equations are found

$$\begin{bmatrix} \begin{bmatrix} y_1 \\ y_1^{(1)} \\ \vdots \\ y_1^{(r_1)} \end{bmatrix}^{\mathrm{T}}, & \dots, & \begin{bmatrix} y_m \\ y_m^{(1)} \\ \vdots \\ y_m^{(r_m)} \end{bmatrix}^{\mathrm{T}} \end{bmatrix} \boldsymbol{\theta}_y^j$$
$$= \begin{bmatrix} \begin{bmatrix} u_1 \\ u_1^{(1)} \\ \vdots \\ u_1^{(r^*)} \end{bmatrix}^{\mathrm{T}}, & \dots, & \begin{bmatrix} u_m \\ u_m^{(1)} \\ \vdots \\ u_m^{(r^*)} \end{bmatrix}^{\mathrm{T}} \end{bmatrix} \boldsymbol{\theta}_u^j, \tag{9}$$

where $r^* \leq \max_i r_i, \forall i \in \{1,\cdots,m\}$ and the feedforward controller parameter matrices $\boldsymbol{\theta}_y^j \in \mathbb{R}^{\sum(r_i+1)\times m}$ and $\boldsymbol{\theta}_u^j \in \mathbb{R}^{m(r^*+1)\times m}$. Each column $k \in \{1,\dots,m\}$ of the matrices $\boldsymbol{\theta}_y^j$ and $\boldsymbol{\theta}_u^j$ are directly built reordering the terms of $\boldsymbol{\Psi}_k^x$ and $\boldsymbol{\Psi}_{k,\cdot}^u$. For the well-conditioned of the feedforward controller, each output's highest dynamics is a weighted sum of the outputs, the inputs and their derivatives and is linearly independent of the other highest output derivatives, i.e. the matrix $\begin{bmatrix} \boldsymbol{\theta}_y^j \\ \boldsymbol{\theta}_u^j \end{bmatrix}$ must be full column rank.

This paper proposes to use the input-output relation (9) as the structure of a feedforward controller. This representation is advantageous as it prevents classical numerical difficulties associated with matrix inversion during parameter identification or integration of unstable dynamics for feedforward control of non-minimum phase systems. Also, this structure does not possess any states; hence no observability problem can appear. The output and input must be smooth enough in the sense that their time derivatives are well defined; this assumption is usually verified for arbitrary physical systems where the input and output cannot physically *jump* but always change smoothly within a small enough time window. Finally, merging controllers' parameters is straightforward, as each parameter has a unique physical interpretation, independent of the operating point.

In the following of this paper, an efficient method to identify the controller parameters from noisy measurement data is proposed. It is shown to be robust against model order selection and benefits from a numerically efficient total least squares formulation. Also, a simple method only requiring to solve a linear least squares problem to design the necessary inputs to follow a prescribed output trajectory is presented. The proposed feedforward controller is consequently straightforward to calibrate, only consisting of physically interpretable parameters. Furthermore, its computational load is low enough to consider a future hardware implementation.

Section 3 describes the proposed method to use (9) as a feedforward controller, assuming already identified $\boldsymbol{\theta}_y(\boldsymbol{\rho})$ and $\boldsymbol{\theta}_u(\boldsymbol{\rho})$. The identification of the controller parameters $\boldsymbol{\theta}_y(\boldsymbol{\rho})$ and $\boldsymbol{\theta}_u(\boldsymbol{\rho})$ is discussed in Section 4 where first a controller is identified at each operating point, and then a nonlinear aggregation of all the feedforward controllers is built from transient measurements. The performances of the proposed method are evaluated and compared to classical control methods in Section 5 using a high-fidelity simulation platform of a diesel engine air path.

3. Input trajectory design

The feedforward controller should provide a trajectory of the inputs $\mathbf{u}$ so that the system outputs $\mathbf{y}$ follow a trajectory prescribed by the high-level controller. This section proposes a robust method to realise such an output tracking using the relation (9) and a parametrisation of the input with basis functions. Regularisation is added to the resulting least squares algorithm to ensure bounded inputs even when the system exhibits non-minimum phase behaviour.

3.1 Input parametrisation with basis functions

The output trajectory tracking task can be seen as finding the input trajectory such that the Equation (9) is fulfilled at each time. Assuming that the output reference trajectory and its derivatives are known, and the parameters $\boldsymbol{\theta}_y(\boldsymbol{\rho})$ and $\boldsymbol{\theta}_u(\boldsymbol{\rho})$ identified as in Section 4, a linear system of ordinary differential equations has to be solved to estimate the required input trajectory.

A collocation method is proposed in this paper, as it has already shown successful results for solving ordinary differential equations that are usually difficult to solve with integration methods (Mai-Duy, 2005). Indeed, when the zero dynamics of the system is unstable, i.e. non-minimum phase system, the right-hand side of (9) has at least one unstable eigenmode.

The underlying idea of using a collocation method is to approximate the input infinite-dimensional function space with a finite set of functions

$$u_i = \boldsymbol{\varphi}\boldsymbol{\gamma}_{u_i}, \quad \forall i \in \{1, \ldots, m\}, \tag{10}$$

with each parameter vector $\boldsymbol{\gamma}_{u_i} \in \mathbb{R}^L$ and a set of L linearly independent functions

$$\boldsymbol{\varphi} = [\varphi_1, \ldots, \varphi_L] \in \mathbb{R}^{1\times L} \tag{11a}$$

$$\varphi_k : \mathbb{R} \to \mathbb{R}, \quad \forall k \in \{1, \ldots, L\}. \tag{11b}$$

Gaussian functions are chosen to create a radial basis function network that has been proven to be a universal function approximator (Liao et al., 2003). Also, these functions are infinitely differentiable, straightforward to parameterise and are non-zero only in a small region, impacting the modelled signal only locally.

To create a radial basis function network, Gaussian functions

$$\varphi_k(t) = e^{-\epsilon_k(t-\tau_k)^2}, \tag{12}$$

are concentrated around regularly spaced time locations τ_k.

The parameter ϵ_k is chosen in a way that neighbouring functions overlap and are sufficiently large to capture local behaviours. By simply plotting the basis functions and the designed inputs, it is straightforward to calibrate ϵ_k to achieve the desired trade-off between smoothness and accurate tracking. Regarding the number of functions, as regularisation is added in the next section, a large value of L will only increase the computational requirements, while a smaller L will, at one point, deteriorate the tracking accuracy. Choosing L large and decreasing its value until the accuracy is negatively impacted constitutes a simple and efficient calibration method.

For a practical implementation of relation (10), the functions φ_k are discretised in N_t samples. The linear system of ordinary differential Equation (9) can be reformulated as

$$\boldsymbol{\Phi}_u\boldsymbol{\gamma}_u = \boldsymbol{\Phi}_y, \tag{13}$$

with the extended parameter vector $\boldsymbol{\gamma}_u \in \mathbb{R}^{Lm}$ defined in (A4), the matrix $\boldsymbol{\Phi}_u \in \mathbb{R}^{N_t m\times Lm}$ and the vector $\boldsymbol{\Phi}_y \in \mathbb{R}^{N_t m}$ as defined in detail in Appendix.

A classical least squares method can be employed to estimate $\boldsymbol{\gamma}_u$ in (13). Nevertheless, a dedicated regularisation is proposed in the following section to keep the inputs bounded.

3.2 Bounded input trajectory with regularisation

Some physical systems are challenging to control with feedforward because they exhibit non-minimum phase behaviours. For example, diesel engine air paths usually exhibit non-minimal phase behaviour because of the turbocharger dynamics (Stürzebecher et al., 2015). For any physical system with unstable zero dynamics, a perfect output trajectory tracking can lead to an unbounded control input when the control horizon is bounded in the negative or positive time direction (Chen & Paden, 1996). In that sense, finding a bounded input trajectory so that Equation (9) perfectly holds at each time is usually not possible. Instead, a bounded input trajectory that minimises the error between both sides of Equation (9) at each point in time is proposed. The resulting output tracking will be shown to be close to the expected trajectory, especially when pre-actuation time is available, and the inputs will remain bounded, i.e. feasible.

This paper proposes to use a modified ridge regression to ensure boundedness of the input trajectory (Ramsay & Silverman, 2005). Taking advantage of the structure of $\boldsymbol{\Phi}_u$ in (13), a penalty directly applied to a specific input and its derivatives is possible.

The coefficients describing the optimal smooth input trajectory $\boldsymbol{\gamma}_u^*$ are directly given as a modified version of the initial Moore–Penrose inverse

$$\boldsymbol{\gamma}_u^* = \left(\boldsymbol{\Phi}_u^{\mathrm{T}}\boldsymbol{\Phi}_u + \mathbf{C}_{\mathrm{reg}}^{\mathrm{T}}\mathbf{C}_{\mathrm{reg}}\right)^{-1}\boldsymbol{\Phi}_u^{\mathrm{T}}\boldsymbol{\Phi}_y, \tag{14a}$$

with $\mathbf{C}_{\mathrm{reg}} \in \mathbb{R}^{N_t m \times Lm}$.

The matrix $\mathbf{C}_{\mathrm{reg}}$ is built as a block diagonal matrix to weight the input and its derivatives independently

$$\mathbf{C}_{\mathrm{reg}} = \mathrm{diag}\left\{\mathbf{C}_{\mathrm{reg},i}\right\}, \quad \forall i \in \{1,\ldots,m\}, \tag{14b}$$

where each matrix $\mathbf{C}_{\mathrm{reg},i}$ weights a specific input and its derivatives

$$\mathbf{C}_{\mathrm{reg},i} = \sum_{k=0}^{r^*} \upsilon_{i,k}\boldsymbol{\varphi}^{(k)^{\mathrm{T}}}, \tag{14c}$$

with $\upsilon_{i,k} \geq 0$ the regularisation parameter for the kth derivative of the ith input and $\boldsymbol{\varphi}^{(k)} \in \mathbb{R}^{N_t \times L}$ corresponding to the sampled kth derivatives of the functions defined in (11a). The proposed regularisation plays an essential role in numerical stability to ensure that the least squares problem (13) is well-posed. Also, when the system exhibits non-minimum phase behaviour, regularisation ensures that the inputs remain bounded. In such a case, perfect output tracking is, in theory, only possible with an infinite pre-actuation time (Chen & Paden, 1996; Isidori, 1995). Nevertheless, with enough pre-actuation time, e.g. a few seconds for a diesel engine air path, perfect output tracking can still be realised up to numerical precision. The proposed feedforward controller takes advantage of this possibility; it is, therefore, non-causal, in the sense that the EGR and VGT trajectories are designed in advance for a prescribed horizon.

4. Controller parameter identification

The controller parameters $\boldsymbol{\theta}_y(\boldsymbol{\rho})$ and $\boldsymbol{\theta}_u(\boldsymbol{\rho})$ are function of the scheduling variable $\boldsymbol{\rho}$ introduced in Section 2.1. A local learning approach is used to reduce the identification complexity and gain meaningful information from the model structure (Hametner & Jakubek, 2013). First, the local controllers are identified in Section 4.1, and then a nonlinear aggregation of the local controllers is parameterised in Section 4.2 to create a parameter-varying controller.

4.1 Local controller parameter identification

The identification of the controller parameters $\boldsymbol{\theta}_y^j$ and $\boldsymbol{\theta}_u^j$ at a fixed operating point $\boldsymbol{\rho}_j$ in (9) corresponds to the identification of the parameters of a system of ordinary differential equations (ODE). Also, because the physical system may exhibit a non-minimum phase behaviour locally, integration methods for the parameter identification may be difficult (Mai-Duy, 2005). A method based on principal differential analysis is therefore chosen to ensure numerical stability and accuracy (Ramsay & Silverman, 2005).

The measured signals during identification, i.e. input and output, are individually modelled with a weighted sum of basis functions, similarly as in (10). The weighted coefficients are calibrated with the available measurements. Consequently, all the necessary time derivatives of the inputs and outputs can be estimated from the basis functions derivatives. The system of ODE (9), for a constant scheduling vector $\boldsymbol{\rho}_j$, can be written as

$$\boldsymbol{\beta}\boldsymbol{\theta}^j = \mathbf{0}, \tag{15}$$

with $\boldsymbol{\theta}^{j\mathrm{T}} = \left[\boldsymbol{\theta}_u^{j\,\mathrm{T}} \;\; \boldsymbol{\theta}_y^{j\,\mathrm{T}}\right]$ the controller parameters to be identified and $\boldsymbol{\beta}$ a matrix being the concatenation of all the required inputs, outputs, and their derivatives as shown in (9).

Because the measured outputs contain noise, and because all the signals are modelled with basis functions, the signals in $\boldsymbol{\beta}$ are only approximations of reality. A total least squares (TLS) method is used to consider these perturbations during the controller parameter identification. The TLS method is used to find the parameters matrix $\boldsymbol{\theta}^j$ that exactly fulfils (15) for a theoretical signals matrix $\bar{\boldsymbol{\beta}}$, assumed with no measurement error and no smoothing approximation. Therefore, the matrix $\boldsymbol{\beta}$ is decomposed into a theoretical *true signals* $\bar{\boldsymbol{\beta}}$ and additive noise $\tilde{\boldsymbol{\beta}}$

$$\boldsymbol{\beta} = \bar{\boldsymbol{\beta}} + \tilde{\boldsymbol{\beta}}. \tag{16}$$

Applying the TLS approach, the signals noise matrix is estimated as the matrix with the minimum Frobenius norm that makes $\bar{\boldsymbol{\beta}}$ m-rank deficient

$$\bar{\boldsymbol{\beta}} = \arg\min_{\bar{\boldsymbol{\beta}}} \left\{\|\boldsymbol{\beta} - \bar{\boldsymbol{\beta}}\|_F\right\}, \tag{17a}$$

$$\mathrm{rank}(\bar{\boldsymbol{\beta}}) = \mathrm{rank}(\boldsymbol{\beta}) - m. \tag{17b}$$

A solution to this constrained minimisation (17a)–(17b) can be found using the singular value decomposition of the matrix $\boldsymbol{\beta}$

$$\boldsymbol{\beta} = \mathbf{U}\begin{pmatrix}\Sigma_1 & \mathbf{0}\\ \mathbf{0} & \Sigma_2\end{pmatrix}\left(\mathbf{V}_1^{\mathrm{T}} \;\; \mathbf{V}_2^{\mathrm{T}}\right)^{\mathrm{T}}, \tag{18}$$

where the m smallest singular values are collected in Σ_2 with the corresponding right singular vectors $\mathbf{V}_2^{\mathrm{T}}$. Removing only the smallest m eigenvalues of $\boldsymbol{\beta}$ would lead to the matrix $\bar{\boldsymbol{\beta}}$ minimising the Frobenius norm (17a) while fulfilling (17b) according to the Eckart–Young–Mirsky theorem (Eckart & Young, 1936). The estimated nullspace of $\boldsymbol{\beta}$ can be directly identified as the remaining part of the singular value decomposition (18), and will be the subspace where each ith column of the estimated parameters matrix lies

$$\boldsymbol{\theta}_i^j \in \langle\mathbf{V}_2^{\mathrm{T}}\rangle, \quad \forall i \in \{1,\ldots,m\}, \tag{19}$$

and with all columns of $\boldsymbol{\theta}^j$ being linearly independent.

Given that the matrix $(\mathbf{V}_1^{\mathrm{T}} \;\; \mathbf{V}_2^{\mathrm{T}})^{\mathrm{T}}$ is orthonormal, the m column vectors of $\mathbf{V}_2^{\mathrm{T}}$ are all orthogonal unit vectors. In that sense, and without loss of generality, taking $\boldsymbol{\theta}^j = \mathbf{V}_2^{\mathrm{T}}$ is a reasonable choice and does not need any specific re-scaling.

The proposed TLS method is only optimal within the assumption of Gaussian noise (Eckart & Young, 1936), yet gives sensibly better results than standard least-squares methods as experienced by the authors. Also, the collected measurement data must persistently excite the system within the whole operating frequency range to accordingly capture the system dynamics.

4.2 Local controller network

To create a parameter-varying feedforward controller (9), the parameters of multiple controllers identified at various operating points must be merged. A substantial advantage of the proposed method is that all the local controllers share the same structure. It is, therefore, possible to interpolate between each feedforward model set of parameters to create a local controller network, equivalent to a local *model* network of *controllers* (Hunt & Johansen, 1997). Additionally, local controller models with different output relative degrees can also be merged, adding a zero coefficient to all the missing input and output derivatives.

To capture the nonlinearities of the air path with respect to the engine speed and load, the feedforward controller parameters are defined as a nonlinear aggregation of the parameters of the N local controllers

$$\boldsymbol{\theta}_u(\boldsymbol{\rho}) = \sum_{j=1}^{N} \tilde{\phi}_j(\boldsymbol{\rho})\, \boldsymbol{\theta}_u^j, \tag{20a}$$

$$\boldsymbol{\theta}_y(\boldsymbol{\rho}) = \sum_{j=1}^{N} \tilde{\phi}_j(\boldsymbol{\rho})\, \boldsymbol{\theta}_y^j, \tag{20b}$$

with $\tilde{\phi}_j : \mathbb{R}^2 \to \mathbb{R}$ the validity function associated with the jth local model whose parameters are $\boldsymbol{\theta}_u^j$ and $\boldsymbol{\theta}_y^j$. Furthermore, at any operating point, the weighted sum of all the controller parameters is constrained to be unitary to guarantee model consistency and interpretability

$$\sum_{j=1}^{N} \tilde{\phi}_j(\boldsymbol{\rho}) = 1. \tag{21}$$

Gaussian radial basis functions are employed to provide a simple identification while ensuring a modular and interpretable LMN. The validity functions are parameterised as

$$\phi_j(\boldsymbol{\rho}) = e^{\left(-\boldsymbol{\tau}_j^{\mathrm{T}}\left(\boldsymbol{\rho}-\boldsymbol{\rho}_j\right)^2\right)}. \tag{22}$$

The parameters $\boldsymbol{\tau}_j$ are configurable and define the activation range in each scheduling vector dimension. The Gaussian functions (22) could be normalised to meet the requirement (21) without complexifying the optimisation of $\boldsymbol{\tau}_j$. Also, such a normalisation usually suffers from the so-called *reactivation* issue (Anzar & Azeem, 2004); a validity function can be not close to zero in a region far away from its centre $\boldsymbol{\rho}_j$.

To avoid reactivation, the validity function of each local model is forced to reach zero asymptotically outside of a predefined activation region. These activation regions are defined using sigmoid functions in all $\tilde{n}$ directions of the scheduling vector

$$\phi_{\mathrm{act}_j}(\boldsymbol{\rho}) = \prod_{k=1}^{\tilde{n}} \left[\frac{1}{1+e^{\left(\tau_{\mathrm{act}}^k\left(\rho^k-\rho_j^k-\sigma^k\right)^2\right)}} + \frac{1}{1+e^{\left(\tau_{\mathrm{act}}^k\left(-\rho^k+\rho_j^k-\sigma^k\right)^2\right)}} \right], \tag{23}$$

with $\boldsymbol{\sigma}^k$ a predefined characteristic length scale in the kth-direction of the scheduling vector and $\boldsymbol{\tau}_{\mathrm{act}}^k$ the associated transition smoothness parameter in that direction.

For each local model, its validity function used in (20a) and (20b) results from the normalisation of the product of its raw activation function ϕ_j and the corresponding activation region function ϕ_{act_j}

$$\tilde{\phi}_j(\boldsymbol{\rho}) = \frac{\phi_j(\boldsymbol{\rho})\,\phi_{\mathrm{act}_j}(\boldsymbol{\rho})}{\sum_{k=1}^{N}\left(\phi_k(\boldsymbol{\rho})\,\phi_{\mathrm{act}_k}(\boldsymbol{\rho})\right)}. \tag{24}$$

The validity function parameters $\boldsymbol{\tau}_j$ are directly identified with measurement data for a variable engine operating point. For that purpose, an interior point method is employed to minimise the square difference between the input computed using the current parameter-varying controller and the measured input. The weighting of each local model parameter results in the activation of the jth local model only in the surroundings of its identification region, i.e. for $\boldsymbol{\rho}_j$ close to $\boldsymbol{\rho}$ in the sense of the Euclidean norm.

5. Simulation results

This section demonstrates the effectiveness of the proposed automated feedforward controller identification method using an experimentally validated simulation platform of a heavy-duty diesel engine (Stefan et al., 2013). All controllers in this section track a randomly generated output trajectory that mimics P_{exh} and NO_x concentration under real scenarios. The reference output trajectory is known in advance, and the output measurements are corrupted with realistic noise during parameter identification. The EGR and VGT are considered as input variables and except in the end of Section 5.4, the input is never saturated.

First, the robustness of the local controller identification is discussed in Section 5.1, especially regarding model order selection. Then, Section 5.2 shows the performances of the proposed feedforward method when applied to an operating point where the system exhibits non-minimum phase behaviour. A PI controller is then added to remove steady-state output tracking error in Section 5.3. Finally, in Section 5.4 a parameter-varying feedforward controller is identified and compared to classical control methods to realise accurate output tracking on the entire engine operating region.

5.1 Local controller identification

This section emphasises the advantage of directly identifying a feedforward controller, as proposed in Section 4, compared to the inversion of a forward model (1) as detailed in Section 2.2, i.e. indirect identification. For the direct identification, the basis functions (12) are sampled at 50 ms, and spaced every 0.6 s with $\epsilon_k = 0.7$ to balance accuracy and complexity.

When identifying a feedforward controller from the inversion of a forward model, the model order selection greatly influences the feedforward controller accuracy and stability as depicted in Figure 4. For a small model order, the accuracy is

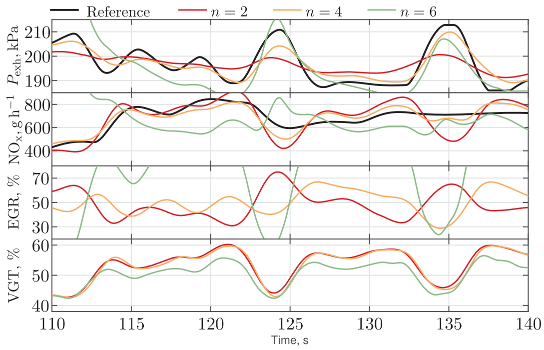

Figure 4. Open loop output tracking using different model orders n to identify a feedforward controller from model inversion, for a fixed engine operating point $N_{\mathrm{ice}} = 1200$ rpm, $T_{\mathrm{ice}} = 1000$ N m.

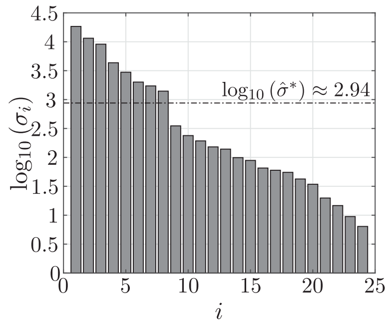

Figure 6. Singular values σ_i of $\boldsymbol{\beta}$ using up to the 5-th derivative of each input and output. The estimated optimal truncation threshold $\hat{\sigma}^*$ is also represented.

not enough to achieve accurate control. In contrast, some instabilities occur for a high model order because the observability matrix (2a) defined in Section 2.2 is close to being singular.

Directly identifying a feedforward controller from measurement data is more robust to high model order selection, as shown in Figure 5. All the proposed parametrisations in Figure 5 show almost identical results for a sufficiently high model order. When adding additional model parameters, i.e. higher model order, some of these parameters are kept to nearly zero. Another advantage is the ability to independently choose the model order for each output and input. In that sense finding the minimum number of model parameters can be possible, mainly thanks to the TLS method introduced in Section 4.1.

Indeed, with the TLS method and a large number of output and input derivatives, the optimal SVD truncation of (18) can be found as given in Gavish and Donoho (2014). The experimentally computed singular values and the optimal truncation are depicted in Figure 6 using 5th order derivatives for both the output and the input. Ten signals should be kept, as the optimal truncation leads to eight meaningful singular values, and the system has two inputs/outputs according to (17b). A fourth-order model can be chosen, with $r_1 = r_2 = 2$ and $r^* = 1$. This analysis coincides with the discussed results shown in Figure 5.

5.2 Feedforward control at a non-minimum phase operating point

A diesel engine air path can exhibit non-minimum phase behaviour when operated at specific operating points, for example, at a high rotational speed of 2000 rpm and a low load of 100 N m, when the VGT is actuated to modify the $\mathrm{NO_x}$ mass flow. At this operating point, when the VGT is set proportionally to the desired $\mathrm{NO_x}$ concentration, a typical non-minimum-phase behaviour occurs as shown in Figure 7; the output goes in the opposite direction at the beginning of each step.

At this operating point, and for this reduced SISO case, an identified forward model usually has an unstable zero. As a result, when an identified model is inverted to create a feedforward controller, the trajectory designed as proposed in Section 3 necessitates some regularisation to keep the input bounded. Two different levels of regularisation are depicted in Figure 7. Output oscillations and overshoots are reduced with a strong regularisation, but the tracking is still not accurate.

When a feedforward controller is directly identified from measurement data, the input relative degree can be set to a small value to achieve better output tracking accuracy with fewer

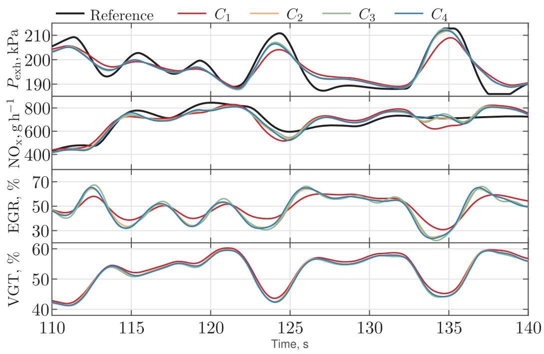

Figure 5. Open loop output tracking using different numbers of input/output derivatives to identify a feedforward controller with the TLS method, for a fixed engine operating point $N_{\mathrm{ice}} = 1200$ rpm, $T_{\mathrm{ice}} = 1000$ N m. ($C_1 : r_1 = r_2 = 1, r^* = 1$; $C_2 : r_1 = r_2 = 2, r^* = 1$; $C_3 : r_1 = r_2 = 2, r^* = 2$; $C_4 : r_1 = r_2 = 3, r^* = 1$).

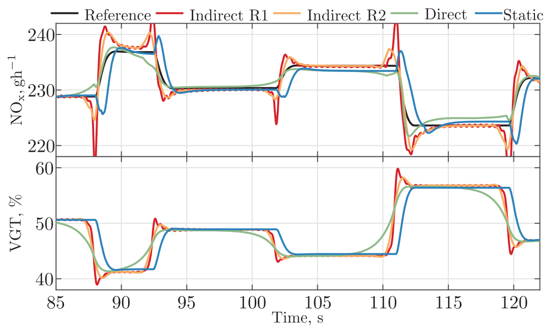

Figure 7. Open loop feedforward control of VGT for a fixed operating point $N_{\mathrm{ice}} = 2000$ rpm, $T_{\mathrm{ice}} = 100$ N m, EGR = 50%, where the system shows non-minimum phase behaviour. (R1: light regularisation, R2: strong regularisation)

oscillations. Indeed, in Figure 7, this latter method, referred to as *direct* identification, shows fewer oscillations and a more accurate output tracking, taking advantage of predictive knowledge regarding the desired output trajectory. With the direct method, regularisation is also needed but is much less sensitive than for the indirect case. Indeed, the regularisation parameters $\upsilon_{i,k}$ in (14c) have been set to 0.1 for each input and each input derivative. Still, noticeably identical results are found whenever the regularisation coefficients are taken in the range $[0.01, 0.5]$.

A *static* controller is also employed in Figure 7 to emphasise the non-minimum phase behaviour of the system at this specific operating point. This controller solely corresponds to a static gain applied to the desired output. At the beginning of each step, the output, i.e. NO_x, starts to change in the wrong direction before reaching the desired setpoint. This behaviour occurs because of the non-minimum phase property of the system and is responsible for the numerical difficulties encountered when using a feedforward controller with the indirect method.

5.3 Two-degree-of-freedom control

The proposed feedforward controller based on Equation (9) only constitutes an open-loop controller. As a result, steady-state errors are not compensated. Therefore, a PI controller is added to work along with the feedforward controller C_2 presented in Figure 5. The PI gains are manually calibrated to asymptotically reach the reference during steady states, with a unique parametrisation for the entire engine operating region. The PI calibration is kept very simplistic, as the PI feedback controller only aims at slowly removing steady-state error.

A schematic representation of this two-degree-of-freedom controller (2DoF) is presented in Figure 8. For this study, the output measurements are considered without noise to emphasise only the feedforward performances. The resulting output tracking of this 2DoF strategy is depicted in Figure 9. The results using only the feedforward controller are also displayed to emphasise the importance of the feedforward part compared to the PI contribution.

5.4 Varying engine operating point

In this section, multiple local controllers identified at various engine operating points are merged to create a single parameter-varying controller. After adding a PI feedback loop to this parameter-varying controller, the resulting 2DoF controller is compared to classical controllers for a varying engine operating point.

After identifying local controllers, the validity functions parameters of the parameter-varying controller are optimised

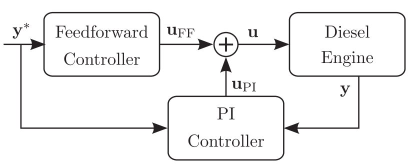

Figure 8. Diagram of the two-degree-of-freedom controller (2DoF).

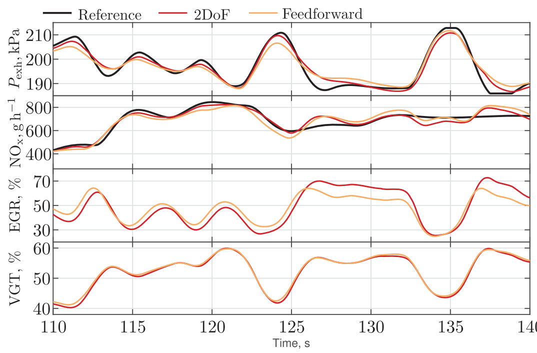

Figure 9. Comparison between a feedforward and a 2DoF controller, for a fixed engine operating point $N_{ice} = 1200$ rpm, $T_{ice} = 1000$ N m.

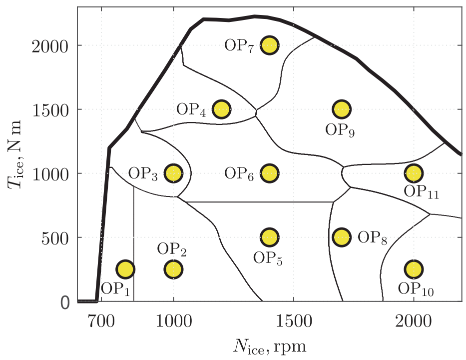

Figure 10. Region of highest activation for each local model (OP_j) around its identification centre.

with an interior-point method using transient operating point measurement data. Each local model has the highest validity function of them all around its operating point of identification, as shown in Figure 10. The use of regularisation and region of activation, as defined in (24), impedes reactivation and ensures that each local model has a validity function near unity around its corresponding operating point.

The parameter-varying feedforward controller is implemented with a PI controller calibrated with constant gains. This resulting 2DoF controller performances are shown in Figure 11 for a varying engine operating point and compared to:

- Only the PI controller from the 2DoF strategy. This strategy is neither adaptive nor predictive but is highly convenient regarding calibration effort and computational requirements;
- A network of full-state feedback controllers with integration of the control error. It is composed of multiple state feedback controllers identified at various operating points (Gregorcic & Lightbody, 2010). This control method is adaptive but not predictive, as it only uses the current desired output and system measurements;
- A flatness-based MPC as proposed in Euler-Rolle et al. (2021) so that the local model parameters can be

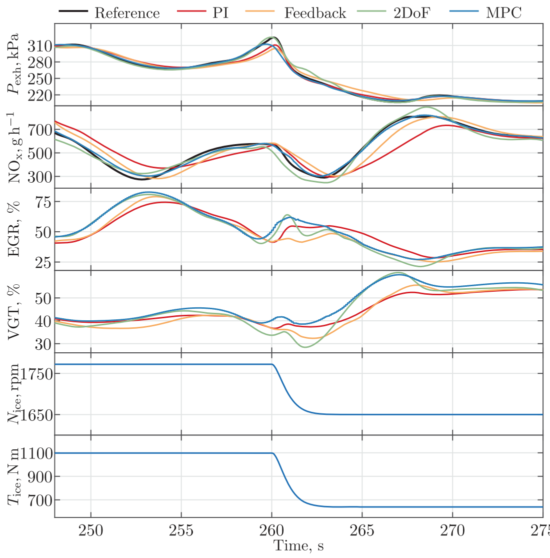

Figure 11. Closed-loop results using different controllers, without input saturation and for a varying engine operating point.

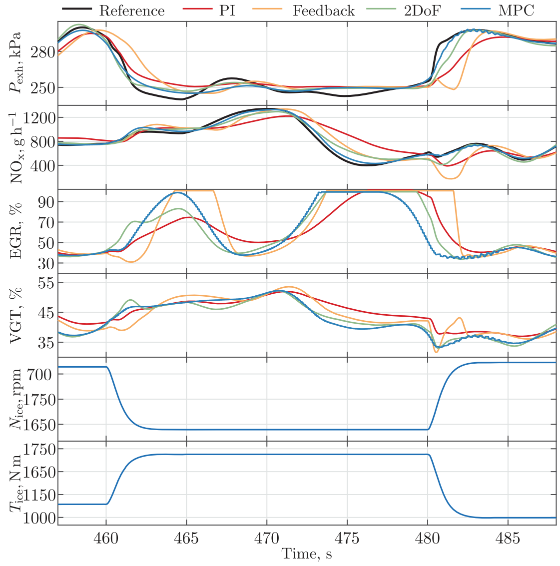

Figure 12. Closed-loop results using different controllers, with input saturation and for a varying engine operating point.

directly merged, creating a time-varying controller at each iteration. This adaptive and predictive strategy requires a significant computational effort, making its implementation on current hardware impractical.

The reference tracking regarding the first output, the exhaust pressure P_{exh}, is almost identical for all controllers. Only the non-predictive controllers, i.e. PI and state feedback controllers, are slightly less accurate before large pressure variations. Regarding the second output, the NO_x mass flow, output tracking is inaccurate for the PI controller during transient phases. The state feedback controller is faster than the PI controller but fails to accurately follow the desired reference NO_x signal during large transients. These observations are confirmed by a lower coefficient of determination detailed in Table 1 for the non-predictive controllers, especially regarding the second output NO_x.

The proposed 2DoF controller is more precise for both outputs during transient phases as it inherently considers predictive information. The 2DoF method is almost as accurate as the MPC and can still be improved with a more sophisticated feedback loop. Indeed, the MPC is primarily relying on its feedback information to control the outputs during transient engine operating points. The 2DoF, with its simple PI feedback loop, cannot perfectly follow the outputs during transient operating points,

Table 1. Coefficients of determination for different controllers proposed in Figure 11.

Controller	R^2-P_{exh}	R^2-NO_x
PI	0.984	0.613
Feedback	0.963	0.857
2DoF	0.991	0.947
MPC	0.992	0.987

Table 2. Coefficients of determination for different controllers proposed in Figure 12.

Controller	R^2-P_{exh}	R^2-NO_x
PI	0.837	0.600
Feedback	0.676	0.709
2DoF	0.946	0.922
MPC	0.965	0.984

but the control error is immediately corrected after the engine operating point returns to a steady state.

Another reference output trajectory tracking is presented in Figure 12 for the same controllers. Nevertheless, this time, the input is saturated for all the controllers as the reference is not reachable between 475 and 480 seconds. Especially the exhaust pressure cannot be accurately followed, even with the adaptive MPC, resulting in lower coefficients of determination given in Table 2 compared to the previous case summarised in Table 1.

The same observation as in the previous case still holds, with non-predictive methods being slower and, therefore, less accurate. During and shortly after an input saturation, the 2DoF method is almost as precise as the adaptive MPC but with significantly smaller computation requirements. Also, compared to the PI or the state feedback controllers, the 2DoF method is much faster at removing a steady-state error after an input saturation phase.

6. Conclusion and outlook

This paper proposes an automated method for identifying a feedforward controller for output tracking of a nonlinear physical system. The proposed structure benefits from its modularity, making it applicable to any physical system modelled with an LPV model. Additionally, the controller parameters can be directly identified from measurement data, guaranteeing robustness against model order selection and ensuring numerical stability. Also, with the suggested TLS identification approach, the model order can be estimated without prior knowledge regarding the physical system.

A significant advantage of the proposed feedforward identification method is that multiple local controllers can be merged. Because they share an identical structure, their parameters can be combined to create a local controller network. Using a single least squares algorithm, the resulting parameter-varying controller can design an entire input trajectory given a desired output trajectory. Moreover, the input trajectory is guaranteed to be smooth and bounded thanks to regularisation, even if the system exhibits non-minimum phase behaviour.

The proposed feedforward controller, implemented with a simple PI feedback loop, i.e. two-degree-of-freedom controller, is compared to classical controllers using a detailed physical simulation of an engine air path. The accuracy during transient output tracking is improved using the proposed strategy compared to non-predictive methods. The 2DoF controller performs almost as well as an adaptive MPC, even with input constraints, but uses only a fraction of its complexity. The input trajectory can therefore be easily recomputed anytime a new and more accurate operating point trajectory or output reference trajectory is available.

Future work is focusing on communicating the generated input trajectory to the high-level controller to improve the setpoints definition and assess input constraints. Additionally, the practical implementation of the proposed controller, e.g. on a diesel engine testbed, is the next step to validate the proposed feedforward strategy. Finally, a theoretical study regarding the optimality of the proposed feedforward controller is also under consideration.

Acknowledgments

The financial support by the Austrian Federal Ministry for Digital and Economic Affairs, the National Foundation for Research, Technology and Development, the Christian Doppler Research Association as well as AVL List GmbH, Austria is gratefully acknowledged.

Disclosure statement

No potential conflict of interest was reported by the author(s).

ORCID

Alexis Benaitier http://orcid.org/0000-0001-7946-1640

References

Anzar, M., & Azeem, M. F. (2004). Effect of normalization of membership functions in premise region of generalized adaptive neuro-fuzzy inference system. In *Proceedings of the IEEE INDICON 2004. First India annual conference* (pp. 294–298). IEEE.

Brunovský, P. (1970). A classification of linear controllable systems. *Kybernetika*, *6*(3), 173–188. http://eudml.org/doc/28376

Chen, D., & Paden, B. (1996). Stable inversion of nonlinear non-minimum phase systems. *International Journal of Control*, *64*(1), 81–97. https://doi.org/10.1080/00207179608921618

Eckart, C., & Young, G. (1936). The approximation of one matrix by another of lower rank. *Psychometrika*, *1*(3), 211–218. https://doi.org/10.1007/BF02288367

Euler-Rolle, N., Krainer, F., Jakubek, S., & Hametner, C. (2021). Automated synthesis of a local model network based nonlinear model predictive controller applied to the engine air path. *Control Engineering Practice*, *110*(October 2019), Article 104768. https://doi.org/10.1016/j.conengprac.2021.104768

Fliess, M., Levine, J., Martin, P., & Rouchon, P. (1995). Flatness and defect of non-linear systems: introductory theory and examples. *International Journal of Control*, *61*(6), 1327–1361. https://doi.org/10.1080/00207179508921959

Gavish, M., & Donoho, D. L. (2014). The optimal hard threshold for singular values is $4/\sqrt{3}$. *IEEE Transactions on Information Theory*, *60*(8), 5040–5053. https://doi.org/10.1109/TIT.2014.2323359

Gregorcic, G., & Lightbody, G. (2010). Nonlinear model-based control of highly nonlinear processes. *Computers & Chemical Engineering*, *34*, 1268–1281. https://doi.org/10.1016/j.compchemeng.2010.03.011

Hametner, C., & Jakubek, S. (2013). Local model network identification for online engine modelling. *Information Sciences*, *220*, 210–225. Online Fuzzy Machine Learning and Data Mining, https://www.sciencedirect.com/science/article/pii/S0020025512000138

Harris McClamroch, N., & Al-Hiddabi, S. A. (1998). A decomposition based control design approach to output tracking for multivariable nonlinear non-minimum phase systems. In *Proceedings of the 1998 IEEE international conference on control applications (Cat. No.98CH36104)* (Vol. 2, pp. 1414–1418). IEEE.

Hirata, M., Hayashi, T., Takahashi, M., Yamasaki, Y., & Kaneko, S. (2019). A nonlinear feedforward controller design taking account of dynamics of turbocharger and manifolds for diesel engine air-Path system. *IFAC-PapersOnLine*, *52*(5), 341–346. 9th IFAC Symposium on Advances in Automotive Control AAC 2019, https://www.sciencedirect.com/science/article/pii/S2405896319306767

Hunt, K. J., & Johansen, T. A. (1997). Design and analysis of gain-scheduled control using local controller networks. *International Journal of Control*, *66*(5), 619–652. https://doi.org/10.1080/002071797224487

Isidori, A. (1995). *Nonlinear control systems* (3rd ed.). Springer London.

Jean-Francois, S., Ferdinand, S., & Kennel, R. (2009). Trajectory tracking control with flat inputs and a dynamic compensator. In *Proceedings of the european control conference* (pp. 248–253). IEEE.

Jiang, W., & Shen, T. (2019). Lyapunov-based nonlinear feedback control design for exhaust gas recirculation loop of gasoline engines. *Journal of Dynamic Systems, Measurement and Control, Transactions of the ASME*, *141*(5), 1–11. https://doi.org/10.1115/1.4042146

John Hauser, G. M., & Sastry, S. (1992). Nonlinear control design for slightly non-minimum phase systems: Application to V/STOL aircraft. *Automatica*, *28*(4), 665–679. https://www.sciencedirect.com/science/article/pii/000510989290029F

Kang, M., & Shen, T. (2017). Experimental comparisons between LQR and MPC for spark-ignition engine control problem. In *Chinese Control Conference, CCC* (pp. 2651–2656). IEEE.

Liao, Y., Fang, S.-C., & Nuttle, H. L. W. (2003). Relaxed conditions for radial-basis function networks to be universal approximators. *Neural Networks*, *16*(7), 1019–1028. https://www.sciencedirect.com/science/article/pii/S0893608002002277

Mai-Duy, N. (2005). Solving high order ordinary differential equations with radial basis function networks. *International Journal for Numerical Methods in Engineering*, *62*, 824–852. https://doi.org/10.1002/(ISSN)1097-0207

Murilo, A., Alamir, M., & Alberer, D. (2014). A general NMPC framework for a diesel engine air path. *International Journal of Control*, *87*(10), 2194–2207. https://doi.org/10.1080/00207179.2014.905708

Ortner, P., & Re, L. (2007). Predictive control of a diesel engine air path. *IEEE Transactions On Control Systems Technology*, *32*(2), 449–456. https://doi.org/10.1109/TCST.2007.894638

Plianos, A., & Stobart, R. K. (2011). Nonlinear airpath control of modern diesel powertrains: A fuzzy systems approach. *International Journal of Systems Science*, *42*(2), 263–275. https://doi.org/10.1080/00207721.2010.521864

Poe, W. A., & Mokhatab, S. (2017). Chapter 3–process control. In W. A. Poe & S. Mokhatab (Eds.), *Modeling, control, and optimization of natural gas processing plants* (pp. 97–172). Gulf Professional Publishing.

https://www.sciencedirect.com/science/article/pii/B9780128029619000036
Qiu, L., & Davison, E. J. (1993). Performance limitations of non-minimum phase systems in the servomechanism problem. *Automatica*, *29*(2), 337–349. https://www.sciencedirect.com/science/article/pii/000510989390127F
Ramsay, J., & Silverman, B. W. (2005). *Functional data analysis*. Springer-Verlag New York.
Schenkendorf, R., & Mangold, M. (2014). Parameter identification for ordinary and delay differential equations by using flat inputs. *Theoretical Foundations of Chemical Engineering*, *48*(5), 594–607. https://doi.org/10.1134/S0040579514050224
Shi, H., & Shen, T. (2021). Design and experimental validation for nonlinear control of internal combustion engines with EGR and VVT. *SICE Journal of Control, Measurement, and System Integration*, *14*(1), 51–58. https://doi.org/10.1080/18824889.2021.1874680
Silverman, L. (1969). Inversion of multivariable linear systems. *IEEE Transactions on Automatic Control*, *14*(3), 270–276. https://doi.org/10.1109/TAC.1969.1099169
Sira-Ramírez, H., & Agrawal, S. K. (2004). *Differentially flat systems* (1st ed.). CRC Press.
Spirito, M., & Marconi, L. (2022). Inner-outer decomposition for strictly proper linear time invariant systems and non-minimum phase performance limitations. In *2022 IEEE 61st conference on decision and control (CDC)* (pp. 5492–5497). IEEE.
Stefan, P., Michael, K., Efstratios, F., & Atzler, H. (2013). Model-based production calibration–the efficient way of variant development. *MTZ Worldwide*, *74*(10), 18–25. https://doi.org/10.1007/s38313-013-0096-2
Stürzebecher, C., Reß, J., Bohn, C., Märzke, F., & Prase, R. (2015). A diesel engine model including exhaust flap, intake throttle, LP-EGR and VGT. Part II: Identification and validation. *IFAC-PapersOnLine*, *28*(15), 60–65. http://dx.doi.org/10.1016/j.ifacol.2015.10.009
Waldherr, S., & Zeitz, M. (2008). Conditions for the existence of a flat input. *International Journal of Control*, *81*(3), 439–443. https://doi.org/10.1080/00207170701561443
Waldherr, S., & Zeitz, M. (2010). Flat inputs in the MIMO case. *IFAC Proceedings Volumes (IFAC-PapersOnline)*, *43*(14), 695–700. https://doi.org/10.3182/20100901-3-IT-2016.00147
Zhang, J., Amini, M. R., Kolmanovsky, I., Tsutsumi, M., & Nakada, H. (2022). Benefits of feedforward for model predictive airpath control of diesel engines. In *10th IFAC symposium on robust control design*. Elsevier.

Appendix. Matrices for the feedforward least squares formulation

This appendix provides details for re-writing (9) into the form (13) where the input parametrization $\boldsymbol{\gamma}_u$ appears linearly. First, the desired outputs signals are discretised in N_t samples, and so are the basis functions given in (11a), i.e. $\varphi_k \in \mathbb{R}^{N_t}$ leading to $\mathbf{y}_i \in \mathbb{R}^{N_t}, \forall i \in \{1, \dots, m\}$. Additionally, the parameters of the controller structure (9) are also discretised

$$\bar{\boldsymbol{\theta}}_y = \boldsymbol{\theta}_y(\boldsymbol{\rho}(t)), \tag{A1}$$

with $\boldsymbol{\rho}(t)$ the discretised operating trajectory provided by the high-level controller. The model parameters are ordered in a three dimensional matrix, i.e. $\bar{\boldsymbol{\theta}}_y \in \mathbb{R}^{n\times m\times N_t}$.

With the discretised expected outputs and their derivatives, the left-hand side of (9) is trivially computed. Also, the resulting m columns of N_t samples are stored in a column vector $\boldsymbol{\Phi}_y$ of $N_t m$ elements

$$\boldsymbol{\Phi}_y = \begin{bmatrix} \sum_{k=1}^{m}\left(\sum_{l=0}^{r_k}\left(y_k^l \odot \bar{\boldsymbol{\theta}}_y\left(l+1+\sum_{i=1}^{k-1} r_i + 1, 1, \cdot\right)\right)\right) \\ \vdots \\ \sum_{k=1}^{m}\left(\sum_{l=0}^{r_k}\left(y_k^l \odot \bar{\boldsymbol{\theta}}_y\left(l+1+\sum_{i=1}^{k-1} r_i + 1, m, \cdot\right)\right)\right) \end{bmatrix}, \tag{A2}$$

with $\bar{\boldsymbol{\theta}}_y(l+1+\sum_{i=1}^{k-1} r_i+1, k, \cdot) \in \mathbb{R}^{N_t}, \forall l \in \{0, \dots, r_k\}, \forall k \in \{1, \dots, m\}$. The notation $\odot$ refers to the standard Hadamard product, resulting in the column vector $\boldsymbol{\Phi}_y \in \mathbb{R}^{N_t m}$.

The right-hand side of (9) is discretised in N_t samples, with $\bar{\boldsymbol{\theta}}_u \in \mathbb{R}^{m(r^*+1)\times m\times N_t}$ created identically as $\bar{\boldsymbol{\theta}}_y$. The inputs are parameterised with basis functions as shown in (10). It follows that in the right-hand side of (9) all the inputs and their derivatives can be written

$$\left[\bar{\mathbf{u}}_1, \quad \bar{\mathbf{u}}_1^{(1)}, \quad \dots, \quad \bar{\mathbf{u}}_m^{(r^*)}\right] = \left[\boldsymbol{\varphi}\boldsymbol{\gamma}_{u_1}, \quad \boldsymbol{\varphi}^{(1)}\boldsymbol{\gamma}_{u_1}, \quad \dots, \quad \boldsymbol{\varphi}^{(r^*)}\boldsymbol{\gamma}_{u_m}\right]. \tag{A3}$$

In Equation (9), the right-hand side can be expressed as done for the left-hand side (A2), just changing the output signals with the inputs and $\bar{\boldsymbol{\theta}}_y$ by $\bar{\boldsymbol{\theta}}_u$. Using the relation (A3), and collecting all the unknown variables,

$$\boldsymbol{\gamma}_u = \left[\boldsymbol{\gamma}_{u_1}^{\mathrm{T}}, \quad \boldsymbol{\gamma}_{u_2}^{\mathrm{T}}, \quad \dots, \quad \boldsymbol{\gamma}_{u_m}^{\mathrm{T}}\right]^{\mathrm{T}}, \tag{A4}$$

the right-hand side of (9) becomes

$$\boldsymbol{\Phi}_u = \begin{bmatrix} \sum_{k=1}^{m}\left(\sum_{l=0}^{r^*}\left(\boldsymbol{\varphi}^l \odot \bar{\boldsymbol{\theta}}_u\left(l+1+(k-1)\left(r^*+1\right), 1, \cdot\right)\right)\gamma_{u_k}\right) \\ \vdots \\ \sum_{k=1}^{m}\left(\sum_{l=0}^{r^*}\left(\boldsymbol{\varphi}^l \odot \bar{\boldsymbol{\theta}}_u\left(l+1+(k-1)\left(r^*+1\right), m, \cdot\right)\right)\gamma_{u_k}\right) \end{bmatrix}. \tag{A5}$$

From (A5), all contributions $\gamma_{u_k}, \forall k \in \{1, \dots, m\}$ can be collected to become a linear operation with respect to $\boldsymbol{\gamma}_u$

$$\boldsymbol{\Phi}_u\boldsymbol{\gamma}_u = \begin{bmatrix} \begin{bmatrix} \sum_{l=0}^{r^*}\left(\boldsymbol{\varphi}^{(l)} \odot \bar{\boldsymbol{\theta}}_u\left(l+1+(1-1)\left(r^*+1\right), 1, \cdot\right)\right) \\ \vdots \\ \sum_{l=0}^{r^*}\left(\boldsymbol{\varphi}^{(l)} \odot \bar{\boldsymbol{\theta}}_u\left(l+1+(m-1)\left(r^*+1\right), 1, \cdot\right)\right) \end{bmatrix} \\ \vdots \\ \begin{bmatrix} \sum_{l=0}^{r^*}\left(\boldsymbol{\varphi}^{(l)} \odot \bar{\boldsymbol{\theta}}_u\left(l+1+(1-1)\left(r^*+1\right), m, \cdot\right)\right) \\ \vdots \\ \sum_{l=0}^{r^*}\left(\boldsymbol{\varphi}^{(l)} \odot \bar{\boldsymbol{\theta}}_u\left(l+1+(m-1)\left(r^*+1\right), m, \cdot\right)\right) \end{bmatrix} \end{bmatrix} \boldsymbol{\gamma}_u, \tag{A6}$$

with $\boldsymbol{\Phi}_u \in \mathbb{R}^{N_t m \times Lm}$.

Curriculum vitæ

Alexis Benaitier

benaitier.alexis@gmail.com
linkedin.com/in/alexis-benaitier-a9ba68138

EDUCATION

PhD candidate | *Control Theory* — Jan. 2020 – Jun. 2024
Institut für Mechanik und Mechatronik: TU Wien — Vienna, Austria
Supervisor: Associate Prof. Dipl.-Ing. Dr.techn. Christoph Hametner

Master of Science | *Mechanics & Electronic* — Sep. 2014 – Jul. 2019
University Bourgogne Franche-Comté — Nevers, France
Supervisor: Dipl.-Ing. Dr.techn. PREVOST Vivien

WORK EXPERIENCE

Project assistant — Jan. 2020 – Jun. 2024
Institut für Mechanik und Mechatronik: TU Wien — Vienna, Austria

Research project on hybrid vehicle monitoring and control with AVL List GmbH. *Scientific research, journal publications, scientific conferences, reporting to industrial partners, and project scheduling.*

University activities - Lecturer for Master lectures, Master thesis supervision, student work supervision, laboratory experiments. *Scientific knowledge transfer, project proposal and management, and participation in lecture note creation.*

Research scientist — Jul. 2019 – Dec. 2019
IFP Energies Nouvelles — Rueil Malmaison, France

Energetic study of hybrid and electric vehicles. *Conducting scientific projects, reporting to project partners, and writing technical reports.*

Master internship Jan. 2019 – Jun. 2019
IFP Energies Nouvelles Rueil Malmaison, France

Sizing, adaptation and optimization of hybrid powertrain components. *Conducting scientific project, reporting to project partners, writing technical report.*

Auto-entrepreneur Feb. 2019 – Dec. 2019
Self-employed Paris, France

VBA macros for Excel database to automatize statistical report generation. *Project proposal and management, private lecturing, VBA coding, code delivery and maintenance.*

R&D Electronic Technician Jul. 2018 – Aug. 2018
Sepro Group Vendée, France

Electrical drawing of multi-axis robots to equip injection molding machines. *Electrical drawing, manufacturing and assembling process plans.*

Bachelor internship Jul. 2017 – Dec. 2017
AVL Powertain UK Ltd Basildon, UK

Hybrid powertrain simulation and testing. *Data logging and analysis, strategy development, customer report.*

SKILLS

Languages: English (fluent), French (native), German (intermediate), Spanish (basics)
Programming: Matlab, VBA, Python, Javascript, C/C++
CAE: AVL AST, SolidWorks, CATIA V5, LabVIEW, OpenFOAM
Prototyping: dSpace, Quanser, Arduino
Reporting: Microsoft Office Suite, LaTex
Tools: Windows, Linux, Git

LIST OF SCIENTIFIC PUBLICATIONS

International Journals

- **A. Benaitier**, F. Krainer, S. Jakubek, and C. Hametner. A Modular Approach for Cooperative Energy Management of Hybrid Electric Vehicles Considering Predictive Information. *IEEE Access*, Vol. 12 (2024), pages 60588-60600, DOI: 10.1109/ACCESS.2024.3395019

- **A. Benaitier**, F. Krainer, S. Jakubek, and C. Hametner. Optimal energy management of hybrid electric vehicles considering pollutant emissions during transient operations. *Applied Energy*, Vol. 344 (2023), pages 121267, DOI: 10.1016/j.apenergy.2023.121267
- **A. Benaitier**, S. Jakubek, F. Krainer, and C. Hametner. Automated nonlinear feedforward controller identification applied to engine air path output tracking. *International Journal of Control*, Vol. 1 (2023), pages 1-12, DOI: 10.1080/00207179.2023.2227740

International Conferences

- **A. Benaitier**, F. Krainer, S. Jakubek, and C. Hametner. Robust physical quantities estimation for diesel engine emission reduction using sensor fusion. *2022 IEEE Conference on Control Technology and Applications (CCTA)*, Trieste, Italy; 22.08.2022 - 25.08.2022
  DOI: 10.1109/CCTA49430.2022.9966196
- **A. Benaitier**, F. Krainer, S. Jakubek, and C. Hametner. Optimal control of aftertreatment electric heaters for mild hybrid vehicles during cold start. *2022 IEEE Vehicle Power and Propulsion Conference (VPPC)*, Merced, CA, USA; 01.11.2022 - 04.11.2022
  DOI: 10.1109/VPPC55846.2022.10003358
- D. Köppel, **A. Benaitier**, L. Kügerl, and C. Hametner. Efficient optimization-based control of a fuel cell hybrid electric vehicle with torque vectoring. *IEEE 2023 Vehicle Power and Propulsion*, Milan, Italy; 24.10.2023 - 27.10.2023
  DOI: 10.1109/VPPC60535.2023.10403338

Patents

- F. Krainer, C. Hametner, and **A. Benaitier**. *Verfahren zur Identifizierung eines Gesetzes zur Vorwärtssteuerung eines Steuerungsparameters eines Antriebsstrangs aus Messdaten.* Status: patent granted (European Patent Office number DE102023111180)
- F. Krainer, C. Hametner, and **A. Benaitier**. *Kontrollverfahren und Kontrollsystem für einen Hybridantriebsstrang.* Status: patent submitted (Austrian registration number: A50304/2022)